

On the physics potential to study the gluon content of proton and deuteron at NICA SPD

A. Arbuzov^a, A. Bacchetta^{b,c}, M. Butenschoen^d, F.G. Celiberto^{b,c,e,f}, U. D'Alesio^{g,h}, M. Deka^a, I. Denisenko^a, M. G. Echevarria^l, A. Efremov^a, N.Ya. Ivanov^{a,j}, A. Guskov^{a,k}, A. Karpishkov^{l,a}, Ya. Klopota^{a,m}, B. A. Kniehl^d, A. Kotzinian^{j,o}, S. Kumano^p, J.P. Lansberg^q, Keh-Fei Liu^r, F. Murgia^h, M. Nefedov^l, B. Parsamyan^{a,n,o}, C. Pisano^{g,h}, M. Radici^c, A. Rymbekova^a, V. Saleev^{l,a}, A. Shipilova^{l,a}, Qin-Tao Song^s, O. Teryaev^a

^aJoint Institute for Nuclear Research, 141980 Dubna, Moscow region, Russia

^bDipartimento di Fisica, Università di Pavia, via Bassi 6, I-27100 Pavia, Italy

^cINFN Sezione di Pavia, via Bassi 6, I-27100 Pavia, Italy

^dII. Institut für Theoretische Physik, Universität Hamburg, Luruper Chaussee 149, 22761 Hamburg, Germany

^eEuropean Centre for Theoretical Studies in Nuclear Physics and Related Areas (ECT*), I-38123 Villazzano, Trento, Italy

^fFondazione Bruno Kessler (FBK), I-38123 Povo, Trento, Italy

^gDipartimento di Fisica, Università di Cagliari, I-09042 Monserrato, Italy

^hINFN Sezione di Cagliari, I-09042 Monserrato, Italy

ⁱDpto. de Física y Matemáticas, Universidad de Alcalá, 28805 Alcalá de Henares (Madrid), Spain

^jYerevan Physics Institute, 0036 Yerevan, Armenia

^kMoscow Institute of Physics and Technology, Moscow Region, 141700, Russia

^lSamara National Research University, 443000 Samara, Russia

^mBogolyubov Institute for Theoretical Physics, 03143 Kiev, Ukraine

ⁿDipartimento di Fisica, Università di Torino, Via Peitro Giuria 1, 10125 Torino, Italy

^oINFN Sezione di Torino, Via Peitro Giuria 1, 10125 Torino, Italy

^pInstitute of Particle and Nuclear Studies, High Energy Accelerator Research Organization (KEK), Oho 1-1, Tsukuba, Ibaraki, 305-0801, Japan

^qUniversité Paris-Saclay, CNRS, IJCLab, 91405 Orsay, France

^rDepartment of Physics and Astronomy, University of Kentucky, Lexington, KY 40506, USA

^sSchool of Physics and Microelectronics, Zhengzhou University, Zhengzhou, Henan 450001, China

Abstract

The Spin Physics Detector (SPD) is a future multipurpose experiment foreseen to run at the NICA collider, which is currently under construction at the Joint Institute for Nuclear Research (JINR, Dubna, Russia). The physics program of the experiment is based on collisions of longitudinally and transversely polarized protons and deuterons at \sqrt{s} up to 27 GeV and luminosity up to 10^{32} cm⁻² s⁻¹. The SPD will operate as a universal facility for the comprehensive study of the unpolarized and polarized gluon content of the nucleon, using complementary probes such as: charmonia, open charm, and prompt photon production processes.

The aim of this work is to provide a thorough review of the physics objectives that can potentially be addressed at the SPD, underlining related theoretical aspects and discussing relevant experimental results when available. Among different pertinent phenomena particular attention is drawn to the study of the gluon helicity, gluon Sivers and Boer-Mulders functions in the nucleon, as well as the gluon transversity distribution in the deuteron, via the measurement of single and double spin asymmetries.

Contents

1	Introduction	2
2	Gluon probes at NICA SPD	3
2.1	Charmonium production	4
2.2	Open charm production	7
2.3	Prompt photon production	7

3	Theoretical motivation	9
3.1	Gluon TMDs	9
3.2	Hadron structure and mechanisms of charmonium hadroproduction	11
3.3	TMD factorization with gluon probes	17
3.4	Gluon content of the proton spin from Lattice QCD	18
4	Gluon content of unpolarized proton and deuteron	20
4.1	Gluons at large x and perturbative QCD	20
4.2	Linearly polarized gluons in unpolarized nucleon	22
4.2.1	Parton-hadron correlators and TMD distribution functions	22
4.2.2	Probing the density $h_1^{\perp g}$ with heavy flavor production	23
4.2.3	Azimuthal distributions in heavy-quark hadroproduction	24
4.3	Non-nucleonic degrees of freedom in deuteron	27
5	Gluon content of polarized proton and deuteron	27
5.1	Gluon helicity with longitudinally polarized beams	27
5.2	Gluon-related TMD and twist-3 effects with transversely polarized beams	30
5.3	Gluon transversity in deuteron	35
5.4	Tensor-polarized gluon distribution in deuteron	39
5.5	Deuteron tensor polarization and shear forces	40
6	Summary	41

1. Introduction

Gluons, along with quarks, are the fundamental constituents of the nucleon. They play a key role in generation of the mass of the nucleon and carry about half of its momentum in hard (semi)inclusive processes. The spin of the nucleon is also defined by its constituents and is built up from the intrinsic spin of the valence and sea quarks (spin-1/2) and gluons (spin-1), and their orbital angular momenta. Notwithstanding the progress achieved during the last decades in the understanding of the quark contribution to the nucleon spin, the gluon sector is much less developed. One of the difficulties is the lack of the direct probes to access the gluon content in high-energy processes. While the quark contribution to the nucleon spin was determined quite precisely in semi-inclusive deep-inelastic scattering (SIDIS) experiments like EMC, CLAS, HERMES, and COMPASS, the gluon contribution, determined through the gluon helicity Parton Distribution Function is still not well-constrained experimentally and is expected to be significant.

In recent years, the three-dimensional partonic structure of the nucleon, in particular the spatial and momentum distributions of its constituents, became a subject of a careful study. Precise mapping of the three-dimensional structure of the nucleon is crucial for our understanding of Quantum Chromodynamics (QCD). One of the ways to go beyond the usual collinear approximation in the momentum space, is to take into consideration intrinsic transverse-motion of partons in the nucleon *i.e.* assuming non-zero transverse momentum vector \mathbf{k}_T for partons. Then the spin-structure of the nucleon in semi-inclusive hard processes is described by the so-called Transverse-Momentum-Dependent Parton Distribution Functions (TMD PDFs) [1–6].

One of the most powerful tools to study quark TMD PDFs are the measurements of the nucleon spin (in)dependent azimuthal asymmetries in SIDIS [1, 4, 5, 7, 8] and Drell–Yan processes [9, 10]. Complementary information on TMD fragmentation process, necessary for the interpretation of SIDIS data, is obtained from e^+e^- measurements [11]. Being an actively developing field, TMD physics triggers a lot of experimental and theoretical interest all over the world, stimulating new measurements and developments in TMD extraction techniques oriented on existing and future data from lepton-nucleon, hadron-hadron and electron-positron facilities at CERN, DESY, JLab, FNAL, BNL, and KEK. For recent reviews on experimental and theoretical advances on TMDs see Refs. [12–19]. These efforts improved significantly the phenomenological modeling of quark Sivers, transversity and Boer-Mulders TMD PDFs.

Recently a remarkable progress has been achieved in modeling of gluon TMD PDFs and phenomenological calculations for azimuthal asymmetries in gluon-sensitive channels including *e.g.* open heavy-flavor and charmonia production in hard processes, see Refs. [20–23] and the references therein. However experimental data relevant for the study of gluon TMD PDFs are still scarce [24–29].

Whereas the experimental efforts are mostly focused on the study of the partonic content of the proton, the gluon structure of the deuteron hides interesting peculiarities. The simplest model of the deuteron describes it as a weakly-bound state of a proton and a neutron mainly in the S-wave with a small admixture of the D-wave state [30]. This approach is not fully reliable in the description of the deuteron structure at large Q^2 ¹. In particular, possible non-nucleonic degrees of freedom in deuteron could play an important role in the understanding of the nuclear modification of PDFs (the EMC effect [31]). Since the gluon transversity operator requires two-unit helicity-flip, it cannot be defined for spin-1/2 nucleons [32]. Hence, proton and neutron gluon transversity functions can not contribute directly to the gluon transversity of the deuteron. A non-zero deuteron transversity would then be an indication of a non-nucleonic component, or some other exotic hadronic mechanisms within the deuteron.

Most of the existing experimental results on spin-dependent gluon distributions in nucleon are obtained in the experiments at DESY (HERMES), CERN (COMPASS), and BNL (STAR and PHENIX). Study of polarized gluon content of the proton and nuclei is an important part of future projects in Europe and the United States such as AFTER@LHC and LHCSpin at CERN, and EIC at BNL [33–36].

Experiments with hadronic collisions are used to access gluons at the Born level without involvement of electromagnetic couplings, which is an important advantage over SIDIS measurements. The Spin Physics Detector (SPD) project [37–40] at the NICA collider that is under construction at JINR (Dubna, Russia) aims to investigate the nucleon spin structure and polarization phenomena in polarized p - p and d - d collisions. The planned center-of-mass energy can reach up to 27 GeV while the luminosity L is expected to be of order of 10^{32} cm⁻² s⁻¹ in p - p collisions at maximal energy [41]. The d - d collisions can be performed at $\sqrt{s_{NN}} \leq 13.5$ GeV with about one order of magnitude lower luminosity. Asymmetric p - d collisions at $\sqrt{s_{NN}} \leq 19$ GeV are also under discussion. It is planned to achieve beam polarization of up to 70%. The SPD experimental setup (see Fig. 1) is being designed as a universal 4π -acceptance detector equipped with advanced tracking and particle identification systems. The silicon vertex detector (VD) will provide good resolution for the vertex position ($\lesssim 100$ μ m) ensuring reliable identification of secondary vertices of D -meson decays. The straw-tube based tracking system (ST) to be placed in the solenoidal magnetic field (up to 1 T at the detector axis) will provide the transverse momentum resolution $\sigma_{p_T}/p_T \approx 2\%$ for particles with momentum about 1 GeV. The time-of-flight system (PID in the Fig. 1) with a time resolution of about 60 ps will provide 3σ π/K and K/p separation for hadrons with momenta up to about 1.2 GeV and 2.2 GeV, respectively. The usage of an aerogel-based Cherenkov detector could extend the momentum range of the PID-system. The detection of photons will be performed by the sampling electromagnetic calorimeter (ECal) with an energy resolution of $5\%/\sqrt{E/\text{GeV}}$. To reduce multiple scattering and photon conversion effects, the detector material will be minimized throughout the inner part of the spectrometer. The muon (range) system (RS) will be set up for muon identification. It can also act as a rough hadron calorimeter. A pair of beam-beam counters (BBC) and zero-degree calorimeters will be responsible for the local control of polarimetry and luminosity. To minimize possible systematic effects, SPD will be equipped with a triggerless data acquisition system [42]. Spin physics program at the SPD is expected to start after year 2025 and to extend for about 10 years.

This Review has the following structure. Section 2 describes peculiarities of gluon probes such as charmonium (2.1), open charm (2.2), and prompt photon production (2.3) in the SPD kinematic domain. Section 3: subsection 3.1 serves as a theoretical and phenomenological introduction into physics of gluon TMD PDFs, in 3.2 heavy quarkonium hadroproduction is discussed, in 3.3 peculiarities of TMD-factorization for heavy-quarkonium production are addressed, while the proton spin problem from the point of view of contemporary lattice QCD is reviewed in 3.4. Beam-polarization-independent measurements are discussed in section 4. In subsections 4.1, 4.2 and 4.3 we address the determination of the gluon PDFs at high x , linearly polarized gluons in unpolarized nucleon and possible non-nucleonic content in deuteron, respectively. Section 5 is dedicated to beam-polarization-dependent measurements that are feasible at SPD. Gluon helicity function $\Delta g(x)$ and related measurements are discussed in 5.1. The study of TMD and twist-3 effects is the main topic of Sec. 5.2. Section 5.3 is dedicated to the gluon transversity in deuteron. Gluon contribution to the tensor structure of deuteron is reviewed in 5.5. Section 6 summarizes the discussion on the physics program with gluons at the SPD.

2. Gluon probes at NICA SPD

Within perturbative QCD, the partonic content of a nucleon is described by (TMD)PDFs. To ensure the validity of this description, one needs to restrict to hard inclusive reactions on nucleons. The hard scale (Q^2 or μ^2) in

¹We use Q^2 (or μ^2) as a generic notation for the hard scale of a reaction: the invariant mass square of lepton pairs in Drell-Yan processes, Q^2 , transverse momentum square p_T^2 of produced hadron or its mass square M^2 .

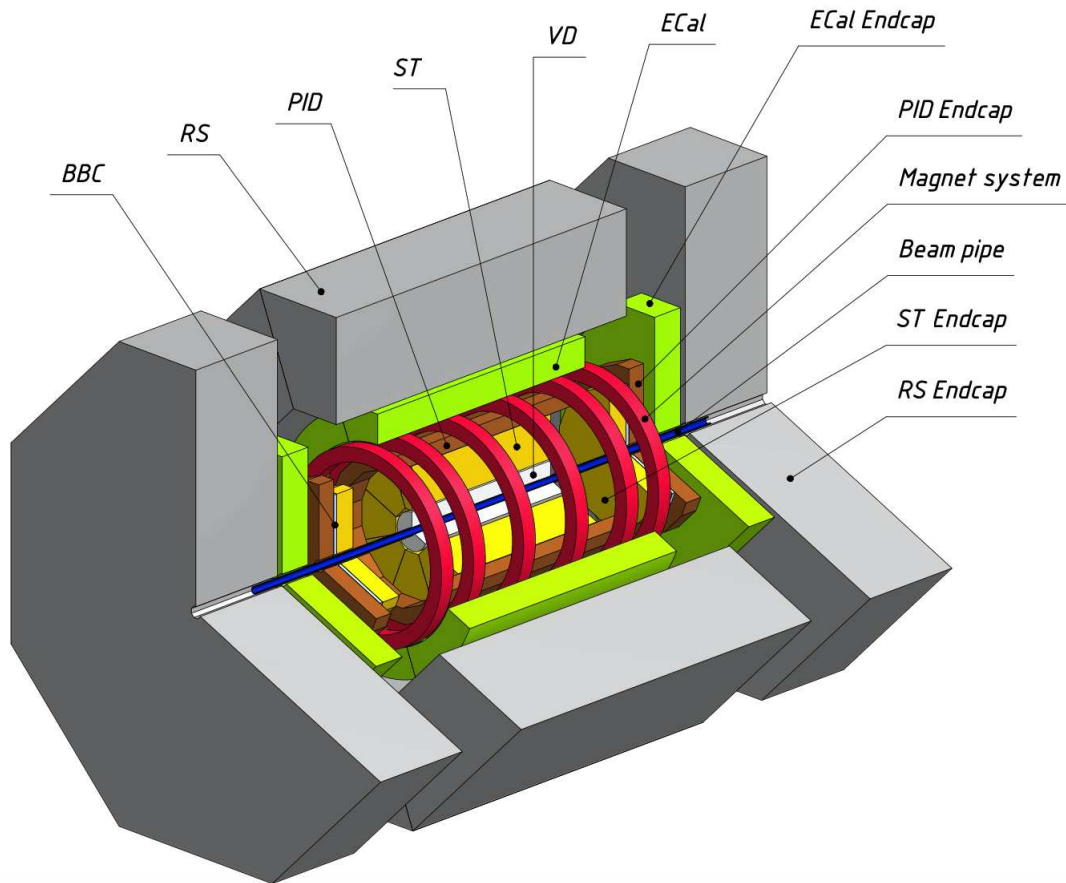


Figure 1: General layout of the SPD setup [42].

these reactions is provided for (SI)DIS by a) the virtuality of exchanged photon, Q^2 , or b) by the high transverse momentum of selected final particle or jet, p_T , or c) by the heavy mass of the observed hadron, for example $m_{J/\psi}$. For the hadronic reactions, the selections b) and c) provide access to the partonic content of a nucleon.

The (un)polarized gluon content of the proton and deuteron at intermediate and high values of Bjorken x will be investigated at the SPD using three main probes: the inclusive production of charmonia, open charm, and prompt photons. The study of these processes is complementary to the usual approaches to access the partonic structure of the nucleon in hadronic collisions such as the inclusive production of hadrons at high transverse momentum and the Drell-Yan process. Unfortunately, the latter channel is unlikely to be accessible at SPD due to the small cross-section and unfavourable background conditions. For an efficient detection of the aforementioned gluon probes, the SPD setup is planned to be equipped with muon-identification system, an electromagnetic calorimeter, a time-of-flight system, and a silicon vertex detector. Nearly a 4π coverage of the setup and a low material budget in the inner part of the setup should provide a large acceptance for the detection of the desired final states. In Fig. 2, the kinematic phase-space in x and Q^2 to be accessed by the SPD is compared to the corresponding ranges of previous, present and future experiments. The parameters of the experimental facilities planning to contribute to gluon physics with polarized beams are listed in Tab. 1. Figure 3 illustrates the behavior of the cross sections for the inclusive production of J/ψ , ψ' , D -mesons and high- p_T prompt photons in p - p collisions as a function of \sqrt{s} .

2.1. Charmonium production

From the experimental point of view, for the SPD energy range, the hadronic production of charmonia seems to be particularly suited to access gluon content in hadrons due to the clean signal from $J/\psi \rightarrow \mu^+\mu^-$ decay ($BF = 0.06$). The production of prompt J/ψ -mesons looks most attractive, since the corresponding cross section is experimentally known to be significant. A large data set of $J/\psi \rightarrow \mu^+\mu^-$ events is accumulated in beam-dump experiments (where only a muon pair is detected) with proton and pion beams at \sqrt{s} close to 20 GeV. However J/ψ -meson is not the cleanest probe of the proton structure, since a significant fraction of J/ψ -mesons

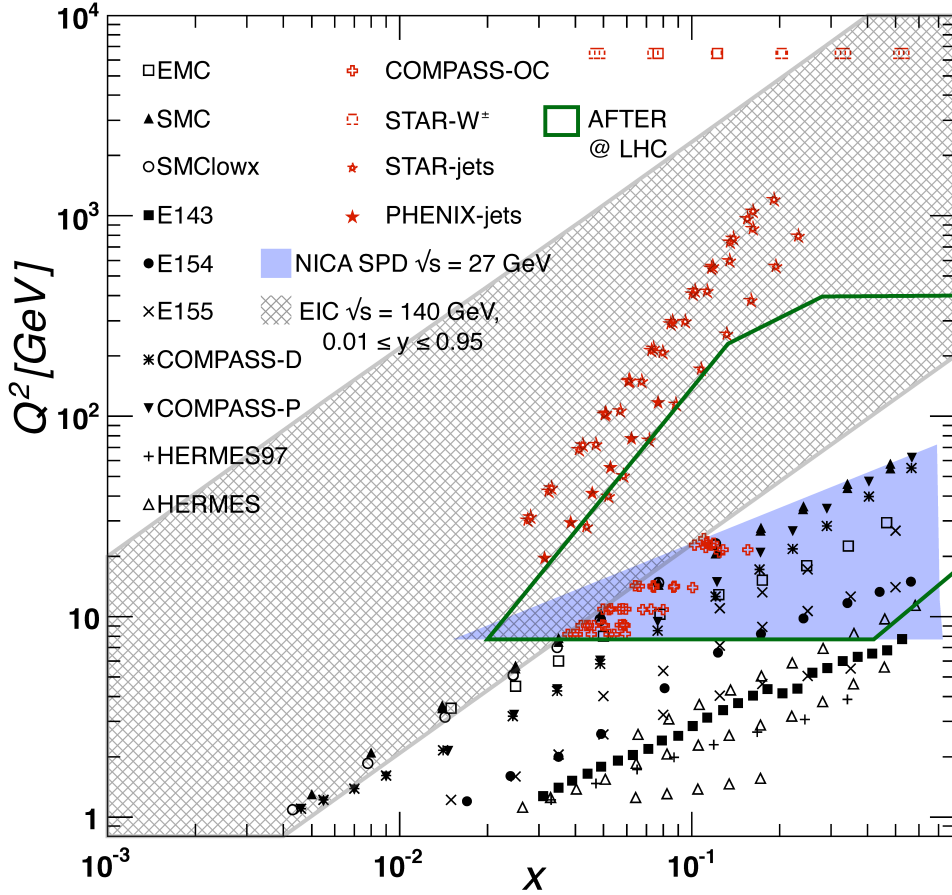


Figure 2: The kinematic coverage, in the (x, Q^2) plane, of the hadronic cross-section data used for determination of the NNPDFpol1.1 set of the polarized PDFs [43]. The kinematic domains expected to be covered by the NICA SPD at $\sqrt{s} = 27$ GeV and AFTER [34] by charmonium, open-charm and prompt-photon production are shown. The EIC kinematic domain for $\sqrt{s} = 140$ GeV and $0.01 \leq y \leq 0.95$ is also presented according to Ref. [36]. The figure is adapted from [43] © (2014) by Elsevier.

observed in hadronic collisions is produced indirectly through decays of χ_{cJ} and $\psi(2S)$ (the so-called feed-down contribution). The feed-down fraction is p_T and collision-system-dependent, it varies between 20% [46] in pA and $\sim 40\%$ in pp -collisions [47] (see the detailed discussion in Ref. [48]). Accounting for this contribution introduces additional uncertainties into the theoretical calculations of inclusive J/ψ cross-sections. Hence, to provide additional constraints to production models, it is important to study production of χ_{cJ} and $\psi(2S)$ separately, through their decays $\chi_{cJ} \rightarrow \gamma J/\psi$ ($BF = 0.014, 0.343$ and 0.19 for $J = 0, 1$ and 2) and $\psi(2S) \rightarrow J/\psi \pi^+ \pi^-$ ($BF = 0.347$). The latter state is of special interest, because it is essentially free from feed-down contamination from higher charmonium states, due to the proximity of $D^0 \bar{D}^0$ -threshold. However, the separation of the $\chi_{c0,1,2}$ signals is a challenging experimental task due to the small mass difference between the states, which requires good energy resolution of the electromagnetic calorimeters for soft photons. The measurement of η_c -meson production cross-section at SPD NICA, using $\eta_c \rightarrow p\bar{p}$ decay mode ($BF = 1.45 \times 10^{-3}$) is also under discussion, but might be challenging.

Besides, the task of accessing gluon distributions using heavy quarkonia is rather challenging also from the theoretical point of view. The heavy quark-antiquark pair couples directly to gluons from initial-state hadrons

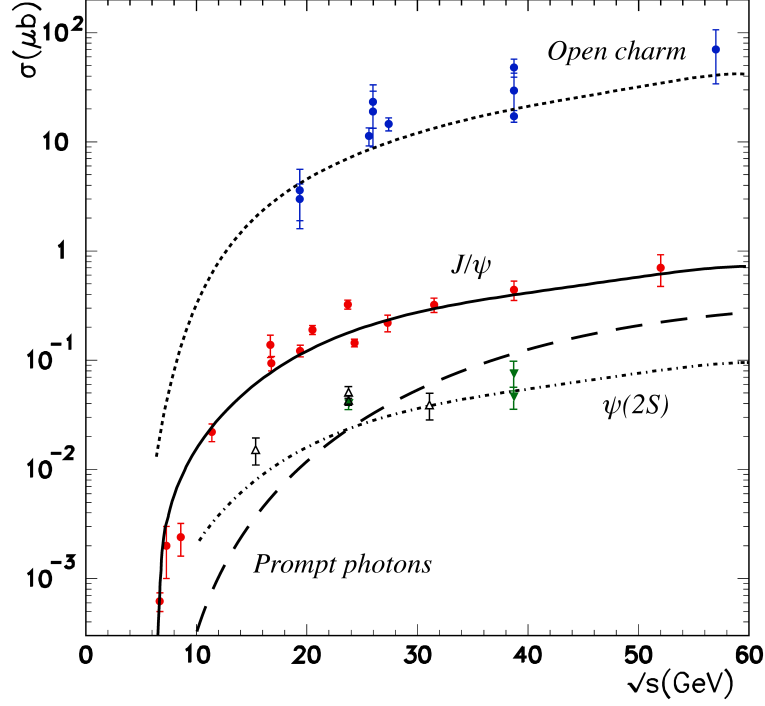


Figure 3: Cross-section for open charm, J/ψ and $\psi(2S)$ production from CEM-NLO model (colour evaporation model combined with NLO pQCD matrix elements) and prompt photon production cross-section for $p_T > 3$ GeV as a function of center-of-mass energy. Model-calculations are compared with available experimental data sets. The figure is adapted from Ref. [44] ©(2002) by The European Physical Journal.

Table 1: Main present and future gluon-spin-physics experiments.

Experimental facility	SPD @NICA [41]	RHIC [45]	EIC [36]	AFTER @LHC [34]	LHCspin [35]
Scientific center	JINR	BNL	BNL	CERN	CERN
Operation mode	collider	collider	collider	fixed target	fixed target
Colliding particles & polarization	$p^\uparrow-p^\uparrow$ $d^\uparrow-d^\uparrow$ $p^\uparrow-d, p-d^\uparrow$	$p^\uparrow-p^\uparrow$	$e^\uparrow-p^\uparrow, d^\uparrow, {}^3\text{He}^\uparrow$	$p-p^\uparrow, d^\uparrow$	$p-p^\uparrow$
Center-of-mass energy $\sqrt{s_{NN}}$, GeV	≤ 27 ($p-p$) ≤ 13.5 ($d-d$) ≤ 19 ($p-d$)	63, 200, 500	20-140 (ep)	115	115
Max. luminosity, $10^{32} \text{ cm}^{-2} \text{ s}^{-1}$	~ 1 ($p-p$) ~ 0.1 ($d-d$)	2	1000	up to ~ 10 ($p-p$)	4.7
Physics run	>2025	running	>2030	>2025	>2025

(Fig. 4(a)) and its production can be perturbatively calculated, because the hard scale of the process is limited from below by the heavy quark mass, providing the direct access to polarized and unpolarized gluon distributions. However, the process of the transition of the heavy quark-antiquark pair into a physical bound-state is presently

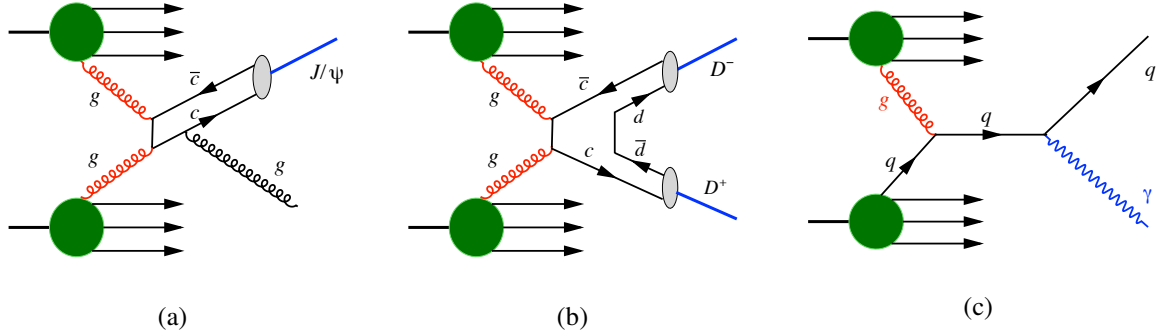


Figure 4: Diagrams illustrating three probes to access the gluon content of proton and deuteron in polarized collisions at NICA SPD: production of (a) charmonium (color-singlet model for J/ψ , $\psi(2S)$), (b) open charm, (c) prompt photons.

not well understood [48–51] and can become a source of significant theoretical uncertainties. We review modern status of the theory of quarkonium production in more detail in Sec. 3.2 to explain the latter point.

Hence, quarkonium production can be used to study the structure of hadrons only with a great caution and only if the results consistent with other probes will eventually emerge. The study of the hadronic structure and the heavy quarkonium production mechanism should be treated as complementary analyses. The best strategy for quarkonium measurements at SPD is to study the yields and the polarization of different quarkonium states in a wide kinematic range, at various energies, both in polarized and non-polarized hadronic collisions. This would serve as an input to develop and to constrain the theory and to validate or exclude various models. When the theory of production of heavy quarkonia is firmly established, it will become an invaluable tool to study the details of hadronic structure.

2.2. Open charm production

It is well known that the heavy flavor production offers direct probes of the gluon distributions in hadrons, see e.g. [52] and references therein. The basic mechanism responsible for charm pair production in pp collisions is the gluon fusion (GF, see Fig. 4(b)). In the framework of pQCD, the GF contributes to the hadron cross-section as $\mathcal{L}_{gg} \otimes \hat{\sigma}_{c\bar{c}}$, where the gluon luminosity \mathcal{L}_{gg} is a convolution of the gluon densities in different protons, $\mathcal{L}_{gg} = g \otimes g$. At leading order in pQCD, $\mathcal{O}(\alpha_s^2)$, the partonic cross-section $\hat{\sigma}_{c\bar{c}}$ describes the process $gg \rightarrow c\bar{c}$. For different theoretical estimates of p_T and Feynman variable x_F -differential D -meson hadroproduction cross-section an NICA energies see the Fig. 5.

The GF contribution to the charmonia production in pp collisions has the form $\mathcal{L}_{gg} \otimes \hat{\sigma}_{(c\bar{c})+X} \otimes W_{c\bar{c}}$. (For more details, see recent review [48]). At the Born level, the partonic cross-section $\hat{\sigma}_{(c\bar{c})+X}$ is of the order of α_s^3 because its basic subprocess is $gg \rightarrow (c\bar{c}) + g$ in the color-singlet model of charmonium production. Moreover, the quantity $W_{c\bar{c}}$, describing the probability for the charm pair to form a charmonium, imposes strong restrictions on the phase space of the final state.² For these two reasons, the α_s -suppression and phase space limitation, the cross-sections for charmonia production are almost two orders of magnitude smaller than the corresponding ones for open charm, see Figs. 2 (b).

To analyze the kinematics of a DD pair, each of D -mesons has to be reconstructed. The decay modes $D^+ \rightarrow \pi^+ K^- \pi^+$ (BF=0.094) and $D^0 \rightarrow K^- \pi^+$ (BF=0.04) can be used for that. In order to suppress the combinatorial background at SPD, the D -meson decay vertices that are about 100 μm away from the interaction point (the $c\tau$ values are 312 and 123 μm for the charged and neutral D -mesons, respectively) have to be selected. Identification of a charged kaon in the final state can be done using the time-of-flight system. The production and the decay of D^* -mesons can be used as an additional tag for open-charm events. Single-reconstructed D -mesons also carry reduced but still essential information about gluon distribution that is especially important in the low-energy region with a lack of statistics.

2.3. Prompt photon production

Photons emerging from the hard parton scattering subprocess, the so-called prompt photons, serve as a sensitive tool to access the gluon structure of hadrons in hadron-hadron collisions. Inclusive direct photon production

²To form a charmonium, the momenta of the produced quark and antiquark should be sufficiently close to each other.

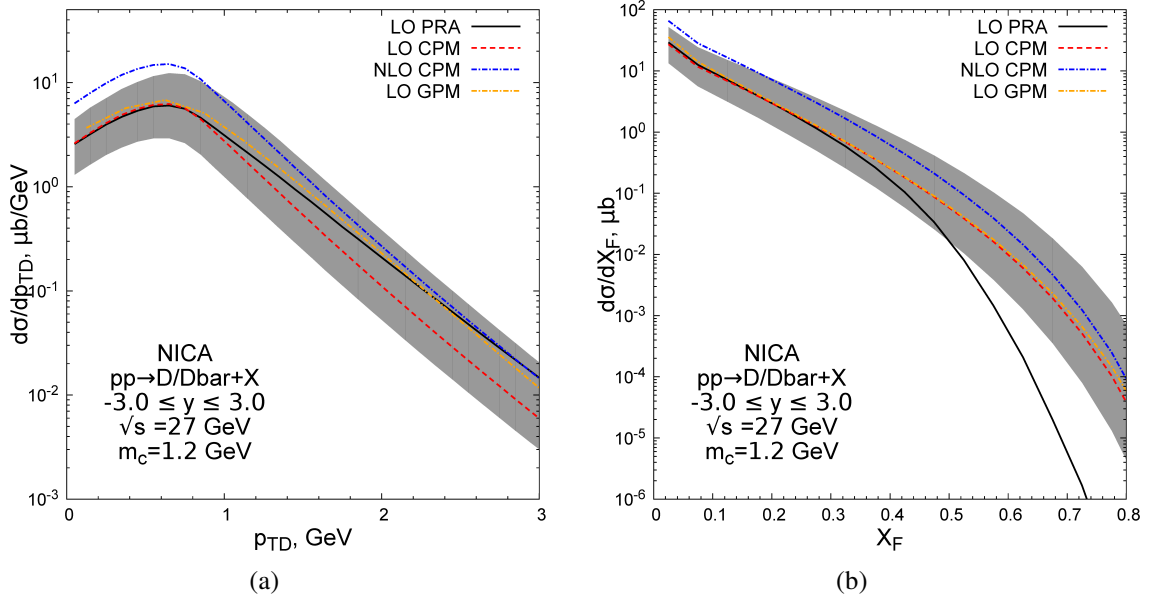


Figure 5: Theoretical predictions for $p_T(D)$ - (a) and x_F -differential (b) inclusive D -meson production cross-section in the LO of CPM, PRA, GPM and NLO of CPM

proceeds without fragmentation, i.e. the photon carries the information directly from the hard scattering process. Hence this process measures a combination of initial k_T -effects and hard scattering twist-3 processes. There are two main hard processes for the production of direct photons: gluon Compton scattering, $gq(\bar{q}) \rightarrow \gamma q(\bar{q})$ (Fig. 4(c)), which dominates, and quark-antiquark annihilation, $q\bar{q} \rightarrow \gamma g$. Contribution of the latter process to the total cross-section is small.

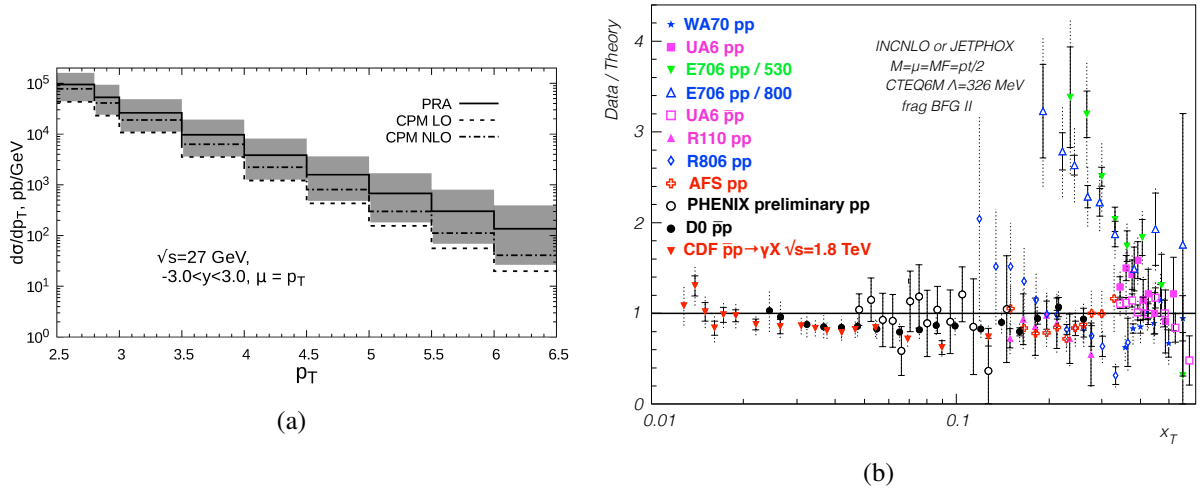


Figure 6: (a) Prediction for prompt photon transverse momentum spectrum at $\sqrt{s} = 27$ GeV obtained in LO (dashed line) and NLO (dash-dotted line) approximations of CPM and LO of PRA (solid line). Uncertainty bands for PRA predictions are due to factorization/renormalization scale variation only. (b) Data-to-theory ratio for the fixed-target and collider experiments. Reprinted figure with permission from [53] © (2006) by the American Physical Society.

Theoretical predictions for transverse momentum spectrum for inclusive prompt photon production at the energy of $\sqrt{s} = 27$ GeV are shown in Fig. 6(a). Calculations are performed in LO and NLO approximations of Collinear Parton Model (CPM), as well as in the Parton Reggeization Approach (PRA) [54], which is a QCD and QED gauge-invariant version of k_T -factorization. They include direct and fragmentation contributions, the latter one is about 15-30%. The K-factor between LO and NLO calculations in the CPM is about ~ 1.8 and slightly depends on $p_{T\gamma}$ [55]. LO prediction of PRA coincides with the result of NLO CPM calculation at moderate trans-

verse momenta ($p_T < 4$ GeV) while at higher p_T PRA predicts somewhat harder p_T -spectrum. Figure 6(b) [53] presents the comparison of the p_T spectra ($x_T = 2p_T / \sqrt{s}$) measured in a wide kinematic range of \sqrt{s} in different fixed-target and collider experiments and the theoretical NLO calculations performed within the JETPHOX package [56]. While high-energy collider results exhibit rather good agreement with the expectations, the situation at high- x_T is complicated. The results from E706 ($\sqrt{s} = 31.6$ and 38.8 GeV) [57] and R806 ($\sqrt{s} = 63$ GeV) [58] experiments diverge significantly from the theory and follow an evident trend, which could be an indication of possible systematic effects that have not been fully understood yet.

Table 2: Expected cross-section and event counts (without the acceptance correction) for each of the gluon probes per one year of SPD running (10^7 s). For η_c cross-section, the central LO PRA NRQCD (see Sec. 3.2) estimate for $\sqrt{s} = 24$ GeV is given, for other estimates see Fig. 9.

Probe	$\sigma_{27 \text{ GeV}},$ nb (\times BF)	$\sigma_{13.5 \text{ GeV}},$ nb (\times BF)	$N_{27 \text{ GeV}},$ 10^6	$N_{13.5 \text{ GeV}},$ 10^6
Prompt- γ ($p_T > 3$ GeV/c)	35	2	35	0.2
J/ψ $\rightarrow \mu^+ \mu^-$	200 12	60 3.6	12	0.36
$\psi(2S)$ $\rightarrow J/\psi \pi^+ \pi^- \rightarrow \mu^+ \mu^- \pi^+ \pi^-$ $\rightarrow \mu^+ \mu^-$	25 0.5 0.2	5 0.1 0.04	0.5 0.2	0.01 0.004
$\chi_{c1} + \chi_{c2}$ $\rightarrow \gamma J/\psi \rightarrow \gamma \mu^+ \mu^-$	200 3.0		3.0	
η_c $\rightarrow p \bar{p}$	400 0.6		0.6	
Open charm: $D\bar{D}$ pairs	14000	1300		
Single D -mesons				
$D^+ \rightarrow K^- 2\pi^+ (D^- \rightarrow K^+ 2\pi^-)$	520	48	520	4.8
$D^0 \rightarrow K^- \pi^+ (\bar{D}^0 \rightarrow K^+ \pi^-)$	360	33	360	3.3

In experiments prompt photons are detected alongside with a much larger number of photons from decays of secondary π^0 and η mesons (minimum-bias photons). The main challenge is to subtract these decay contributions and filter the photons directly emitted from hard collisions. This kind of background is especially important at small transverse momenta of produced photons (p_T) and gives the lower limit of the accessible p_T range. Therefore the prompt-photon contribution with $p_T \leq 2 - 3$ GeV is usually unreachable in the experiment [59].

A pair of prompt photons can be produced in hadronic interactions in $q\bar{q}$ annihilation, quark-gluon scattering, and gluon-gluon fusion hard processes (at the leading, next-to-leading, and next-to-next-leading orders, respectively). The double prompt photon production in nucleon interactions at low energies is not yet well studied experimentally. The production cross-section for proton-carbon interaction at $\sqrt{s} = 19.4$ GeV/c has been measured by the CERN NA3 experiment [60]. Based on this result one can expect the cross-section of the double photon production with $p_T > 2$ GeV/c for each photon to be at the level of about 0.5 nb.

Estimations of the expected event rates are evaluated for p - p collisions at $\sqrt{s} = 27$ and 13.5 GeV for the projected integrated luminosity 1.0 and 0.1 fb^{-1} , respectively that corresponds effectively to one year of data taking (10^7 s). The results are listed in Tab. 2.

3. Theoretical motivation

3.1. Gluon TMDs

The full list of leading-twist polarized gluon TMDs was first introduced in Ref. [61]. Tab. 3 contains the eight leading-twist gluon TMDs that are defined for a spin-1/2 hadron, using the naming scheme proposed in Ref. [62],

		gluon pol.		
		U	circular	linear
nucleon pol.	U	f_1^g		$h_1^{\perp g}$
	L		g_1^g	$h_{1L}^{\perp g}$
	T	$f_{1T}^{\perp g}$	g_{1T}^g	$h_1^g, h_{1T}^{\perp g}$

Table 3: Nucleon gluon TMD PDFs at twist-2. U , L , T describe unpolarized, longitudinally polarized and transversely polarized nucleons. U , ‘circular’, ‘linear’ stand for unpolarized, circularly polarized and linearly polarized gluons. Functions $h_1^{\perp g}$ and g_{1T}^g are T -even. Functions f_1^g and g_1^g are T -even and survive integration over the transverse momentum. Functions $f_{1T}^{\perp g}$, h_1^g , $h_{1T}^{\perp g}$ and $h_{1L}^{\perp g}$ are T -odd. For brevity functional dependence on x and k_T^2 as well as hard-scale dependence is omitted.

analogous to that of quark TMDs (see also [63]). In Ref. [64], the study of gluon TMDs was extended to spin-1 hadrons, leading to the definition of 11 new functions.

The TMDs depend on the light-cone momentum fraction x and the parton transverse momentum k_T . In Tab. 3 they are listed in terms of both the polarization of the gluon itself and of its parent spin-1/2 hadron. The two gluon TMDs on the diagonal of the table have the simplest physical interpretation: $f_1^g(x, k_T^2)$ is the distribution of unpolarized gluons inside an unpolarized hadron, and $g_1^g(x, k_T^2)$ is the distribution of circularly polarized gluons inside a longitudinally polarized hadron. Upon integration over k_T all TMD PDFs for spin-1/2 hadron vanish, except $f_1^g(x, k_T^2)$ and $g_1^g(x, k_T^2)$, which correspond to the well-known collinear unpolarized $f^g(x)$ and helicity $g_1^g(x)$ gluon PDFs, respectively. The collinear (k_T -integrated) gluon transversity PDF, $h_1^g(x)$, which is equal to zero for spin-1/2 hadrons, may be non-zero for spin-1 case (see Sec. 5.3 of this review). The collinear unpolarized gluon PDF, $f^g(x)$, is at present the only gluon function that is known to a good extent, while we have a fair knowledge of the helicity PDF $g_1^g(x)$, but still with large uncertainties [65] (see Sec. 5.1 for further discussion).

As for quarks TMDs, gluon TMDs receive contributions from the resummation of logarithmically-enhanced terms in perturbative calculations. They could be called the ‘‘perturbative part’’ of the TMDs. Much is known about them [66–68], but very little is known about the nonperturbative components.

The distribution of linearly polarized gluons in an unpolarized nucleon, $h_1^{\perp g}(x, k_T^2)$, *i.e.* the gluonic counterpart of the Boer-Mulders function, is particularly interesting because it gives rise to spin effects even in collisions of unpolarized hadrons [17, 69–73]. Analogous effects are generated at high transverse momentum by perturbative QCD: part of these contributions can be resummed and represent the perturbative part $h_1^{\perp g}(x, k_T^2)$ [67] (for further discussion see Sec. 4.2).

The Sivers function, $f_{1T}^{\perp g}(x, k_T^2)$, which encodes the distribution of unpolarized gluons in a transversely polarized nucleon, has a very important role in the description of transverse-spin asymmetries (see Sec. 5.2).

The precise definition of gluon TMDs should also take into account the fact that they can contain (at least) two different gauge-link configurations. This leads to the distinction between f -type and d -type gluon TMDs, also known as Weizsäcker-Williams (WW) and dipole TMDs [74–76]. In practice, each gluon TMD in Tab. 3 actually represents two distinct TMDs.

The WW TMDs contain either $[+, +]$ or $[-, -]$ Wilson line gauge links³, while the dipole TMDs contain either $[+, -]$ or $[-, +]$ gauge links. The WW type gluon TMDs occur in processes where the gluon interacts with a color-singlet initial particle (e.g., a photon in a DIS process) producing two colored final states (e.g., two jets). In processes where a gluon interacts with another gluon (color-octet state) and produces a color-singlet state (e.g., Higgs production), the relevant gluon TMDs have a $[-, -]$ gauge link structure. TMD factorization is expected to work in all these processes, and these relations are expected to follow from time-reversal invariance

$$f_1^{g[+,+]}(x, k_T^2) = f_1^{g[-,-]}(x, k_T^2) \quad (\text{T-even}), \quad (1)$$

$$f_{1T}^{g\perp[+,+]}(x, k_T^2) = -f_{1T}^{g\perp[-,-]}(x, k_T^2) \quad (\text{T-odd}). \quad (2)$$

The dipole gluon TMDs, instead, occur when a gluon interacts with a colored initial particle and produces a colored final particle as, e.g., in photon-jet production in pp collisions. In this case, TMD factorization has not been proven to work and may be affected by color-entanglement problems [77]. More complicated gauge-link

³Here + (–) indicates the direction of the future- (past-) pointing Wilson lines corresponding to final (initial) state interactions.

structure are involved in processes where multiple color states are present both in the initial and final state [78]. In these cases, TMD factorization can be even more questionable.

Experimental information on gluon TMDs is very scarce. First attempts to perform phenomenological studies of the unpolarized gluon TMD have been presented in Refs. [18, 79, 80]. Experimental and phenomenological results related to the gluon Sivers function can be found in Refs. [20, 22, 28, 29, 81].

At high transverse momentum and at low- x , the unpolarized and linearly polarized gluon distributions $f_1^g(x, \mathbf{k}_T^2)$ and $h_1^{\perp g}(x, \mathbf{k}_T^2)$ are connected [76] to the Unintegrated Gluon Distribution (UGD), defined in the BFKL approach [82–85] (see Refs. [86–96] for recent applications).

Since the information on gluon TMDs is at present very limited, it is important to study some qualitative features using relatively simple models. Pioneering work in this direction was done in the so-called *spectator-model* approach [61, 97, 98]. Originally developed for studies in the quark-TMD sector [62, 99–103], this family of models relies on the assumption that the struck nucleon emits a gluon, together with remnants that are treated as a single, on-shell particle. With this model, it is possible to generate all TMD densities at twist-2 (Table 3). A recent calculation for T -even distributions has been presented in Ref. [23]. In that work, at variance with previous studies, the spectator mass is allowed to take a continuous range of values weighted by a spectral function, which provides the necessary flexibility to reproduce both the small- and the moderate- x behaviour of gluon collinear PDFs.

Predictions obtained in Ref. [23] for the unpolarized gluon TMD, $x f_1^g(x, \mathbf{k}_T^2)$, and for the linearly-polarized gluon TMD, $x h_1^{\perp g}(x, \mathbf{k}_T^2)$, are shown in Fig. 7 as functions of the transverse momentum squared, \mathbf{k}_T^2 , for $x = 10^{-3}$ and at the initial scale, $Q_0 = 1.64$ GeV (*i.e.*, without the application TMD evolution). Predictions are given as a set of 100 replicas, which are statistically equivalent and reproduce well the collinear PDFs $f_1^g(x)$ and $g_1^g(x)$. Each line in the plot shows a single replica, with the black solid line corresponding to the most representative replica (n. 11), which has the minimal quadratic distance to the mean values of parameters obtained in the fit. Apart from details, it is important to note that: i) even if all replicas reproduce similar collinear PDFs, they predict very different results for the TMDs, ii) each TMD exhibits a peculiar trend both in x and \mathbf{k}_T^2 . For instance, the unpolarized function presents a clearly non-Gaussian shape in \mathbf{k}_T^2 , and goes to a small but non-vanishing value for $\mathbf{k}_T^2 \rightarrow 0$. The linearly-polarized gluon TMD is large at small \mathbf{k}_T^2 and decreases fast. Both of them are increasingly large at small x .

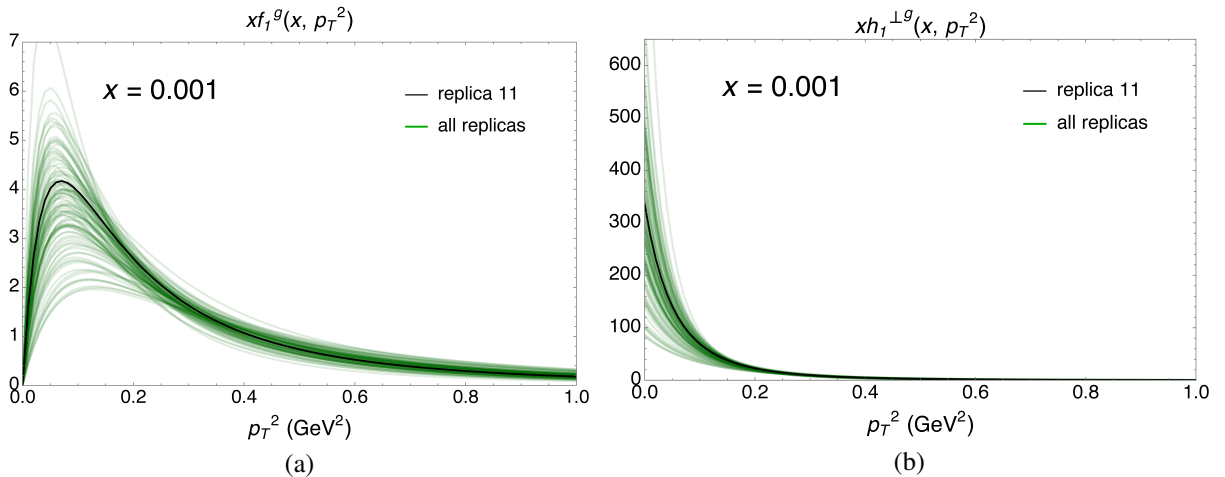


Figure 7: Examples of model calculations of the unpolarized(a) and Boer-Mulders (b) gluon TMDs as functions of \mathbf{k}_T^2 , for $x = 10^{-3}$ and at the initial scale, $Q_0 = 1.64$ GeV. The figures are adapted from Ref. [23] ©(2020) by The European Physical Journal.

3.2. Hadron structure and mechanisms of charmonium hadroproduction

In this section, we give a short overview of the current status of the theory of heavy-quarkonium production with an emphasis on possible applications of heavy-quarkonium measurements for studies of the gluon content of hadrons.

The hadroproduction of heavy quarkonia proceeds in two stages: firstly, a heavy quark-antiquark pair is produced at short distances, via gluon-gluon fusion but also with a non-negligible contribution of $q\bar{q}$ and qg -initiated subprocesses, depending on the collision energy. The second stage is represented by the hadronization

process of the quark-antiquark pair into a physical quarkonium state, which happens at large distances (low energy scales/virtualities) and is accompanied by a complicated rearrangement of color via exchanges of soft gluons between the heavy quark-antiquark pair and other colored partons produced in the collision. At present, two approaches aimed to describe hadronization stage are most well-explored: the Non-Relativistic QCD factorization (NRQCD-factorization) [104] formalism and the (Improved-)Color-Evaporation Model (CEM) [105–114], see e.g. recent reviews [48–51].

Let us first discuss the conceptually simpler CEM. In this model, inspired by the idea of (local) quark-hadron duality, all color and angular-momentum states of $c\bar{c}$ -pair with invariant masses below the threshold of production of open-charmed meson pair contribute to the production of charmonium-state $\mathcal{H} = \eta_c, J/\psi, \chi_c$ with some constant probability $F_{\mathcal{H}}$, i.e. the ICEM cross-section is:

$$d\sigma(p + p \rightarrow \mathcal{H} + X) = F_{\mathcal{H}} \int_{m_{\mathcal{H}}}^{2m_D} dM_{c\bar{c}} \frac{d\sigma(p + p \rightarrow c + \bar{c} + X)}{dM_{c\bar{c}}}, \quad (3)$$

where the cross-section $d\sigma(p + p \rightarrow c + \bar{c} + X)$ can be computed to any order in QCD perturbation theory and particular lower-limit of integration $M_{c\bar{c}}^{(\min)} = m_{\mathcal{H}}$ corresponds to ICEM [110–112], while in traditional CEM [107–109] it has been set to $2m_c$. Also, due to $M_{c\bar{c}} \neq m_{\mathcal{H}}$, the three-momentum of $c\bar{c}$ -pair is different from the momentum of produced charmonium, which in some approximation incorporates effects of soft-gluon emissions at hadronisation stage. This recoil effect is usually [110, 113] taken into account using simple rescaling $\mathbf{p}_{\mathcal{H}} = \mathbf{p}_{c\bar{c}} \times m_{\mathcal{H}}/M_{c\bar{c}}$, which is the correct prescription in the limit $M_{c\bar{c}} - m_{\mathcal{H}} \ll m_{\mathcal{H}} \ll |\mathbf{p}_{\mathcal{H}}|$ and assuming isotropic gluon emission, while in some studies the soft-gluon recoil is neglected [111, 112]. Due to steep decrease of the p_T -spectra, this kind of small momentum shifts are important and may lead to $O(10\%)$ change of probabilities $F_{\mathcal{H}}$.

Despite its simplicity, the ICEM is remarkably successful in describing p_T -dependence of ratios of yields of different charmonium states [110], the general shape of p_T -spectra of prompt J/ψ and $\psi(2S)$ production at moderate transverse-momenta and even describes the unpolarized production of J/ψ at high- p_T in agreement with experimental data [112]. However the detailed shape of p_T spectra, in particular at large p_T , can not be reproduced in this model even at NLO in α_s for the short-distance cross-section $d\sigma(p + p \rightarrow c + \bar{c} + X)$, as it was shown in recent studies [114, 115]. Moreover, when the CEM is applied to the charmonium pair-production with hadronisation-probabilities, $F_{\mathcal{H}}$ fitted to the prompt single-production data, it underestimates the total and differential cross-sections in whole phase-space by up to two orders of magnitude [114]. A similar problem arises with the estimation of $e^+e^- \rightarrow J/\psi + c\bar{c}$ cross-section in CEM [48]. We will discuss implications of latter findings in the context of NRQCD factorization below.

The NRQCD-factorization framework is based on the Non-Relativistic QCD (NRQCD) effective field theory which consists in a systematic expansion of usual QCD Lagrangian in powers of squared velocity of constituent heavy-quarks in a bound state – v^2 . Simple potential-model estimates lead to $v^2 \simeq 0.3$ for charmonia and $\simeq 0.1$ for bottomonia (see e.g. Sec. A in Ref. [104]), so v^2 is assumed to be a good expansion parameter. The degrees of freedom of NRQCD are fields (field-operators) of non-relativistic quarks (annihilation-operator) $\psi(x)$ and anti-quarks (creation-operator) $\chi(x)$, as well as fields $A_{\mu}(x)$ of long-wavelength gluons with virtualities much smaller than m_c . All the effects caused by short-wavelength gluons and light-quarks are incorporated into matching-coefficients in front of local operators forming the NRQCD Lagrangian. The latter ones are perturbatively computable to any order in α_s . The production of $c\bar{c}$ -pair at short distance is also represented as a perturbative matching coefficient, while the subsequent evolution of a $c\bar{c}$ state into a quarkonium is described by Long-Distance Matrix-Elements (LDMEs) of local operators, constructed from the NRQCD fields $\psi(x)$, $\chi(x)$ and $A_{\mu}(x)$.

Inclusive heavy-quarkonium production cross-section depends on LDMEs of operators [104]:

$$\sum_X |\langle X + \mathcal{H} | \psi^\dagger(0) \kappa_i \chi(0) | 0 \rangle|^2 = \langle 0 | \mathcal{O}_i^{(\mathcal{H})}(0) | 0 \rangle = \langle \mathcal{O}_{\mathcal{H}}[i] \rangle, \quad (4)$$

where $\mathcal{O}_i^{(\mathcal{H})}(x) = \chi^\dagger(0) \kappa_i^\dagger \psi(0) a_{\mathcal{H}}^\dagger a_{\mathcal{H}} \psi^\dagger(0) \kappa_i \chi(0)$ with $a_{\mathcal{H}}^\dagger(a_{\mathcal{H}})$ being the creation(annihilation) operators for the physical state \mathcal{H} . The operators κ_i are polynomials in Pauli matrices, covariant derivatives and QCD field-strength tensors, which project out a particular color-singlet (CS,⁽¹⁾) or color-octet (CO,⁽⁸⁾) Fock-state of $c\bar{c}$ -pair $i = {}^{2S+1}L_J^{(1,8)}$ where the spectroscopic notation for spin – S and orbital-momentum – L has been used. To ensure the gauge-invariance of the LDMEs for color-octet states and the expected factorization properties of infra-red divergences in NRQCD perturbation theory, Wilson-line factors depending on $A_{\mu}(x)$ should be added [116, 117] to the operators $\mathcal{O}_i^{(\mathcal{H})}(x)$, making them non local. Further complications in the definition of NRQCD operators arise when more than one heavy-quarkonium state is considered in the final-state [118].

In contrast to Eq. (4), the inclusive decay rate of quarkonium \mathcal{H} depends on different kind of LDMEs:

$$\sum_X |\langle X | \chi^\dagger(0) \kappa_i^\dagger \psi(0) | \mathcal{H} \rangle|^2 = \langle 0 | a_{\mathcal{H}} \chi(0) \kappa_i \psi^\dagger(0) \chi^\dagger(0) \kappa_i^\dagger \psi(0) a_{\mathcal{H}}^\dagger | 0 \rangle, \quad (5)$$

which, for the case of color-octet states, cannot be related to LDMEs (4) without further approximations.

The velocity-scaling rules (VSRs) [104, 119] for LDMEs allow one to truncate to a desired order in v^2 the infinite tower of local NRQCD-operators which otherwise might contribute to the production of a state \mathcal{H} . As such, they are the cornerstone of phenomenological applications of NRQCD factorization. These scaling-rules assign specific scaling power in v to the NRQCD fields $\psi(x)$, $\chi(x)$, $A_\mu(x)$ and to the covariant-derivative $D_\mu = \partial_\mu + ig_s A_\mu(x)$ (see the Tab. 1 in Ref. [119]). The latter one is particularly important, because one factor of D enters into operator κ_i for each unit of orbital momentum L , leading to $(v^2)^L$ -suppression of LDMEs of states with high values of L . Another key ingredient of the derivation of VSRs for LDMEs is the v^2 -expansion for the physical quarkonium states, originating from the physical picture of non-relativistic bound-state in Coulomb gauge for gluon fields. The latter expansion e.g. for J/ψ has the form (see the discussion in Sec. D of Ref. [104]):

$$\begin{aligned} |J/\psi\rangle = a_{J/\psi}^\dagger |0\rangle &= O(1) \left[c\bar{c} \left[{}^3S_1^{(1)} \right] \right] + O(v) \left[c\bar{c} \left[{}^3P_J^{(8)} \right] g \right] \\ &+ O(v^{3/2}) \left[c\bar{c} \left[{}^1S_0^{(8)} \right] g \right] + O(v^2) \left[c\bar{c} \left[{}^3S_1^{(8)} \right] gg \right] + \dots, \end{aligned}$$

where, by $O(v^n)$, we denote the order of velocity-suppression of the corresponding Fock-state. Therefore, an additional v^2 suppression, besides the v^2 -factor coming from the structure of operators κ_i , comes in for decay-LDMEs (5) resulting into the intricate structure of v^2 -suppression for LDMEs with various labels i , shown in the Tab. 4. It is further assumed that production LDMEs (4) follow the same pattern of v^2 -suppression as the decay-LDMEs (5) and this assumption is supported by the results of higher-order perturbative calculations [116, 117]. The color-singlet LDMEs in the LO of v^2 -expansion are proportional to the modulus-squared of the radial part of the wave-function of potential model $-|R(0)|^2$ (or $|R'(0)|^2$ for P -wave states), thus connecting the NRQCD-factorization with the original *Color-Singlet Model* of heavy-quarkonium production [120]. The numerical smallness of color-octet LDMEs relatively to color-singlet also has been observed in global LDME-fits for charmonia [121–127] and bottomonia [128–131].

Table 4: Velocity-scaling rules for LDMEs [132] in the NRQCD-factorization formalism.

	${}^1S_0^{(1)}$	${}^3S_1^{(1)}$	${}^1S_0^{(8)}$	${}^3S_1^{(8)}$	${}^1P_1^{(1)}$	${}^3P_0^{(1)}$	${}^3P_1^{(1)}$	${}^3P_2^{(1)}$	${}^1P_1^{(8)}$	${}^3P_0^{(8)}$	${}^3P_1^{(8)}$	${}^3P_2^{(8)}$
η_c	1		v^4	v^3					v^4			
J/ψ		1	v^3	v^4						v^4	v^4	v^4
h_c			v^2		v^2							
χ_{c0}				v^2		v^2						
χ_{c1}				v^2			v^2					
χ_{c2}				v^2				v^2				

The description of detailed shapes of p_T spectra of prompt charmonia [121–124, 124–127] and bottomonia [128–130] with $p_T > 3 - 5$ GeV, produced in pp and $p\bar{p}$ collisions at Tevatron and LHC in the framework of global NRQCD fits at NLO in CPM is one of the main phenomenological achievements of NRQCD factorization so far. The global NLO fit [121–124] which attempts to describe charmonium production cross-section in e^+e^- , pp and ep collisions leads to the dominance of ${}^3S_1^{(8)}$ and ${}^3P_J^{(8)}$ states at $p_T \gg M_{J/\psi}$. At high- p_T the ${}^3S_1^{(8)}$ state is typically produced in a fragmentation of an almost on-shell gluon $g \rightarrow c\bar{c} \left[{}^3S_1^{(8)} \right]$, resulting into the predominantly-transverse polarization of this state in the helicity frame. The ${}^3P_{J=1,2}^{(8)}$ -states also give significant contribution to the transverse polarization of final quarkonium at NLO. There is no mechanism to de-polarize this states at leading-order in v , since the polarization is carried by heavy-quark spin, so the transverse polarization of produced quarkonium at high- p_T for those fits in which ${}^3S_1^{(8)}$ and ${}^3P_J^{(8)}$ -states dominate at high p_T is one of the most solid predictions of NRQCD.

Unfortunately, this prediction is by now clearly disfavored by experimental measurements of p_T dependence of charmonium [133] and bottomonium [134] polarization parameters at the LHC, see the Ref. [49] for a global survey of heavy-quarkonium polarization data. All experimental data are consistent with unpolarized production at high- p_T , with $\psi(2S)$ data even consistent with small longitudinal polarization, in contradiction with predictions of the fit [121–124]. On the other hand, if the consistency with unpolarized production is imposed, then agreement of the fit with e^+e^- and photo-production data is lost [123, 124]. In the literature, this situation is called “heavy-quarkonium polarization puzzle”.

Another prediction, based on the standard picture of VSRs in the NRQCD factorization is the relation between LDMEs of Fock states different by the flipping of the spin of a heavy-quark – the so-called Heavy-Quark Spin Symmetry (HQSS) relations, for example:

$$\begin{aligned}\langle \mathcal{O}^{\eta_c} [^1S_0^{(1/8)}] \rangle &= \frac{1}{3} \langle \mathcal{O}^{J/\psi} [^3S_1^{(1/8)}] \rangle + \mathcal{O}(v^5), \\ \langle \mathcal{O}^{\eta_c} [^3S_1^{(8)}] \rangle &= \langle \mathcal{O}^{J/\psi} [^1S_0^{(8)}] \rangle + \mathcal{O}(v^4), \\ \langle \mathcal{O}^{\eta_c} [^1P_1^{(8)}] \rangle &= 3 \langle \mathcal{O}^{J/\psi} [^3P_0^{(8)}] \rangle + \mathcal{O}(v^5), \\ \langle \mathcal{O}^{\eta_c} [^1P_1^{(1)}/^1S_0^{(8)}] \rangle &= 3 \langle \mathcal{O}^{v\epsilon_0} [^3P_0^{(1)}/^3S_1^{(8)}] \rangle + \mathcal{O}(v^3).\end{aligned}$$

These relations had been confronted with phenomenology in Ref. [135] by taking CO LDMEs from several available NRQCD-fits of J/ψ production, converting J/ψ LDMEs to η_c -ones and predicting the η_c transverse-momentum spectrum, which can be compared with the measurement by LHCb [136, 137]. The firm result of this investigation is, that LHCb data are perfectly compatible with predominantly direct production of η_c via CS $^1S_0^{(1)}$ -state. The feed-down from h_c has been found to be negligible and addition of CO-contributions leads to overestimation of high- p_T cross-section by more than order of magnitude above experimental data. This findings suggest the significant violation of VSRs for η_c LDMEs, since CO contributions for η_c are of the same order as for the J/ψ (Tab. 4) and corrections to the HQSS relations are of higher-order in v . Nevertheless, in Refs. [138, 139] it was shown that it is possible to improve the description of the J/ψ and η_c cross-sections as well as J/ψ -polarization in common LDME fits compatible with the HQSS-relations if one discards the data with $p_T < 7$ GeV from the fit. However, besides the fact that there is no explanation for such a high value of the p_T -threshold within the NRQCD-factorization formalism, tensions in the data description either remain or are newly introduced: The CS LDME values fitted in Ref. [138] differ from those obtained from potential models or decay widths, while the LDME fit of Ref. [139] still leads to significant transverse J/ψ polarization at higher p_T , see also related Ref. [140].

Comparing the CEM and NRQCD-factorization formalisms to each-other, one finds [132], that CEM can be understood as NRQCD-factorization without v^2 -suppression between S -wave CS and CO LDMEs. This suppression is characteristic for NRQCD, see Tab. 4. The absence of the suppression is also clearly disfavored by recent studies of J/ψ pair-production in NRQCD [141–143] and CEM [114]. These studies show that the bulk of the double- J/ψ cross-section is explained by double- $^3S_1^{(1)}$ CS-state production [144, 145], while the CEM prediction, dominated by CO states of $c\bar{c}$ -pair, fails to describe the data.

Concluding our mini-review of heavy-quarkonium production theory we emphasize, that neither CEM, nor NRQCD-factorization in its pure form can describe all available data on heavy-quarkonium production and polarization, and probably some hybrid of this two models should be constructed. Presently, the study of the heavy-quarkonium production mechanism is an active field of research, with new approaches, such as subleading-power fragmentation [146] and soft-gluon factorization [147–149], being proposed recently.

Due to the theoretical problems described above and multitude of competing theoretical approaches and models available on the market, our lack of quantitative understanding of the mechanism of hadronization of charm quarks into charmonium can become a source of significant theoretical uncertainties if charmonium production is to be used as a tool to study the proton structure. The Fig. 8 provides an insight on this situation at NICA SPD. In this figure, predictions of three models for the p_T spectra of J/ψ (Fig. 8(a)) and η_c mesons (Fig. 8(b)) are compared. Furthermore, in the Fig. 10, predictions for the p_T -dependence of the polarization parameter λ_θ in the \hat{s} -channel helicity frame are presented. The dashed curve with solid uncertainty bend in Fig. 8(a) represents the NLO calculation in collinear parton model (with LO being $\mathcal{O}(\alpha_s^3)$, see Fig. 4(a)) for the short-distance part of the cross-section matched to the NRQCD-factorization formalism for the long-distance part, with LDMEs of the latter tuned to charmonium production data in hadronic collisions, DIS and e^+e^- -annihilation [121–124]. For the prediction represented by solid histogram in the Fig. 8(a), the short-distance part of the cross-section is calculated in the LO ($\mathcal{O}(\alpha_s^2)$ for color-octet and P -wave contributions and $\mathcal{O}(\alpha_s^3)$ for color-singlet S -wave ones) of PRA [54], while LDMEs in this calculation had been fitted to the charmonium hadroproduction data from RHIC, Tevatron

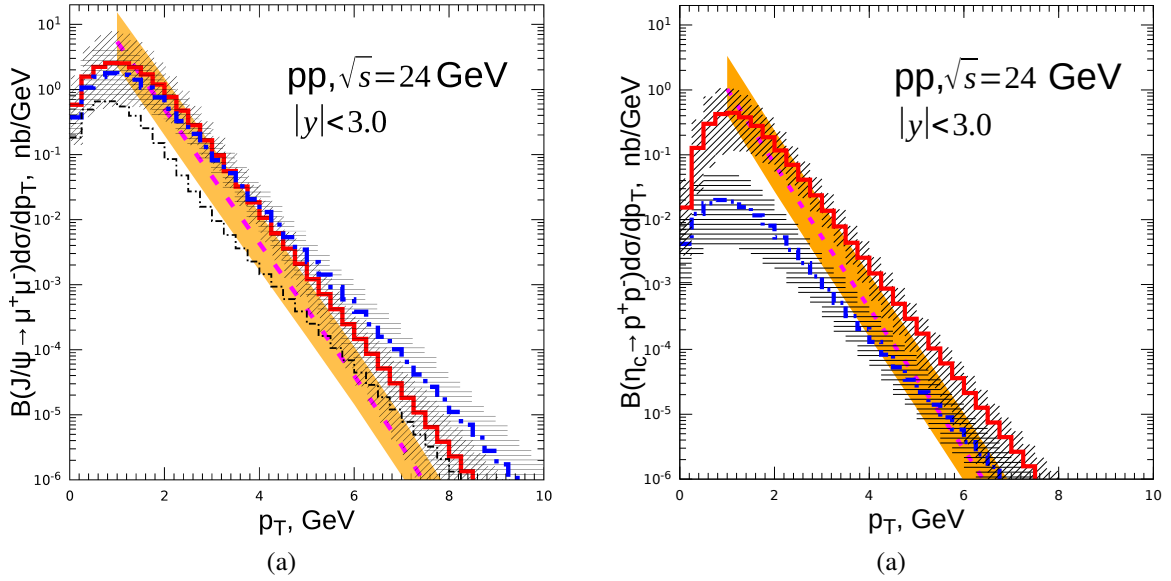


Figure 8: Theoretical predictions for the inclusive J/ψ p_T -spectrum (a) and the η_c p_T -spectrum (b) in various models: NLO of CPM + NRQCD-factorization (thick dashed line with solid uncertainty band) [121, 122], LO of PRA + NRQCD-factorization (thick solid histogram with diagonally-shaded uncertainty band) [150, 151], and LO PRA [54] + Improved Color Evaporation Model (thick dash-dotted histogram with horizontally-shaded uncertainty band) [112]. The contribution of the $q\bar{q}$ -annihilation channel to the central ICEM prediction is depicted by the thin dash-dotted histogram. Uncertainty bands are due to the factorization/renormalization scale variation only.

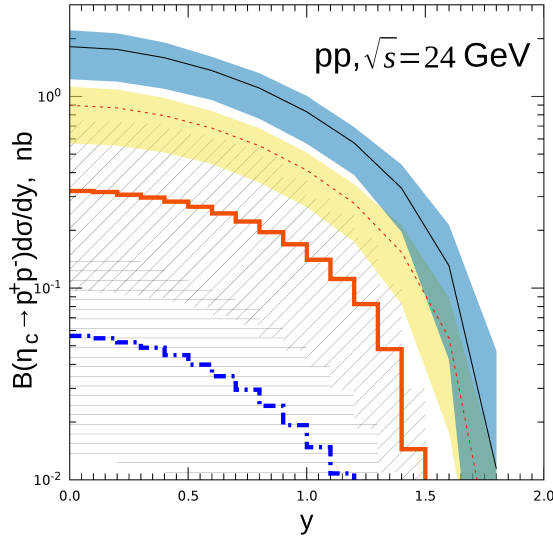


Figure 9: Theoretical predictions for the rapidity-differential cross-section of η_c -production. Thin dashed and solid lines – LO and NLO CPM + NRQCD predictions with optimized factorization-scale choice [152, 153], uncertainty bands – PDF and renormalization-scale uncertainties added in quadratures. Thick solid line – LO PRA + NRQCD, dash-dotted line – LO PRA + ICEM, full uncertainty bands. Last two predictions performed with the same model as predictions in the Fig. 8(b).

and LHC [150, 151]. The thick dash-dotted histogram is calculated in the LO ($O(\alpha_s^2)$) of PRA with the same unintegrated PDFs as for the LO PRA+NRQCD prediction, but interfaced with an improved Color-Evaporation Model (ICEM) of Ref. [112] for description of hadronization. Non-perturbative parameters of the ICEM had been taken from the Ref. [112] where they had been fitted to charmonium hadroproduction data at Tevatron and LHC energies. Predictions of all three models for the inclusive J/ψ p_T spectrum at NICA SPD appear to be consistent within their uncertainty bands, see Fig. 8(a). However, the structure of this predictions is significantly different, with NRQCD-based predictions being dominated by gluon-gluon fusion subprocess, while ICEM prediction containing significant contamination from $q\bar{q}$ -annihilation, shown with the thin dash-dotted histogram in the Fig. 8(a). The latter contribution reaches up to 50% at low $p_T < 1$ GeV and contributes up to 10% at higher $p_T > 3$ GeV.

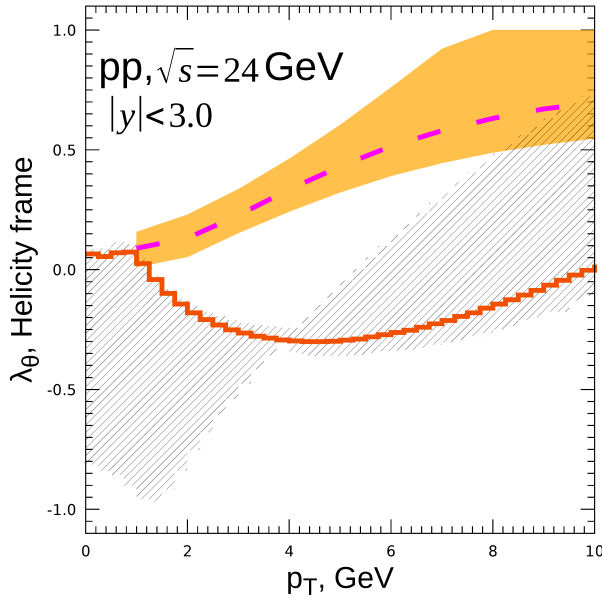


Figure 10: Theoretical predictions for the p_T -dependence of polarization parameter λ_θ in various models: NLO of Collinear Parton Model + NRQCD-factorization (dashed line with solid uncertainty band) [121, 122], LO of PRA + NRQCD-factorization (solid histogram with shaded uncertainty band) [150, 151]. Uncertainty bands are due to the factorization/renormalization scale variation and the variation of LDMEs within their fit-uncertainties.

Also ICEM tends to predict a significantly harder p_T spectrum at $p_T > 5$ GeV, than NRQCD-based PRA prediction which had been performed with the same unintegrated PDFs.

The above discussion shows that the J/ψ p_T -spectrum can be reliably predicted only in the limited range of transverse momenta, approximately from 3 to 6 GeV at $\sqrt{s} = 24$ GeV. At higher p_T the shape of the spectrum becomes highly model-dependent and at lower $p_T < M_{J/\psi}$ the TMD-factorization effects (including possible violation of factorization, see [154, 155]) come into the game and the contribution of $q\bar{q}$ -annihilation subprocess becomes uncertain. Nevertheless, predictions and measurements of the rapidity or x_F -differential cross-sections even in this limited p_T -range could help to further constrain the gluon PDF, e.g. to rule-out the extreme values of L in the $x \rightarrow 1$ asymptotic limit of the PDF $\sim (1-x)^L$.

In the Fig. 8(b), we perform a similar comparison of model-predictions for η_c -production at SPD-NICA. Taking into account results of Ref. [135] we include only CS $^1S_0^{(1)}$ -contribution to the NLO CPM and LO PRA NRQCD predictions and neglect the possible feed-down from h_c -meson decays. For comparison we also show the LO PRA ICEM prediction for η_c transverse-momentum spectrum, with $F_{\eta_c} = (1.8 \pm 0.8) \times 10^{-2}$ in Eq. (3) tuned to describe LHCb data [136] in the same model. The LO PRA and NLO CPM predictions again agree nicely with each-other, however ICEM-prediction has different slope and magnitude at SPD-NICA, while it describes the LHCb-data as well as the NRQCD prediction. This comparison shows, that studies of η_c -production at SPD-NICA will be instrumental for better understanding of its production mechanism. If the CS-dominated NRQCD-prediction turn out to be correct, then η_c production becomes a unique instrument to study the gluon content of the proton without introducing additional free-parameters, such as CO LDMEs, to the analysis.

Model predictions for rapidity-dependence of p_T -integrated cross-section are presented in the Fig. 9. Here the LO and NLO CPM NRQCD predictions are performed with the optimized value of factorization and renormalization scales: $\mu_R = \mu_F = m_{\eta_c} e^{-A_{\eta_c}}$ with $A_{\eta_c} = 1/2$ dictated by the high-energy behavior of NLO partonic cross-section. This particular scale-choice allows one to avoid the problem of negative NLO cross-sections at high energies [152, 153], however at NICA energies it leads to predictions for p_T -integrated η_c -yield significantly higher than predictions of other models. PRA predictions in the Fig. 9 are based on the same model as PRA predictions in the Fig. 8(b). The latter model allows one to calculate rapidity-differential cross-section, because PRA cross-section is finite in $p_T \rightarrow 0$ limit due to p_T -sparing from unintegrated gluon PDFs. We have used the same scale-choice $\mu_R = \mu_F = \sqrt{m_{\eta_c}^2 + p_T^2}$ (with $\langle p_T \rangle > 1$ GeV, see Fig. 8(b)) for PRA predictions in both Figs. 8(b) and 9. The PRA ICEM cross-section in the Fig. 9 is almost order of magnitude smaller than PRA NRQCD prediction, consistently with Fig. 8(b), thus even measurement of the total cross-section of η_c -production at SPD NICA will

allow to exclude ICEM for this state.

Predictions of NLO CPM and LO of PRA for J/ψ -polarization parameter λ_θ (see the Fig. 10) are significantly different, with PRA predicting mostly unpolarized production ($\lambda_\theta \simeq 0$) while CPM predicts transverse polarization ($\lambda_\theta = +1$) at high p_T . Disagreement of the predictions for polarization parameters mostly reflects the difference of LDMEs obtained in two fits and their large uncertainty bands are due to significant uncertainties of LDMEs. Measurements of heavy quarkonium polarization at NICA energies will provide additional constraints on models, however due to well-known problems with description of polarization at high energies [123, 124] constraints coming from the polarization measurements should be interpreted with great care and one should try to disentangle conclusions for gluon PDF from the results related to heavy quarkonium polarization.

3.3. TMD factorization with gluon probes

The description of hard processes which involve hadrons is based on factorization theorems. In particular, formulation of factorization theorems in terms of the TMD PDFs (see e.g. the monograph [156] or the review [6]) of quarks and gluons is the most important step towards studying the 3D structure of hadrons in momentum space and the nature of their spins.

The field of TMDs has taken a big step forward in the last years. Both the theoretical framework [68, 156–161], mainly focused on the proper definition of TMDs and their properties, and the phenomenological analyses (see e.g. these recent extractions [162–168]), have been developed, together with the appearance of new higher-order perturbative calculations (see e.g. [80, 169–174]). However this progress has mainly been done in the quark sector, due to the difficulty to cleanly probe gluons in high-energy processes.

Several processes have been proposed to access gluon TMDs in lepton-hadron collisions, like open charm production [175–177] and dijet or high- p_T charged dihadron production [178, 179]. However in hadron-hadron collisions the production of a color neutral final state is a must for the TMD factorization not to be broken by Glauber gluon exchanges [77, 180–184]. An example of a process which probes directly gluon TMDs in hadron-hadron collisions is the Higgs boson production [68, 80, 185–187]. However the extraction of gluon TMDs from its transverse momentum distribution is challenging due to the large mass of the boson and small available statistics. In other words, genuine non-perturbative TMD effects are somehow hidden in the spectrum and are thus difficult to constrain. All in all, quarkonium production processes seem to be the best tool at our disposal to probe gluon TMDs, and they have indeed attracted an increasing attention lately [17, 18, 20, 21, 73, 79, 154, 155, 175, 176, 188–200].

The NRQCD factorization formalism, which is briefly reviewed in Sec. 3.2, can only be applied for transverse momentum spectra when the quarkonium state is produced with a relatively large transverse momentum compared to its mass, i.e. $p_T \sim 2m_Q$, with m_Q the mass of the heavy quark. This is because the emissions of soft gluons from the heavy quark pair cannot modify the large transverse momentum of the bound state. The hard process generates this p_T , while the infrared divergences are parameterized in terms of the well-known long-distance matrix elements (LDMEs) and integrated PDFs.

On the contrary, when quarkonium states are produced with a small transverse momentum, soft gluons can no longer be factorized. Indeed, it was found that for quarkonium photo/lepto-production in the endpoint region [201–203], processes which are sensitive to soft radiation and where NRQCD approach fails, the LDMEs need to be promoted to shape functions [154, 155]. In the same way, in order to properly deal with soft gluon radiation at small p_T in a TMD spectrum of quarkonium production, it has recently been found that one needs to promote the LDMEs to the so-called TMD Shape Functions (TMDShFs) [154, 155], which encode the two soft mechanisms present in the process: the formation of the bound-state and soft gluon radiation.

As an example, let us consider the TMD factorization for single quarkonium \mathcal{H} production in hadronic collisions, with mass $m_{\mathcal{H}}$ and rapidity y , which reads

$$\frac{d\sigma}{dy dp_T} = \int \frac{d^2\mathbf{b}_\perp}{(2\pi)^2} e^{-i(\mathbf{p}_T \cdot \mathbf{b}_\perp)} \sum_{i \in \{^1S_0^{[1]}, \dots\}} H^{(i)}(m_{\mathcal{H}}, y, s; \mu) F_{g/A}(x_A, \mathbf{b}_\perp; \mu, \nu) F_{g/B}(x_B, \mathbf{b}_\perp; \mu, \nu) S_{\mathcal{H}}^{(i)}(\mathbf{b}_\perp, \mu, \nu) + O\left(\frac{p_T}{m_{\mathcal{H}}}\right), \quad (6)$$

where y is the quarkonium rapidity, $x_{A,B} = m_{\mathcal{H}} e^{\pm y} / \sqrt{s}$ are the longitudinal momentum fractions, $F_{g/A(B)}$ are the gluon TMD PDFs, $H^{(i)}$ are the process-dependent hard-scattering coefficients and $S_{\mathcal{H}}^{(i)}$ are the polarization-independent quarkonium TMDShFs (for more details see Refs. [154, 155]). μ and ν are the factorization/resummation and rapidity scales, respectively, \mathbf{b}_\perp is the Fourier conjugate of \mathbf{p}_T . The summation is performed over the various

colour and angular momentum configurations. Similarly to LDMEs, the TMDShFs scale with the relative velocity, v , of the heavy quark-antiquark pair in the quarkonium rest frame. Therefore, the factorisation formula is a simultaneous expansion in the relative quark-pair velocity v and $\lambda = p_T/m_H$.

The factorization theorem contains three or more non-perturbative hadronic quantities at low transverse momenta: gluon TMD PDFs and the TMDShFs. Thus, the phenomenological extraction of gluon TMDs from quarkonium production processes is still possible, i.e., a robust factorization theorem can potentially be obtained in any particular case of heavy meson production. However one also needs in principle to model and extract the involved TMDShFs.

Finally, a couple of open questions remain with regard to the factorization formula just discussed. On one hand, the double expansion in λ and v allows for, e.g., terms that are suppressed (i.e. sub-leading) in λ but at the same time are numerically important due to the enhancement in v . Although this double expansion introduces theoretical challenges, it is also an opportunity to observe the contributions to the cross-section from sub-leading factorization or from the terms with higher twist. On the other hand, Glauber gluon exchanges when summing over colour octet final-state channels can spoil the factorization (as in P -wave quarkonium production [204]). However this actually represents an opportunity to quantify these effects in QCD, which connect long and short distance physics. Both of these issues are present in studies of inclusive J/ψ and $\Upsilon(1S)$ production in hadronic colliders. Anyhow, the production of $\eta_{c/b}$ [154], with leading contribution from the channel $^1S_0^{[1]}$, could provide a clean channel for the study of quarkonium TMDShFs.

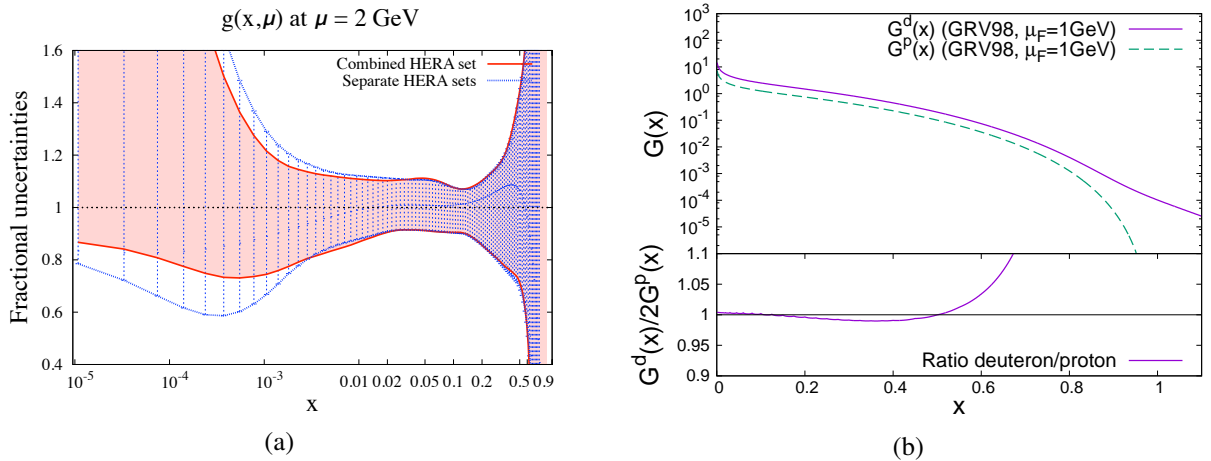


Figure 11: (a) Uncertainty of unpolarized gluon PDF based on HERA data ($\mu = 2$ GeV). Reprinted figure with permission from Ref. [205] © (2010) by the American Physical Society. (b) Comparison of the model-prediction for gluon PDF in the deuteron in comparison with the nucleon. Reprinted figure from [206] © (2018) by Elsevier.

3.4. Gluon content of the proton spin from Lattice QCD

There are at least two different ways to define the gluon content in the nucleon [207, 208]. One is defined in the light-cone frame with the light-cone gauge and the other is frame-independent. They are both measurable but from different experimental observables. They are associated with the two different decompositions of the proton spin and momentum in terms of the quark and gluon contributions that can be defined from the matrix elements of the QCD energy-momentum tensor. There are, in principle, infinitely-many ways to define this decomposition. A meaningful decomposition will depend on whether each component in the division can be measured experimentally. As far as lattice calculations are concerned, it would be desirable if the components can be defined by matrix elements of local operators.

The Jaffe-Manohar decomposition [207] is given as follows:

$$J = \frac{1}{2}\Delta\Sigma + L_q^{JM} + \Delta G + L_G, \quad (7)$$

where $\frac{1}{2}\Delta\Sigma$ (ΔG) is the quark (gluon) spin contribution, and L_q^{JM} (L_G) is the quark (gluon) Orbital Angular Momentum (OAM) contribution. Contributions $\Delta\Sigma$ and ΔG are related to the corresponding helicity-PDFs as $\Delta\Sigma = \int_0^1 dx g_1^q(x)$ and $\Delta G = \int_0^1 dx \Delta g(x)$. This is derived from the canonical energy-momentum tensor in the

infinite-momentum frame with $A^0 = 0$ gauge (or light-cone frame with $A^+ = 0$ gauge). Thus, this is superficially gauge-dependent. Furthermore, while ΔG can be extracted from high energy experiments, it had been thought that it cannot be obtained from a matrix element based on a local operator. This has posed a challenge for the lattice approach for many years.

The Ji decomposition [208] is:

$$J = \frac{1}{2}\Delta\Sigma + L_q^{Ji} + J_G, \quad (8)$$

where $\frac{1}{2}\Delta\Sigma$ is the same quark spin contribution as in Eq. (7), L_q^{Ji} is the quark OAM, and J_G is the gluon angular momentum contribution. This is derived from the energy-momentum tensor in the Belinfante form and each term in Eq. (8) is gauge invariant and can be calculated on the lattice with local operators in the finite momentum frame.

The intriguing difference between these two decompositions and their respective realization in experiments have perplexed the community for many years. The partonic picture of the gluon spin ΔG and OAM are naturally depicted in the light-front formalism with ΔG extracted from high energy pp collisions and OAM from GPDs and GTMDs. Unfortunately, the light-front coordinates are not accessible to lattice QCD calculation since the latter is based on Euclidean path-integral formulation. To bridge the gap between the light-front formulation and the lattice calculation, it was shown that the matrix elements of appropriate equal-time local operator, when boosted to the infinite momentum frame, is the same as those of the gauge-invariant but non-local operator on the light-cone. The proof was first carried out for the gluon spin ΔG [209]. It is also proven for the L_q^{JM} and L_G defined from the generalized transverse momentum distribution (GTMD) [210]. After the usual continuum extrapolation of the lattice results at large but finite momenta in the \overline{MS} scheme at μ , a large momentum effective field theory (LaMET) [209, 211, 212], which takes care of the non-commuting UV and $P_z \rightarrow \infty$ limits, is suggested to match the matrix elements of local operators to those of the non-local operators measured on the light-front.

It is instructive to have a comparison with QED at this point. Many years of experimental study of paraxial light beam on matter has been able to distinguish the different manifestation of the spin and OAM of the beam from the radiation-pressure force (a measure of OAM) and the torque (a measure of spin) on the probed dipole particle [213]. The separation of spin and OAM is based on the canonical energy-momentum tensor in the physical Coulomb gauge. As we learned before, this separation is frame-dependent. Since the light is always in the light-front frame, it is the natural frame to define the spin and OAM of the optical beam. Likewise, boosting the proton to the infinite momentum frame makes the gluons in the proton behave like the photons in the light beam. The transverse size of the proton, like the width of the light beam, admits the existence of OAM of the gluon in the proton. Recently, the experimental evidence for non-zero gluon helicity in the proton Δg was found, see the Sec. 5.1 of this review for detailed discussion and references. These experimental results support the interest in theoretical calculations of gluon contributions to the proton spin.

Following the suggestion of calculating ΔG on the lattice as discussed above, a lattice calculation is carried out with the local operator $S_G = \int d^3x Tr(\mathbf{E} \times \mathbf{A}_{phys})$, where \mathbf{A}_{phys} transforms covariantly under the gauge transformation and satisfies the non-Abelian transverse condition, $D\mathbf{A}_{phys} = 0$ [214]. Thus S_G is gauge invariant. It is shown on the lattice [210] that A_{phys}^i is related to A_c^i in the Coulomb gauge via the gauge transformation, i.e. $A_{phys}^\mu(x) = g_c(x)A_c^\mu g_c^{-1}(x) + \mathcal{O}(a)$, where g_c is the gauge transformation which fixes the Coulomb gauge. As a result, the gluon spin operator

$$S_G = \int d^3x Tr(\mathbf{E} \times \mathbf{A}_{phys}) = \int d^3x Tr(\mathbf{E}_c \times \mathbf{A}_c) \quad (9)$$

can be calculated with both \mathbf{E} and \mathbf{A} in the Coulomb gauge. A lattice calculation with the overlap fermion action is carried out on 5 lattices with 4 lattice spacings and several sea quark masses including one corresponding to the physical pion mass. The result, when extrapolated to the infinite momentum limit, gives $\Delta G = 0.251(47)(16)$ [215] which suggests that the gluon spin contribute about half of the proton spin. However, there is a caveat. It was found that the finite piece in the one-loop large momentum effective theory (LaMET) matching coefficient is very large which indicates a convergence problem for the perturbative series even after one re-sums the large logarithms. Due to above-mentioned perturbative instability of the matching coefficient, the LaMET matching at current stage is not applicable. In this sense, the gluon helicity calculation on the lattice is not completed.

Another approach is to calculate the polarized gluon distribution function $\Delta g(x)$ through the quasi-PDF approach [219] and then take the first moment to obtain ΔG .

To summarize existing LQCD studies regarding the gluon angular momentum contribution to the proton spin (J_G in Eq. (8)) we list obtained values of J_G in Table 5. Also momentum fraction ($\langle x \rangle_g$ or $T_1(0)$) has been calculated; whereas, the gluon angular momenta are the sum of $T_1(0)$ and $T_2(0)$, the anomalous gravitomagnetic moment. In other words, $J_g = 1/2(T_1(0) + T_2(0))$ [208]. We also show the percentage of the J_G contribution to proton spin

Table 5: Values of J_g from different lattice studies.

Pub.	Lattice action	J_g	Scale (Q^2)
[216]	Quenched Fermionic action	28(8)%	4 GeV ²
[217]	2-flavor Twisted-mass (+clover term) at physical pion mass	27(3)%	4 GeV ²
Preliminary [218]	(2+1)-flavor overlap fermion on Domain Wall sea fermion at 400 MeV pion mass	39(10)%	4 GeV ²

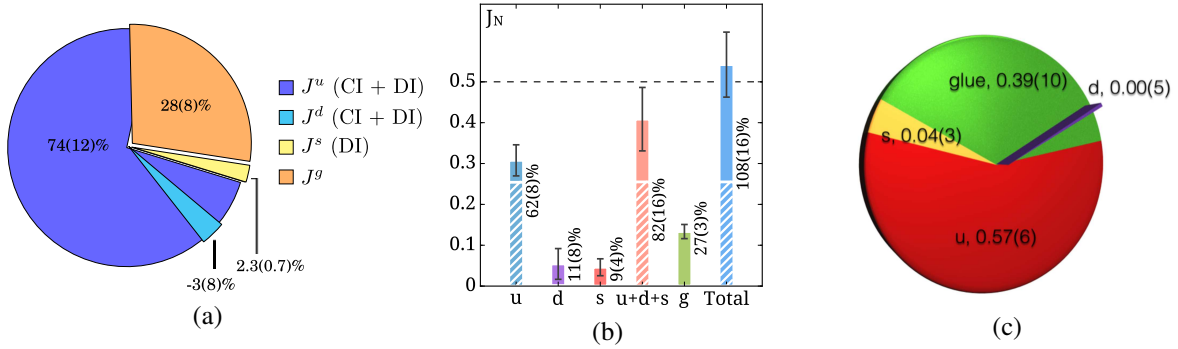


Figure 12: The angular momentum fractions from the quenched clover calculation (a), 2 flavor Twisted-mass (+clover term) fermion calculation at physical pion mass (b), and the non-perturbative renormalized 2+1 flavor overlap fermion on Domain Wall sea with 400 MeV pion mass (c). See Refs. [216–218]. Reprinted figures with permission from Refs. [216, 217] © (2015, 2017) by the American Physical Society.

together with the quark contributions in Fig. 12. It is worth emphasizing again that both $\langle x \rangle_g$ and J_g are gauge invariant.

An exploratory LQCD study of the gluonic structure of the ϕ meson is presented in Ref. [220] that sets the stage for more complex studies of gluonic structure in light nuclei with an exotic gluon.

4. Gluon content of unpolarized proton and deuteron

4.1. Gluons at large x and perturbative QCD

The available data constrain weakly the gluon distribution function in the proton, $g(x, \mu_F)$ ⁴, for x greater than 0.5 [221, 222]. In the high- x region, the gluon density is usually parameterized as $g(x, \mu_F) \sim (1-x)^L$, and values of L extracted from global fits differ considerably from each other. In particular, obtained results for L vary from 3 to 11 at $\mu_F^2 = 1.9 \text{ GeV}^2$ [223]. In Fig. 13(a), the NLO gluon densities from the CT14, MSTW2008 and HERAPDF20 sets of PDFs are compared. One can see sizable difference between these predictions for large x . Note also that the uncertainty bands resulting from the PDF fits are quite large in the region $x > 0.5$, see e.g. Fig. 11(a).

To improve the situation with large x , one needs precise data on the heavy flavor production at energies not so far from the production threshold. Concerning the open charm production in pp collisions, the corresponding cross-sections are poorly known for $\sqrt{s} < 27 \text{ GeV}$ [224, 225].⁵ In this region, only three hundred events on D meson production in pA collisions are presently available [224]. Unfortunately, these results have large uncertainties, and we can only estimate the order of magnitude of the $pp \rightarrow c\bar{c}X$ cross-section at $\sqrt{s} \approx 20 \text{ GeV}$. For this reason, future studies of the open charm production at SPD in pp , pd and dd collisions for $\sqrt{s} \leq 27 \text{ GeV}$ are of special interest. In particular, they will allow to reduce significantly the present uncertainties in the gluon density (as well as in α_s and c -quark mass, m_c) at a GeV scale, especially for high x .

⁴Which is also referred to as $f^g(x, \mu)$

⁵On the contrary, the J/ψ production cross-section is known well enough practically down to the threshold, see Fig. 3.

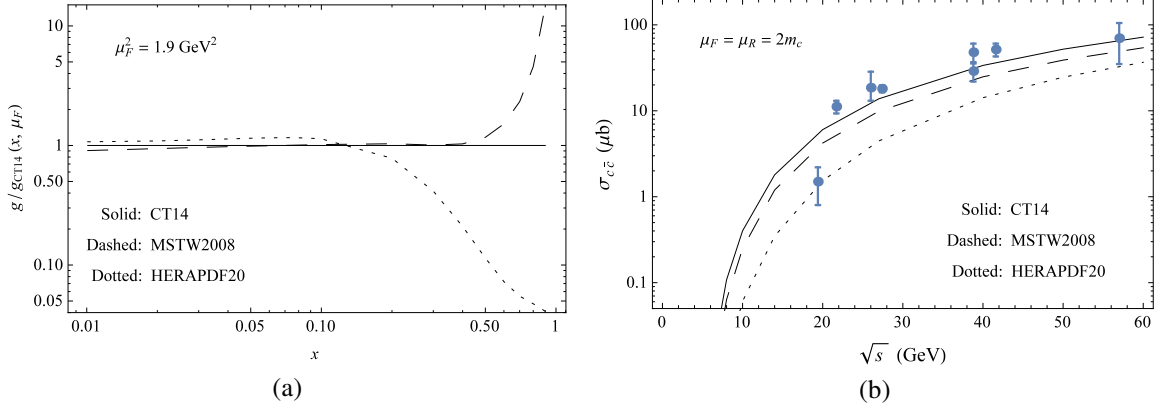


Figure 13: (a) Ratios of the NLO MSTW2008 and HERAPDF20 predictions for the gluon density to the CT14 ones, $g/g_{CT14}(x, \mu_F)$, at $\mu_F^2 = 1.9$ GeV². (b) NLO QCD predictions for the total $pp \rightarrow c\bar{c}X$ cross-section as a function of \sqrt{s} using CT14, MSTW2008 and HERAPDF20 sets of PDFs at $\mu_F = \mu_R = 2m_c$.

In the framework of pQCD, the inclusive $pp \rightarrow Q\bar{Q}X$ cross-section can be written as

$$\sigma_{Q\bar{Q}}(\rho_h) = \sum_{ij} \int_{\rho_h}^1 \frac{dz}{z} \mathcal{L}^{ij}(z, \mu_F) \hat{\sigma}_{ij}(\rho_h/z, \mu_F, \mu_R), \quad (10)$$

$$\mathcal{L}^{ij}(z, \mu_F) = z \int_0^1 dx_1 \int_0^1 dx_2 f^i(x_1, \mu_F) f^j(x_2, \mu_F) \delta(x_1 x_2 - z), \quad (11)$$

where i, j run over all the initial state partons, $\rho_h = 4m^2/s$, m is the heavy-quark mass, μ_R and μ_F are the renormalization and factorization scales, while $f^i(x, \mu_F)$ describes the parton i density in the proton ($i = g, q, \bar{q}$). The partonic total cross-sections, $\hat{\sigma}_{ij}(\rho)$ with $\rho = 4m^2/\hat{s}$ and $\hat{s} = (p_i + p_j)^2 = x_1 x_2 s$, are expanded in $\alpha_s \equiv \alpha_s(\mu_R)$ as follows:

$$\hat{\sigma}_{ij}(\rho, \mu_F, \mu_R) = \frac{\alpha_s^2}{m^2} \left\{ f_{ij}^{(0)}(\rho) + \alpha_s \left[f_{ij}^{(1)}(\rho) + f_{ij}^{(1,1)}(\rho) \ln(\mu_F^2/m^2) \right] \right. \\ \left. + \alpha_s^2 \left[f_{ij}^{(2)}(\rho) + f_{ij}^{(2,1)}(\rho) \ln(\mu_F^2/m^2) + f_{ij}^{(2,2)}(\rho) \ln^2(\mu_F^2/m^2) \right] + \mathcal{O}(\alpha_s^3) \right\}. \quad (12)$$

Main partonic subprocesses of the heavy flavor production are: gluon fusion, $gg \rightarrow Q\bar{Q}X$, $q\bar{q}$ -annihilation, $q\bar{q} \rightarrow Q\bar{Q}X$, and quark-gluon fusion, $qg \rightarrow Q\bar{Q}X$. Presently, the total cross-sections of these processes are known to NNLO in QCD, $\mathcal{O}(\alpha_s^4)$, see Refs. [226–228].⁶ The NLO results for $\hat{\sigma}_{gg}$, $\hat{\sigma}_{q\bar{q}}$ and $\hat{\sigma}_{qg}$ are presented in Ref. [229]. At LO in α_s , the gluon fusion and $q\bar{q}$ -annihilation only contribute:

$$f_{gg}^{(0)}(\rho) = \frac{\pi\rho\beta}{192} \left[\frac{1}{\beta}(\rho^2 + 16\rho + 16) \ln\left(\frac{1+\beta}{1-\beta}\right) - 28 - 31\rho \right], \quad f_{q\bar{q}}^{(0)}(\rho) = \frac{\pi\rho\beta}{27}(2 + \rho), \quad f_{qg}^{(0)}(\rho) = 0, \quad (13)$$

where $\beta = \sqrt{1 - \rho}$.

Due to relatively low c -quark mass, the charm production cross-sections are usually calculated within pQCD at $\mu_F = \mu_R = 2m_c$. Such a choice makes it possible to improve convergence of the perturbative series for $\sigma_{c\bar{c}}$. Unfortunately, the NNLO predictions for the key gluon fusion process are presently available only for the case of $\mu_F = m$, i.e. the dimensionless coefficients $f_{gg}^{(2,1)}$ and $f_{gg}^{(2,2)}$ are unknown [228]. At the same time, it is well known that the cross-section $\sigma_{c\bar{c}}$ is very sensitive to the choice of the factorization scale in the region of a few GeV. For this reason, although the NNLO predictions [226–228] are successfully used in the top quark phenomenology, applicability of these results for description of the charm production is presently questionable. So, we restrict ourselves by consideration of the NLO approximation only.

⁶At NNLO, three more fermion-pair-initiated partonic channels contribute to heavy flavor production: $qq \rightarrow Q\bar{Q}X$, $qq' \rightarrow Q\bar{Q}X$ and $\bar{q}\bar{q}' \rightarrow Q\bar{Q}X$ with $q' \neq q$. However, these contributions are usually ignored due to their numerically negligible sizes.

In Fig. 13(b), the NLO QCD predictions for the total $pp \rightarrow c\bar{c}X$ cross-section are shown as a function of \sqrt{s} using the CT14, MSTW2008 and HERAPDF20 sets of PDFs at $\mu_F = \mu_R = 2m_c$. The experimental data are taken from Ref. [224].⁷ We see essential differences between these predictions, especially at low energies. These differences are due not only to the different threshold behavior of the PDF sets we compare. Main source of these uncertainties are different values of the c -quark mass used in various analyses of the world data. In particular, the mass m_c varies from 1.3 GeV to 1.47 GeV in the PDF sets presented in Fig. 13(b).⁸ On the other hand, the quantities $\alpha_s(\mu_R)$ and $g(x, \mu_F)$ are very sensitive to the values of μ_R and μ_F at a GeV scale. As a result, the pQCD predictions for $\sigma_{c\bar{c}}$ are crucially dependent on the value of c -quark mass in use. Therefore future precise data on the total cross-section $\sigma_{c\bar{c}}$ from NICA SPD should reduce uncertainties in the c -quark mass and improve essentially description of the processes with charm production within pQCD.

To probe the PDFs at high x , one needs to measure the differential cross-sections of the charmed particle production in sufficiently wide region. In particular, the invariant mass of the $c\bar{c}$ pair, $M_{c\bar{c}}^2 = (p_c + p_{\bar{c}})^2$, should be large enough because $M_{c\bar{c}}^2/s < x_1 x_2 < 1$ for x_1 and x_2 in Eq. (11). Therefore to scan high values of x , we need $M_{c\bar{c}}^2/s \sim x$.

Detailed information on the gluon distribution at large x is very important for various phenomenological applications. For instance, it is of current interest to estimate the $b\bar{b}$ pair production cross-section at NICA energies. Such predictions are however presently unreliable due to their strong dependence on the exponent L which is poorly known. Likewise, the threshold behavior of PDFs could be useful in search for various heavy particles beyond the Standard Model. Another example is the DGLAP evolution of the PDFs. Using precise data on $g(x, \mu_F)$ (and α_s) at $\mu_F \sim 2m_c$ as boundary conditions in DGLAP equations, one could reduce essentially the uncertainties in evolution of PDFs for higher values of μ_F .

From the theoretical point of view, the threshold behavior of cross-sections is closely related to the so-called infrared renormalon problem. It is well known that radiative corrections to the production cross-sections contain mass (or threshold) logarithms whose contribution is expected to be sizable near the threshold. These logarithms are usually taken into account within the soft gluon resummation formalism [231–235]. Formally resummed cross-sections are however ill-defined due to the Landau pole contribution, and few prescriptions have been proposed to avoid the renormalon ambiguities [236–239]. Unfortunately, numerical predictions for heavy quark production cross-sections can depend significantly on the choice of resummation prescription. Undoubtedly, anticipated data from SPD on the charm production not so far from the production threshold could clarify the role of soft gluon resummation in the description of heavy flavor production.

Another interesting problem for NICA SPD is to probe the intrinsic charm (IC) content of the proton [240, 241]. The IC contribution to open charm production is expected to be sizable near the threshold because its PDF, $c(x, \mu_F)$, is predicted to be harder than the gluonic one. As a result, the IC density in the proton can be dominant at sufficiently large x independently of its overall normalization [242]. To visualize the IC component, one needs to collect enough events like $D\bar{D}$ pair produced in $pp \rightarrow D\bar{D}$ with a large overall x_F . That events are predicted to be very rare within the GF mechanism and would directly indicate the five-quark component in the proton, $|uudc\bar{c}\rangle$.

Investigation of the open charm production in pp , pd and dd collisions might be one of the key points in the NICA SPD program. The motivation is twofold. On the one hand, production of D -mesons in pp collisions is practically unmeasured at NICA energies. On the other hand, these presently unavailable data on open charm production rates are strongly necessary for determination of the gluon density $g(x, \mu_F)$ at large x where this PDF is practically unknown. Future SPD measurements should also reduce uncertainties in the charm quark mass m_c and α_s at a GeV scale.

Moreover, anticipated results on the open charm production are very important for many other current issues in particle physics: from infrared renormalon ambiguities in cross-sections to intrinsic charm content of the proton.

4.2. Linearly polarized gluons in unpolarized nucleon

4.2.1. Parton-hadron correlators and TMD distribution functions

Search for the polarized quarks and gluons in unpolarized hadrons is of special interest in studies of the spin-orbit couplings of partons and understanding of the proton spin decomposition. The corresponding intrinsic transverse momentum dependent distributions of the transversely polarized quarks, $h_1^{1q}(x, \mathbf{k}_T^2)$, and linearly polarized

⁷Note that $\sigma_{D\bar{D}} = (0.78 \pm 0.03) \sigma_{c\bar{c}}$. For more details, see e.g. [224] and references therein.

⁸In the recent edition of the Review of Particle Physics [230], the following value for the c -quark $\overline{\text{MS}}$ mass is presented: $m_c = 1.27 \pm 0.02$ GeV.

gluons, $h_1^{\perp g}(x, \mathbf{k}_T^2)$, in an unpolarized nucleon have been introduced in Refs. [3] and [61]. Unfortunately, both these functions are presently unmeasured.

Information about parton densities in unpolarized nucleon is formally encoded in corresponding TMD parton correlators. The parton correlators describe the nucleon \rightarrow parton transitions and are defined as matrix elements on the light-front (LF) (i.e., $\lambda^+ = \lambda \cdot n = n^2 = 0$, where n is a light-like vector conjugate to the nucleon momentum, $P \cdot n = 1$). At leading twist and omitting process-dependent gauge links that ensure gauge invariance, the quark correlator is given by [3, 72]

$$\begin{aligned}\Phi_q(x, \mathbf{k}_T) &= \int \frac{d(P \cdot \lambda) d^2 \lambda_T}{(2\pi)^3} e^{ik \cdot \lambda} \langle P | \bar{\psi}(0) \psi(\lambda) | P \rangle_{\text{LF}} \\ &= \frac{1}{2} \left\{ f_1^q(x, \mathbf{k}_T^2) \hat{P} + i h_1^{\perp q}(x, \mathbf{k}_T^2) \frac{[\hat{k}_T, \hat{P}]}{2m_N} \right\},\end{aligned}\quad (14)$$

where m_N and $k = xP + k_T + k^- n$ are the nucleon mass and parton momentum, respectively. $f_1^q(x, \mathbf{k}_T^2)$ denotes the TMD distribution of unpolarized quarks inside unpolarized nucleon. Its integration over \mathbf{k}_T reproduces the well-known collinear momentum distribution, $\int d^2 \mathbf{k}_T f_1^q(x, \mathbf{k}_T^2) = q(x)$. The function $h_1^{\perp q}(x, \mathbf{k}_T^2)$, referred to as Boer-Mulders PDF, is time-reversal (T-) odd and describes the distribution of transversely polarized quarks inside an unpolarized nucleon. Similarly, for an antiquark correlator we have:

$$\begin{aligned}\Phi_{\bar{q}}(x, \mathbf{k}_T) &= - \int \frac{d(P \cdot \lambda) d^2 \lambda_T}{(2\pi)^3} e^{-ik \cdot \lambda} \langle P | \bar{\psi}(0) \psi(\lambda) | P \rangle_{\text{LF}} \\ &= \frac{1}{2} \left\{ f_1^{\bar{q}}(x, \mathbf{k}_T^2) \hat{P} + i h_1^{\perp \bar{q}}(x, \mathbf{k}_T^2) \frac{[\hat{k}_T, \hat{P}]}{2m_N} \right\}.\end{aligned}\quad (15)$$

Omitting process-dependent gauge links, the gluon-nucleon correlator has the form [61]:

$$\begin{aligned}\Phi_g^{\mu\nu}(x, \mathbf{k}_T) &= \frac{n_\rho n_\sigma}{(P \cdot n)^2} \int \frac{d(P \cdot \lambda) d^2 \lambda_T}{(2\pi)^3} e^{ik \cdot \lambda} \langle P | \text{Tr}[F^{\rho\mu}(0) F^{\sigma\nu}(\lambda)] | P \rangle_{\text{LF}} \\ &= \frac{x}{2} \left\{ -g_T^{\mu\nu} f_1^g(x, \mathbf{k}_T^2) + \left(g_T^{\mu\nu} - 2 \frac{k_T^\mu k_T^\nu}{k_T^2} \right) \frac{k_T^2}{2m_N^2} h_1^{\perp g}(x, \mathbf{k}_T^2) \right\},\end{aligned}\quad (16)$$

with the gluon field strength $F_a^{\mu\nu}(x)$ and a transverse metric tensor $g_T^{\mu\nu} = g^{\mu\nu} - \frac{P^\mu n^\nu + P^\nu n^\mu}{P \cdot n}$.

The TMD PDF $f_1^g(x, \mathbf{k}_T^2)$ describes the distribution of unpolarized gluons inside an unpolarized nucleon, and, integrated over \mathbf{k}_T , gives the familiar gluon density, $\int d^2 \mathbf{k}_T f_1^g(x, \mathbf{k}_T^2) = g(x)$. The distribution $h_1^{\perp g}(x, \mathbf{k}_T^2)$ is gluonic counterpart of the Boer–Mulders function; it describes the linear polarization of gluons inside unpolarized nucleon. The degree of their linear polarization is determined by the quantity $r = \frac{k_T^2 h_1^{\perp g}}{2m_N^2 f_1^g}$. In particular, the gluons are completely polarized along the \mathbf{k}_T direction at $r = 1$. Note also that the TMD densities under consideration have to satisfy the positivity bound [61]:

$$\frac{k_T^2}{2m_N^2} |h_1^{\perp g}(x, \mathbf{k}_T^2)| \leq f_1^g(x, \mathbf{k}_T^2).\quad (17)$$

To probe the TMD distributions, the momenta of both heavy quark and anti-quark, \mathbf{p}_Q and $\mathbf{p}_{\bar{Q}}$, should be measured (reconstructed). For further analysis, the sum and difference of the transverse heavy quark momenta are introduced,

$$\mathbf{K}_\perp = \frac{1}{2} (\mathbf{p}_{Q\perp} - \mathbf{p}_{\bar{Q}\perp}), \quad \mathbf{q}_T = \mathbf{p}_{Q\perp} + \mathbf{p}_{\bar{Q}\perp},\quad (18)$$

in the plane orthogonal to the collision axis. The azimuthal angles of \mathbf{K}_\perp and \mathbf{q}_T are denoted by ϕ_\perp and ϕ_T , respectively.

4.2.2. Probing the density $h_1^{\perp g}$ with heavy flavor production

Contrary to its quark version, the TMD density $h_1^{\perp g}$ is T- and chiral-even, and thus can directly be probed in certain experiments. Azimuthal correlations in heavy-quark pair production in unpolarized ep and pp collisions as probes of the linearly polarized gluons have been considered in Refs. [69, 72]. For the case of DIS, the complete angular structure of the pair production cross-section has been obtained in terms of seven azimuthal modulations

containing the angles ϕ_\perp and ϕ_T . However, in the considered kinematics, only two of these modulations are really independent; they can be chosen as the $\cos \varphi$ and $\cos 2\varphi$ distributions, where φ is the heavy quark azimuthal angle [243]. Integrating over the anti-quark azimuth, the following result for the reaction $l(\ell) + N(P) \rightarrow l'(\ell - q) + Q(p_Q) + \bar{Q}(p_{\bar{Q}}) + X$ was obtained:

$$d\sigma_{lp} \propto [1 + (1 - y)^2] d\sigma_2 - y^2 d\sigma_L + 2(1 - y) d\sigma_A \cos 2\varphi + (2 - y) \sqrt{1 - y} d\sigma_I \cos \varphi, \quad (19)$$

where $\sigma_2 = \sigma_T + \sigma_L$, x, y, Q^2 are usual Bjorken variables, m is the heavy-quark mass and $z = \frac{p_Q \cdot P}{q \cdot P}$. The contributions of the linearly polarized gluons to $d\sigma_i$ ($i = 2, L, A, I$) were analyzed in Refs. [244, 245].

First, the LO predictions for the azimuthal asymmetries ($A_{\cos \varphi} = d\sigma_I/d\sigma_2$ and $A_{\cos 2\varphi} = d\sigma_A/d\sigma_2$) and Callan-Gross ratio ($R = d\sigma_L/d\sigma_T$) were discussed in the case when the unpolarized gluons only contribute, i.e. for $r = \frac{q_T^2 h_1^{\perp g}}{2m_N^2 f_1^g} = 0$. It was shown that the maximal values of these quantities allowed by the photon-gluon fusion with unpolarized initial gluons are sizable: $A_{\cos 2\varphi} \leq 1/3$, $|A_{\cos \varphi}| \leq (\sqrt{3} - 1)/2 \simeq 0.366$ and $R \leq \frac{2}{1+12\lambda}$ with $\lambda = m^2/Q^2$. Then the contributions of the linearly polarized gluons to the above distributions were considered. As shown in Refs. [244, 245], the maximal values of the discussed quantities, $A_{\cos 2\varphi}^h$, $A_{\cos \varphi}^h$ and R^h , are very sensitive to the gluon density $h_1^{\perp g}$. In particular, $A_{\cos 2\varphi}^h(r) = \frac{1+r}{3-r}$ and $R^h(r) = \frac{2(1-r)}{1+r+4\lambda(3-r)}$. The functions $A_{\cos 2\varphi}^h(r)$ and $R^h(r)$ are depicted in Figs. 14(a) and 14(b) where their strong dependence on r is seen. Note also an unlimited growth of the Callan-Gross ratio with Q^2 at $r \rightarrow -1$. This is because the transverse cross-section, $d\sigma_T$, vanishes at high Q^2 for $r \rightarrow -1$.

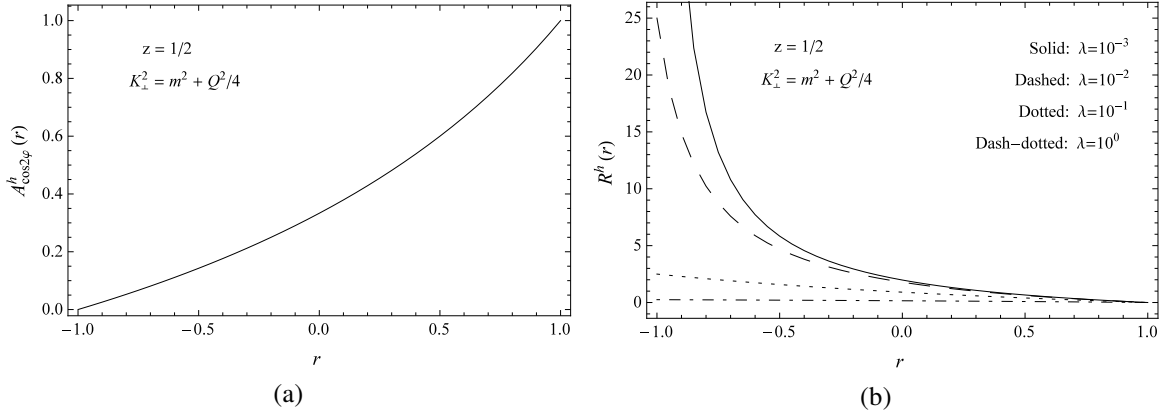


Figure 14: (a) Maximum value of the $\cos 2\varphi$ asymmetry with the contribution of linearly polarized gluons, $A_{\cos 2\varphi}^h(r)$, as a function of r . (b) Maximum value of the Callan-Gross ratio, $R^h(r)$, with the contribution of linearly polarized gluons as a function of r . The figures are reprinted from Refs. [244, 245] © (2018) by Elsevier.

So, we see that the azimuthal distributions and Callan-Gross ratio in heavy-quark leptonproduction are predicted to be large and very sensitive to the gluon density $h_1^{\perp g}$. Taking into account that the $\cos 2\varphi$ asymmetry and Callan-Gross ratio are well defined in pQCD (they are stable both perturbatively and parametrically [246, 247]), one can conclude that the considered quantities could be good probes of the linearly polarized gluons in unpolarized proton.

4.2.3. Azimuthal distributions in heavy-quark hadroproduction

In this Section, we discuss the contributions of the gluon density $h_1^{\perp g}$ to the azimuthal modulations anticipated in the charm quark pair production in pp collisions at NICA SPD. Main goal is to estimate the upper bounds of theoretical expectations for these azimuthal distributions. In our analysis, the effects of initial and final state interactions (and, correspondingly, the problems with factorization) are ignored.⁹ We expect that (possible) factorization breaking contributions are not able to affect essentially the parton model predictions for the order of magnitudes of the azimuthal asymmetries under consideration.

The angular structure of the $p(P_1) + p(P_2) \rightarrow Q(p_Q) + \bar{Q}(p_{\bar{Q}}) + X$ cross-section has the following form [69, 72]:

$$d\sigma_{pp} \propto A(\mathbf{q}_T^2) + B(\mathbf{q}_T^2) \mathbf{q}_T^2 \cos 2(\phi_\perp - \phi_T) + C(\mathbf{q}_T^2) \mathbf{q}_T^4 \cos 4(\phi_\perp - \phi_T). \quad (20)$$

⁹For the details related to TMD factorization, see Sec. 3.3.

Besides \mathbf{q}_T^2 , the terms A , B and C depend on other kinematic variables not explicitly shown: $\mathbf{K}_\perp = \frac{1}{2}(\mathbf{p}_{Q\perp} - \mathbf{p}_{\bar{Q}\perp})$ and $M_{Q\bar{Q}}^2 = (p_Q + p_{\bar{Q}})^2$. At LO in pQCD, $\mathcal{O}(\alpha_s^2)$, the quantities A and B are given by the sum of the gluon fusion, $gg \rightarrow Q\bar{Q}$, and $q\bar{q}$ -annihilation, $q\bar{q} \rightarrow Q\bar{Q}$, subprocesses: $A = A^{g\bar{g}} + A^{q\bar{q}}$ and $B = B^{g\bar{g}} + B^{q\bar{q}}$. In particular,

$$\begin{aligned} A^{q\bar{q}} &= A_0 \left(z, \frac{m^2}{m_\perp^2} \right) \left\{ C [f_1^q f_1^{\bar{q}}] + C [f_1^{\bar{q}} f_1^q] \right\}, \\ A^{g\bar{g}} &= A_1 \left(z, \frac{m^2}{m_\perp^2} \right) C [f_1^g f_1^g] + A_2 \left(z, \frac{m^2}{m_\perp^2} \right) C [w_0 h_1^{\perp g} h_1^{\perp \bar{g}}], \end{aligned} \quad (21)$$

where the variables $m_\perp^2 = m^2 + \mathbf{K}_\perp^2$ and z are related to $M_{Q\bar{Q}}^2$ as follows: $z(1-z)M_{Q\bar{Q}}^2 = m_\perp^2$.

The TMD convolutions $C[wfg]$ are defined as

$$C[wfg] = \int d^2\mathbf{k}_{1T} \int d^2\mathbf{k}_{2T} \delta^2(\mathbf{k}_{1T} + \mathbf{k}_{2T} - \mathbf{q}_T) w(\mathbf{k}_{1T}, \mathbf{k}_{2T}) f(x_1, \mathbf{k}_{1T}^2, \mu_F) g(x_2, \mathbf{k}_{2T}^2, \mu_F), \quad (22)$$

where, at LO in α_s , the light-cone momentum fractions $x_{1,2}$ are related to the rapidities $y_{1,2}$ and $s = (P_1 + P_2)^2$ by $x_{1,2} = \frac{m_\pm}{\sqrt{s}}(e^{\pm y_1} + e^{\pm y_2})$. In the considered reactions, the following weights are used:

$$\begin{aligned} w_0 &= \frac{1}{m_N^4} [2(\mathbf{k}_{1T} \cdot \mathbf{k}_{2T})^2 - \mathbf{k}_{1T}^2 \mathbf{k}_{2T}^2], & w_1 &= \frac{1}{m_N^2} \left[2 \frac{(\mathbf{q}_T \cdot \mathbf{k}_{1T})^2}{\mathbf{q}_T^2} - \mathbf{k}_{1T}^2 \right], \\ w_3 &= \frac{1}{m_N^2} \left[2 \frac{(\mathbf{q}_T \cdot \mathbf{k}_{1T})(\mathbf{q}_T \cdot \mathbf{k}_{2T})}{\mathbf{q}_T^2} - (\mathbf{k}_{1T} \cdot \mathbf{k}_{2T}) \right], & w_2 &= \frac{1}{m_N^2} \left[2 \frac{(\mathbf{q}_T \cdot \mathbf{k}_{2T})^2}{\mathbf{q}_T^2} - \mathbf{k}_{2T}^2 \right], \end{aligned} \quad (23)$$

and $w_4 = 2w_3^2 - \mathbf{k}_{1T}^2 \mathbf{k}_{2T}^2 / m_N^4$. Analogously to Eqs.(21), we have

$$\begin{aligned} \mathbf{q}_T^2 B^{q\bar{q}} &= B_0 \left(z, \frac{m^2}{m_\perp^2} \right) \left\{ C [w_3 h_1^{\perp q} h_1^{\perp \bar{q}}] + C [w_3 h_1^{\perp \bar{q}} h_1^{\perp q}] \right\}, \\ \mathbf{q}_T^2 B^{g\bar{g}} &= B_1 \left(z, \frac{m^2}{m_\perp^2} \right) \left\{ C [w_1 h_1^{\perp g} f_1^g] + C [w_2 f_1^g h_1^{\perp \bar{g}}] \right\}. \end{aligned} \quad (24)$$

Finally, the $\cos 4(\phi_\perp - \phi_T)$ angular distribution of the $Q\bar{Q}$ pair is only due to the presence of linearly polarized gluons inside unpolarized nucleon, $C = C^{g\bar{g}}$:

$$\mathbf{q}_T^4 C^{g\bar{g}} = C_1 \left(z, \frac{m^2}{m_\perp^2} \right) C [w_4 h_1^{\perp g} h_1^{\perp \bar{g}}]. \quad (25)$$

The order α_s^2 predictions for the coefficients $A_{0,1,2}$, $B_{0,1}$ and C_1 in Eqs.(21), (24) and (25) are presented in Ref.[72]. Using these results, one can, in principle, extract the densities $h_1^{\perp q}(x, \mathbf{k}_T^2)$ and $h_1^{\perp g}(x, \mathbf{k}_T^2)$ from azimuthal distributions of the $D\bar{D}$ pairs produced in pp collisions.

Before discussing the anticipated values of the azimuthal asymmetries, we need to resort to models for description of the TMD distributions. It is well known that the heavy flavor production is dominated by the $gg \rightarrow Q\bar{Q}$ subprocess. For this reason, it seems reasonable to begin from the contribution of the gluon fusion mechanism. Usually the TMD density of unpolarized gluons is taken to be a Gaussian:¹⁰

$$f_1^g(x, \mathbf{k}_T^2, \mu_F) = \frac{g(x, \mu_F)}{\pi \langle k_T^2 \rangle} \exp \left(- \frac{\mathbf{k}_T^2}{\langle k_T^2 \rangle} \right), \quad (26)$$

where $g(x, \mu_F)$ is the collinear gluon PDF and $\langle k_T^2 \rangle$ depends implicitly on the scale μ_F .

For description of the linearly polarized gluons in unpolarized proton, we use the parameterization motivated by previous TMD studies [188]:

$$h_1^{\perp g}(x, \mathbf{k}_T^2, \mu_F) = \frac{2m_N^2}{\langle k_T^2 \rangle} \frac{(1-\kappa) g(x, \mu_F)}{\kappa \pi \langle k_T^2 \rangle} \exp \left(1 - \frac{\mathbf{k}_T^2}{\kappa \langle k_T^2 \rangle} \right). \quad (27)$$

¹⁰For more details, see Ref.[248] and references therein.

The model-independent positivity bound (17) is satisfied by Eqs.(26) and (27) with $\kappa < 1$. Usually the value $\kappa = 2/3$ is used that maximizes the second k_T moment of $h_1^{\perp g}$. With the choice (27), all the TMD convolutions $C[w_i f g]$ ($i = 0-4$) with gluon PDFs are simple analytical functions.

Another widely used parameterization of the PDF for linearly polarized gluons is

$$h_1^{\perp g}(x, \mathbf{k}_T^2, \mu_F) = \frac{2m_N^2}{k_T^2} f_1^g(x, \mathbf{k}_T^2, \mu_F). \quad (28)$$

With this choice, one can estimate the upper bounds of the expected values of the azimuthal asymmetries. Throughout this subsection, "Model 1" will refer to the Gaussian form (27) with $\kappa = 2/3$ and "Model 2" to the form (28) saturating the positivity bound.

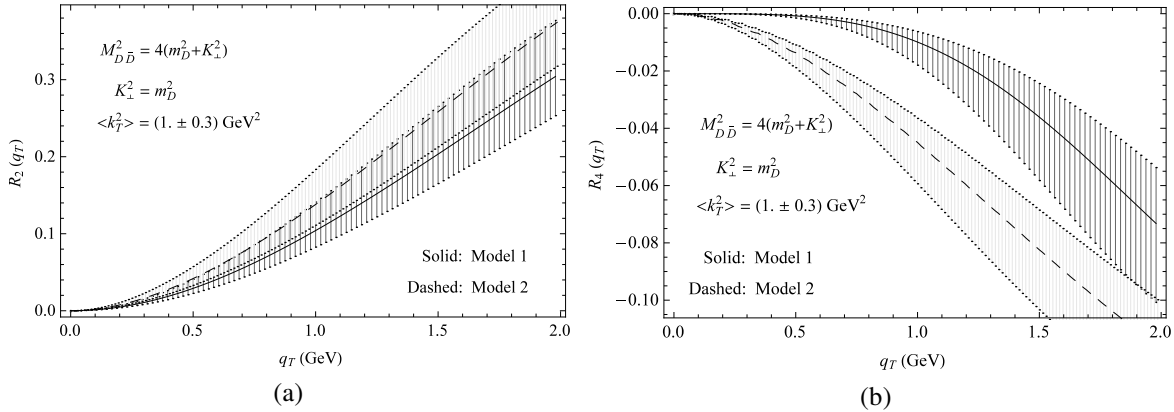


Figure 15: (a) Gluon fusion contribution to the asymmetry $R_2(q_T) = \frac{Bq_T^2}{A}$ in $pp \rightarrow D\bar{D}X$ process at $M_{D\bar{D}}^2 = 4(K_\perp^2 + m_D^2)$ and $K_\perp^2 = m_D^2$. (b) Gluon fusion contribution to the asymmetry $R_4(q_T) = \frac{Cq_T^4}{A}$ in $pp \rightarrow D\bar{D}X$ process at $M_{D\bar{D}}^2 = 4(K_\perp^2 + m_D^2)$ and $K_\perp^2 = m_D^2$.

Let us discuss the gluon fusion contributions to the azimuthal asymmetries defined as

$$R_2(q_T) = \frac{Bq_T^2}{A} = 2\langle \cos 2(\phi_\perp - \phi_T) \rangle, \quad R_4(q_T) = \frac{Cq_T^4}{A} = 2\langle \cos 4(\phi_\perp - \phi_T) \rangle. \quad (29)$$

Our analysis of the functions $A_{1,2}(z, m^2/m_\perp^2)$ and $B_1(z, m^2/m_\perp^2)$ shows that the asymmetry $R_2(q_T, z, m^2/m_\perp^2)$ has an extremum at $z = 1/2$ and $m^2/m_\perp^2 = 1/2$ (i.e., at $M_{Q\bar{Q}}^2 = 4(m^2 + K_\perp^2)$ and $K_\perp^2 = m^2$). This extremum value is $\frac{C[w_1 h_1^{\perp g} f_1^g]}{3C[f_1^g f_1^g - (1/8)C[w_0 h_1^{\perp g} h_1^{\perp g}]}$. One can see that the function R_2 has a maximum at $z = m^2/m_\perp^2 = 1/2$ for all positive values of the convolution $C[w_1 h_1^{\perp g} f_1^g]$ independently of the form of $h_1^{\perp g}$ and f_1^g densities we use.

The gluon fusion predictions for the asymmetry $R_2(q_T) = 2\langle \cos 2(\phi_\perp - \phi_T) \rangle$ in $pp \rightarrow D\bar{D}X$ reaction at $M_{D\bar{D}}^2 = 4(K_\perp^2 + m_D^2)$ and $K_\perp^2 = m_D^2$ are presented in Fig.15(a). The solid line corresponds to the Model 1 described by the gluon density (27) with $\kappa = 2/3$. The dashed line shows the predictions of the Model 2 saturating the positivity bound (17). Both solid and dashed lines are given for $\langle k_T^2 \rangle = 1.0 \text{ GeV}^2$. The uncertainty bands result from the variation of $\langle k_T^2 \rangle$ by 0.3 GeV^2 . Note that the dashed line (Model 2) describes the largest $\cos 2(\phi_\perp - \phi_T)$ asymmetry allowed by the gluon fusion mechanism.

Our analysis of the quantity $C_1(z, m^2/m_\perp^2)$ indicates that the distribution $R_4(q_T, z, m^2/m_\perp^2)$ takes its maximum value at $M_{Q\bar{Q}}^2 \rightarrow s$, i.e. for $x_1 x_2 \rightarrow 1$. However, the heavy flavor production rates vanish at the threshold. For this reason, the gluon fusion predictions for the asymmetry $R_4(q_T) = 2\langle \cos 4(\phi_\perp - \phi_T) \rangle$ are also given in Fig.15(b) at $M_{D\bar{D}}^2 = 4(K_\perp^2 + m_D^2)$ and $K_\perp^2 = m_D^2$. One can see from Figs.15(a) and 15(b) that both the R_2 and R_4 distributions are predicted to be sizable (of the order of 10%) within considered models for $q_T \gtrsim 1 \text{ GeV}$.

Another processes proposed to probe the linearly polarized gluons in unpolarized proton are: pseudoscalar C -even quarkonia (such as η_c and χ_c) [154, 188], di-gamma ($pp \rightarrow \gamma\gamma X$) [249], J/ψ - pair ($pp \rightarrow J/\psi J/\psi X$) [18, 79] and $J/\psi \gamma$ ($pp \rightarrow J/\psi \gamma X$) [73] production. These reactions are TMD factorizable but, unfortunately, strongly suppressed in comparison with $pp \rightarrow D\bar{D}X$.

4.3. Non-nucleonic degrees of freedom in deuteron

The naive model describes the deuteron as a weakly-bound state of a proton and a neutron mainly in S-state with a small admixture of the D-state. However, such a simplified picture failed to describe the HERMES experimental results on the b_1 structure function of the deuteron [250]. Modern models treat the deuteron as a six-quark state with the wave function

$$|6q\rangle = c_1|NN\rangle + c_2|\Delta\Delta\rangle + c_3|CC\rangle, \quad (30)$$

that contains such terms as the nucleon $|NN\rangle$, Δ -resonance $|\Delta\Delta\rangle$ and the so-called hidden color component $|CC\rangle$ in which two color-octet baryons combine to form a color singlet [251]. Such configurations can be generated, for example, if two nucleons exchange a single gluon. The relative contribution of the hidden-color term varies from about 0.1% to 80% in different models [252]. The components other than $|NN\rangle$ should manifest themselves in the high- Q^2 limit. Possible contributions of the Fock states with a valent gluon like $|uuudddg\rangle$ could also be discussed [206, 253].

The unpolarized gluon PDF of the deuteron in the light-front quantization was calculated in the Ref. [206] under the approximation where the input nuclear wave function is obtained by solving the nonrelativistic Schrödinger equation with the phenomenological Argonne v18 nuclear potential as an input. Gluon PDFs calculated per nucleon are very similar for the proton ones in the range of small and intermediate x values while for $x > 0.6$ the difference becomes large due to the Fermi motion (see Fig. 11(b)). A similar work was performed in Ref. [254] for determination of spatial gluon distribution in deuteron for low- x that could be tested in the J/ψ production at EIC. Today the gluon content of deuteron and light nuclei becomes the matter of interest for the lattice QCD studies [255]. Apart from the general understanding of the gluon EMC effect, the measurement of the gluon PDF at high- x for deuteron could provide a useful input for high-energy astrophysical calculation [206].

SPD can perform an explicit comparison of the differential inclusive production cross-sections $d\sigma/dx_F$ for all three gluon probes: charmonia, open charm, and prompt photons using p - p and d - d collisions at $\sqrt{s_{NN}} = 13.5$ GeV and possibly below. Such results could be treated in terms of the difference of unpolarized gluon PDFs in deuteron and nucleon.

5. Gluon content of polarized proton and deuteron

5.1. Gluon helicity with longitudinally polarized beams

The gluon helicity distribution function $\Delta g(x)$ ¹¹ is a fundamental quantity characterizing the inner structure of the nucleon. It describes the difference of probabilities to find a gluon with the same and opposite helicity orientation w.r.t. the spin of the longitudinally polarized nucleon. The integral $\Delta G = \int \Delta g(x)dx$ can be interpreted as the gluon spin contribution to the nucleon spin, as it was discussed in Sec. 3.4. After the EMC experiment discovered that only a small part of proton spin is carried by the quarks: $\Delta\Sigma \approx 0.25$, see Refs. [16, 256], the gluon spin was assumed to be another significant contributor, see Eq. (7) in Sec. 3.4.

The first attempt to measure the gluon polarization in the nucleon was made by the FNAL E581/704 Collaboration using a 200 GeV polarized proton beam and a polarized proton target [257]. They measured the longitudinal double-spin asymmetries A_{LL} for inclusive multi- γ and $\pi^0\pi^0$ production to be consistent with zero within their sensitivities. In the following years a set of SIDIS measurements was performed by the HERMES [258], SMC [259] and COMPASS [260–264] experiments. The production of hadron pairs with high transverse momenta and the production of the open charm where the photon-gluon fusion mechanism dominates were studied. It was figured out that with a large uncertainty the value of ΔG is close to zero. Nevertheless, for gluons carrying a large fraction x of the nucleon momentum, an evidence of a positive polarization has been observed, see Fig. 16(a). The summary of theoretical and experimental results for ΔG can be found in Ref. [265].

New input for ΔG estimation was obtained from the measurement of the A_{LL} asymmetries in the inclusive production of high- p_T neutral [266–269] and charged pions [270], η -mesons [267], jets [271], di-jets [272, 273], heavy flavors [274] and, recently, J/ψ -mesons [275] in polarized p - p collisions at RHIC. These results in general are in agreement with the SIDIS measurements, which indicates the universality of the helicity-dependent parton densities and QCD factorization.

At the moment the most recent sets of polarized PDFs extracted in the NLO approximation are LSS15 [276], DSSV14 [277, 278], NNPDF-pol1.1 [43], and JAM17 [279]. To obtain them, different approaches, parameterizations, and sets of experimental data were used, see Ref. [65] for more details. Fit results for $\Delta g(x)$ from DSSV14

¹¹Here we adopt historical notation for gluon helicity-PDF $\Delta g(x)$ which is also known as $g_1^g(x)$.

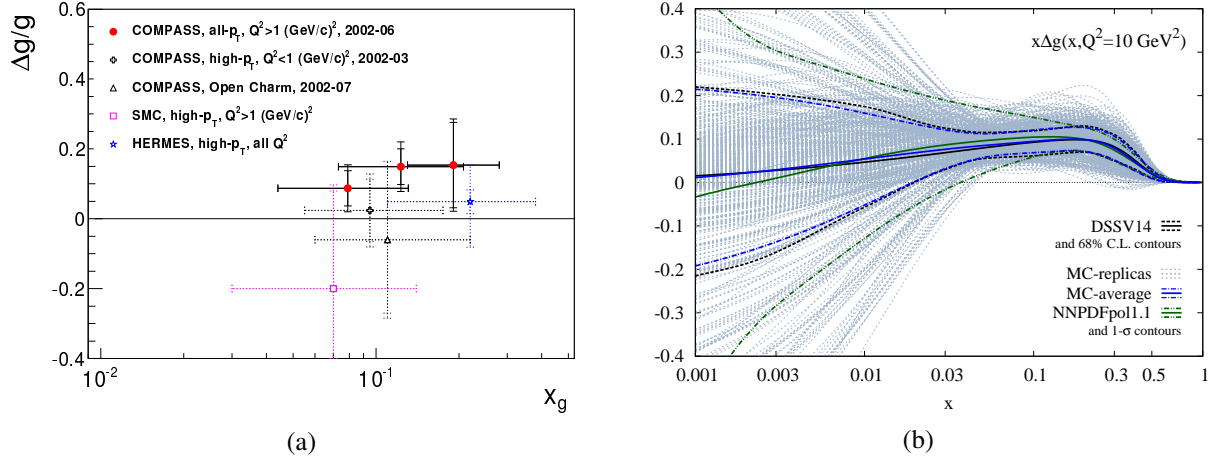


Figure 16: (a) SIDIS data on $\Delta g(x)/g(x)$ extracted in LO [264]. With kind permission of The European Physical Journal (EPJ). (b) Global fit results for the gluon helicity distribution $\Delta g(x)$. Reprinted figure from [278] © (2019) by the American Physical Society under Creative Commons Attribution 4.0 International License.

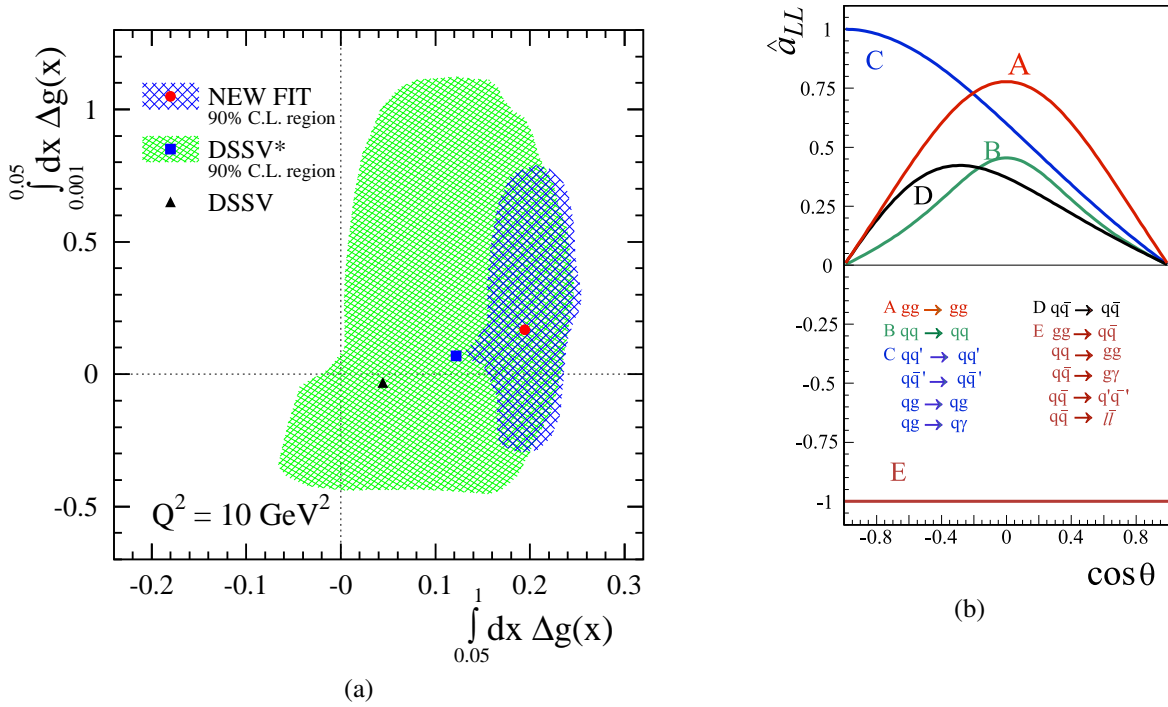


Figure 17: (a) Estimates of contributions of low- x and high- x kinematic ranges into ΔG for the DSSV series of the global fit. The 90% C.L. areas are shown. Reprinted figure with permission from Ref. [277] © (2014) by the American Physical Society. (b) Partonic longitudinal double-spin asymmetries \hat{a}_{LL} for different hard processes as a function of center-of-mass scattering angle [281].

and NNPDF-pol1.1 are presented in Fig. 16(b) [278]. The RHIC p - p data put a strong constraint on the size of $\Delta g(x)$ in the range $0.05 < x < 0.2$ while a constraint on its sign is weaker since in some of the processes only Δg squared is probed (see discussion below). The small x region remains still largely unconstrained and could be covered in the future by measurements at EIC [36]. Region of high x is covered at the moment only by SIDIS measurements which still lack a proper NLO description [280]. The uncertainty of the contribution to ΔG from the kinematic range $0.001 < x < 0.05$ vs. the corresponding contribution from the range $x > 0.05$ for the DSSV global fits is shown in Fig. 17(a) [277].

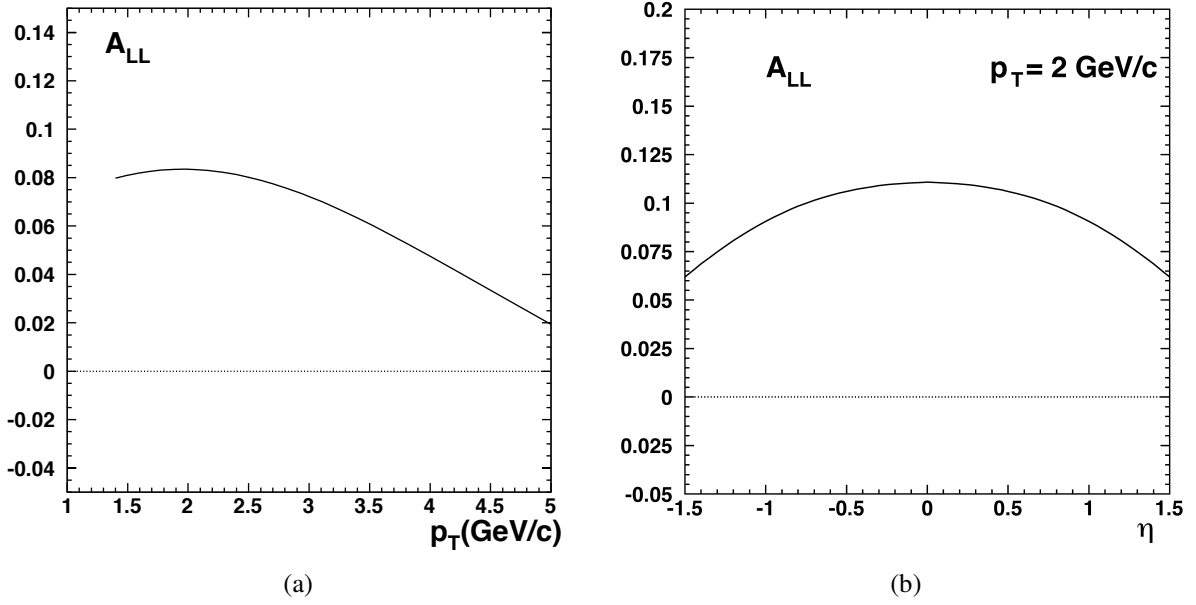


Figure 18: Longitudinal double spin asymmetry A_{LL} for inclusive J/ψ production calculated using LO PDF set A from Ref. [282] for p - p collisions at $\sqrt{s} = 39$ GeV in the LO approximation as a function of a) transverse momentum p_T and b) pseudorapidity η [283].

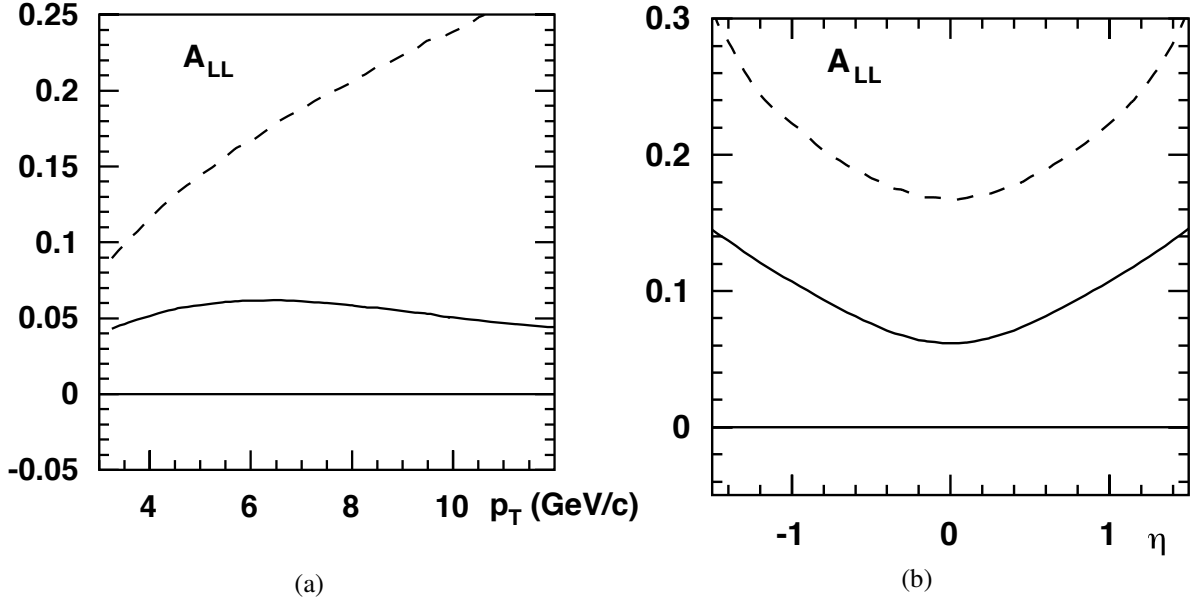


Figure 19: Longitudinal double spin asymmetry A_{LL} for inclusive prompt-photon production calculated for p - p collisions at $\sqrt{s} = 39$ GeV in the LO approximation as a function of a) transverse momentum p_T and b) rapidity η ($p_T = 6$ GeV/c) [283]. The full line corresponds to the NLO 'valence' PDF set from Ref. [284], while the dashed line – to the set A from Ref. [282].

In case of the longitudinally polarized p - p collisions the asymmetry A_{LL} is defined as

$$A_{LL} = \frac{\sigma^{++} - \sigma^{+-}}{\sigma^{++} + \sigma^{+-}}, \quad (31)$$

where σ^{++} and σ^{+-} denote the cross-sections with the same and opposite proton helicity combinations, respectively. For the prompt photons produced via the gluon Compton scattering

$$A_{LL}^\gamma \approx \frac{\Delta g(x_1)}{g(x_1)} \otimes A_{1p}(x_2) \otimes \hat{a}_{LL}^{gq(\bar{q}) \rightarrow \gamma q(\bar{q})} + (1 \leftrightarrow 2). \quad (32)$$

Here $A_{1p}(x)$ is the asymmetry well measured in a wide range of x and $\hat{a}_{LL}^{gq(\bar{q})\rightarrow\gamma q(\bar{q})}$ is the asymmetry of the corresponding hard process. The Fig. 17(b) shows the behavior of \hat{a}_{LL} for different hard processes as a function of the center-of-mass scattering angle. For charmonia and open charm production via the gluon-gluon fusion process the expression for the corresponding asymmetry reads

$$A_{LL}^{c\bar{c}} \approx \frac{\Delta g(x_1)}{g(x_1)} \otimes \frac{\Delta g(x_2)}{g(x_2)} \otimes \hat{a}_{LL}^{gg\rightarrow c\bar{c}X}. \quad (33)$$

This asymmetry on the one hand is more sensitive to the gluon polarization than the corresponding one for the prompt photons due to the quadratic dependence on Δg . On the other hand the sign of the Δg value can not be determined from it. So the measurements with prompt photons and heavy-quark states are complementary. The contribution of $q\bar{q}$ annihilation processes to the above-mentioned asymmetries is negligible despite $\hat{a}_{LL} = -1$ because of the smallness of the sea-quark polarization in the nucleon.

It is important to emphasize that a sizable systematic uncertainty of A_{LL} measurements in the inclusive J/ψ production comes from our limited knowledge of charmonia production mechanisms including the feed-down contribution. Each of them has different partonic asymmetries \hat{a}_{LL} [285]. For the Δg estimation in Ref. [275] the value of $\hat{a}_{LL}^{J/\psi}$ has been forced to -1 . The SPD setup will have the possibility to reconstruct χ_{cJ} states via their radiative decays and resolve J/ψ and $\psi(2S)$ signals in a wide kinematic range and disentangle contributions of direct and feed-down production mechanisms. The quality of the Δg estimation could be significantly improved by measuring A_{LL} separately for each charmonium state.

Predictions for the longitudinal double-spin asymmetries A_{LL} in p - p collisions can be found in Ref. [286] (J/ψ) and [287] (prompt photons). They mostly cover the kinematic range of the RHIC experiments. Some estimates for A_{LL} in charmonia [283] and prompt-photon [283, 284, 288] production at $\sqrt{s} = 39$ GeV (see Figs. 18 and 19, respectively) have been done in preparation of the unrealized HERA- N project.

The authors of the Ref. [289] proposed to extract information about the gluon helicity Δg via studying of the production of high- p_T prompt photons accompanied by Σ^+ hyperons. To do that the single longitudinal spin asymmetry $A_L^{\gamma\Sigma}$ and the polarization of the produced Σ^+ hyperons should be measured. However, further elaboration of this method is needed.

5.2. Gluon-related TMD and twist-3 effects with transversely polarized beams

One of the promising ways to investigate the spin structure of the nucleon is the study of transverse single-spin asymmetries (SSAs) in the inclusive production of different final states in high-energy interactions. The SSA A_N is defined as

$$A_N = \frac{\sigma^\uparrow - \sigma^\downarrow}{\sigma^\uparrow + \sigma^\downarrow}, \quad (34)$$

where σ^\uparrow and σ^\downarrow denote the inclusive production cross-sections with opposite transverse polarization with respect to the production plane, defined by momenta of polarized projectile and produced hadron (or jet). At the moment, more than forty years after the transverse spin phenomena were discovered, a wealth of experimental data indicating non-zero A_N in the lepton-nucleon and nucleon-nucleon interactions were collected, see e.g. [12–16, 290–292] and references therein. However, our understanding of the SSA phenomenon is not yet conclusive.

Theoretically two dual approaches are used to explain transverse single-spin azimuthal asymmetries: the collinear twist-3 formalism and the TMD factorization approach. In the first one at large transverse momenta $p_T \gg \Lambda_{QCD}$ of a produced particle, the collinear factorization involving twist-3 contributions for three-parton (Efremov-Teryaev-Qiu-Sterman) correlations Ref. [293–296] are used, for the review see Ref. [297].¹² An alternative approach, suitable also for less inclusive processes, is based on the TMD factorization, valid for $p_T \ll Q$, in terms of transverse-momentum-dependent parton distributions. In this case, the SSAs originate from the initial-state quark and Gluon Sivers Functions (GSF), which may be related to the mentioned twist-3 correlators, or the final-state Collins fragmentation functions.

The Sivers function $f_{1T}^{\perp,q(g)}(x, \mathbf{k}_T^2)$ is a TMD PDF that describes the left-right asymmetry in the distribution of partons w.r.t. the plane defined by the nucleon spin and momentum vectors. Originating from the correlation between the spin of the nucleon and the orbital motion of partons, it is an important detail of the three-dimensional picture of the nucleon. This function is responsible for the so-called Sivers effect (for both quarks and gluons) that was first suggested in Ref. [298] as an explanation for the large transverse single-spin asymmetries A_N measured in

¹²Here $\Lambda_{QCD} \approx 200$ MeV is the QCD scale.

the inclusive pion production off transversely polarized nucleons. More details on the theoretical and experimental status of the transverse spin structure of the nucleon can be found in Refs. [14, 299, 300]. The first attempt to access the GSF studying azimuthal asymmetries in high- p_T hadron pair production in SIDIS off transversely polarized deuterons and protons, was performed by COMPASS [28]. Using neural network techniques the contribution originating from the Photon–Gluon Fusion (PGF) subprocess has been separated from the leading-order virtual-photon absorption and QCD Compton scattering subprocesses. The extracted combined proton-deuteron PGF-asymmetry was found to be negative and more than two standard deviations below zero, the possible existence of a non-zero GSF. In the meantime, COMPASS did not see any signal for the PGF Collins asymmetry, which can analogously be related to the gluon transversity distribution in nucleon. COMPASS studied the GSF also through Siverson asymmetry in the J/ψ -production channel [29], again obtaining an indication of a negative asymmetry.

Several inclusive processes were proposed to access the gluon-induced spin effects in transversely polarized p - p collisions. Single spin asymmetries for production of charmonia [22, 301] (RHIC, AFTER), open charm [22, 302–305] (RHIC) [305] (AFTER), and prompt photons [295, 306] (E704), [307] (RHIC). The possible gluon induced effects were estimated using both approaches TMD and the collinear twist-three approaches for the experimental conditions of the past, present, and future experiments.

In Ref. [308] a first estimate of the GSF was obtained using the midrapidity data on A_N , as measured in π^0 production in pp collisions at RHIC [24]. The extraction was performed within the GPM framework, a phenomenological extension of the TMD factorization scheme, where TMDs are assumed conditionally universal, using the GRV98-LO set for the unpolarized PDF and available parameterizations for the quark Siverson functions (SIDIS1 from Ref. [309] and SIDIS2 from Ref. [310]).

The GSF is parameterized assuming a factorized Gaussian-like form, as follows:

$$\Delta^N f_{g/p^\dagger}(x, \mathbf{k}_T^2) = \left(-2 \frac{|\mathbf{k}_T|}{M_p} \right) f_{1T}^{\perp g}(x, \mathbf{k}_T^2) = 2 N_g(x) f_{g/p}(x) h(\mathbf{k}_T^2) \frac{e^{-\mathbf{k}_T^2 / \langle k_T^2 \rangle}}{\pi \langle k_T^2 \rangle}, \quad (35)$$

where $f_{g/p}(x)$ is the standard unpolarized collinear gluon distribution, and

$$N_g(x) = N_g x^\alpha (1-x)^\beta \frac{(\alpha + \beta)^{(\alpha + \beta)}}{\alpha^\alpha \beta^\beta}, \quad h(\mathbf{k}_T^2) = \sqrt{2} e \frac{|\mathbf{k}_T|}{M'} e^{-\mathbf{k}_T^2 / M'^2}. \quad (36)$$

We can also define a suitable parameter $\rho = M'^2 / (\langle k_T^2 \rangle + M'^2)$, with $0 < \rho < 1$. By imposing $|N_g| \leq 1$ the positivity bound for the GSF is automatically fulfilled for any value of x and \mathbf{k}_T .

The first \mathbf{k}_T -moment of the GSF is also of relevance

$$\Delta^N f_{g/p^\dagger}^{(1)}(x) = \int d^2 \mathbf{k}_T \frac{|\mathbf{k}_T|}{4M_p} \Delta^N f_{g/p^\dagger}(x, \mathbf{k}_T^2) \equiv -f_{1T}^{\perp(1)g}(x). \quad (37)$$

Two different parameterization of the GSF were obtained using different sets for the fragmentation functions, namely the Kretzer [311] and DSS07 [312] sets, which give significantly different results for gluons. The latter point has a strong impact on the extracted GSF, especially in the low- x region, see Fig. 20, where the first moments of the GSF are shown in Fig. 20(a) and 20(b), respectively for the SIDIS1 and SIDIS2 sets.

We recall that the gluon Siverson function is expected to satisfy the positivity bound defined as twice the unpolarized TMD gluon distribution. Although, some theoretical expectations are that the gluon Siverson function at relatively high x should be about 1/3 of the quark one [300].

An extended version of the GPM, with inclusion of initial- and final-state interactions (ISIs and FSIs respectively) under a one-gluon exchange approximation, was developed, limiting to the quark sector, in Refs. [313, 314]: the so-called color-gauge-invariant GPM (CGI-GPM). In this approach, the effects induced by ISIs and FSIs, leading to the process dependence of the Siverson function, can be collected into modified color factors and moved to the hard partonic parts. In this way, one can still consider a universal Siverson function, as extracted from SIDIS, but this time convoluted with properly modified partonic cross-sections. Interestingly, these coincide with the corresponding hard partonic parts appearing in the collinear twist-three formalism [313]. Moreover, this modified GPM allows to get the expected opposite sign of the Siverson function when moving from SIDIS to DY processes [315, 316].

In Ref. [22] this approach was extended to the gluon Siverson contribution to A_N for D -meson and J/ψ production and, subsequently, in Ref. [81] to the case of inclusive pion and photon production. The main difference w.r.t. the quark case is that for the gluon sector one needs to introduce two different classes of modified partonic cross-sections, corresponding to the two different ways in which a color-singlet state can be formed out of three gluons, *i.e.* either through an anti-symmetric or a symmetric color combination. Each one of them has to be convoluted with

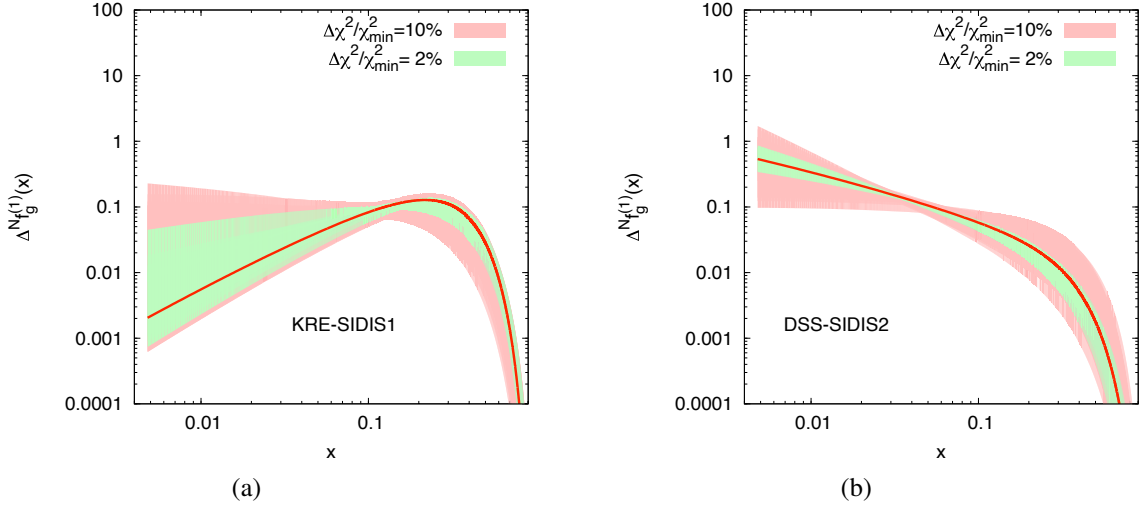


Figure 20: The first k_T -moment of the gluon Sivers function [308] obtained using the SIDIS1 [309] – panel (a) and SIDIS2 [310] – panel (b) extractions of the quark Sivers functions. Reprinted figures from Ref. [308] © (2015) Springer under the Creative Commons Attribution 4.0 International License.

a different gluon Sivers distribution. These two universal and independent distributions are named, respectively, the f -type and d -type gluon Sivers functions [317]: the former is even under charge conjugation, while the latter is odd.

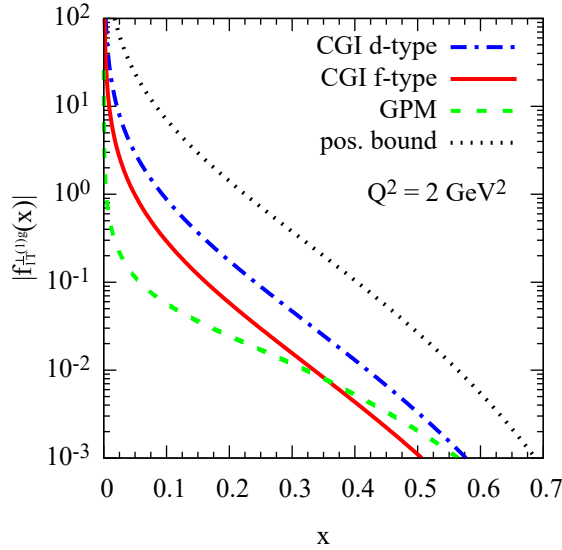


Figure 21: Allowed upper values for the first k_T -moments of the gluon Sivers function in different approaches and scenarios at $Q^2 = 2 \text{ GeV}^2$ [81]: GPM approach (dashed line), CGI-GPM d -type ($N_g^{(d)} = 0.15$, dot-dashed line) and f -type ($N_g^{(f)} = 0.05$, solid line). The positivity bound (dotted line) is also shown.

In Ref. [81] a detailed phenomenological study was carried out, leading to the first preliminary determination of the allowed upper bounds for the two GSFs entering the CGI-GPM approach. This was obtained by analysing the mid-rapidity pion A_N data together with those for D -meson production, from the PHENIX Collaboration [24, 27]. The main outcome of this study is that while pion SSAs are very sensitive to the f -type GSF, being the d -type one dynamically suppressed, the opposite is true in the SSAs for D -meson production, at least at forward rapidities. A combined extraction (in terms of allowed upper bounds) of these two GSFs was therefore possible. The corresponding results for the first moments of the GSF are shown in Fig. 21.

Notice that, while in Ref. [308] a single value $\langle k_T^2 \rangle = 0.25 \text{ GeV}^2$ [318] was adopted for the unpolarized quark

and gluon TMDs, in Ref. [81] for the unpolarized gluon TMD the authors used a different value, $\langle k_T^2 \rangle = 1 \text{ GeV}^2$. This, indeed, gives a better account of the unpolarized cross-sections for J/ψ production at not so large p_T values, without spoiling the description of the inclusive pion production data. Moreover, a different set for the unpolarized PDFs (the CTEQ6L1 set [319]) was employed. For these reasons, an updated extraction of the GSF within the GPM was performed (still adopting the DSS07 set for the unpolarized collinear pion FFs), finding results very similar to those reported in Ref. [308] for the first k_T -moments of the GSF (SIDIS2 case), although with slightly different parameters.

The SSA $A_N^{J/\psi}$ in the J/ψ production was measured by the PHENIX Collaboration in p - p and p - A collisions at $\sqrt{s_{NN}} = 200 \text{ GeV}/c$ [25, 26]. The obtained asymmetries $A_N^{J/\psi}$ are consistent with zero for negative and positive x_F values. Theoretical predictions [301] based on the Color Evaporation Model within a TMD approach and employing the GSF from Ref. [320] for different center-of-mass energies are shown in Fig. 23(a) as functions of the rapidity y . Since the J/ψ production mechanism is not well understood, the measurement of the $A_N^{J/\psi}$ may bring a valuable input to that matter as well.

In this context, a comprehensive analysis adopting different mechanisms for quarkonium production, namely the Color-Singlet Model and its extension to NRQCD, and two TMD schemes, the GPM and the CGI-GPM, has been recently performed in Refs. [21, 197]. In Fig. 22 we show a comparison among these options, adopting maximized gluon Sivvers functions (that is by using $\mathcal{N}_g(x) = 1$ and $\rho = 2/3$ for all GSFs), for A_N at RHIC kinematics, $\sqrt{s} = 200 \text{ GeV}$ and $x_F = 0.1$ (a) and $x_F = -0.1$ (b), vs. p_T . This indeed could be a valuable tool to quantify the potential role of the GSFs and the feasibility of their corresponding extraction. As one can see the f -type contribution in NRQCD (solid lines) suffers from the most effective cancellations, coming from the relative sign of the modified partonic cross-sections. The d -type one (thin dashed lines) is suppressed by the absence of the gg channel, that dominates the unpolarized cross-section (this reflects also into the negligible contribution of the quark Sivvers function). On the opposite side the GPM approach, both within the CS model (thick dashed lines) and in NRQCD (dotted lines), gives the potentially largest contributions. It is worth to remark that within the GPM the differences coming from the production mechanism are small. Moreover, even if to a much lesser extent as compared to the GPM, also within the CGI-GPM one can potentially put some constraints on the size of the f -type GSF even with the few data points available.

These estimates can be certainly affected by uncertainties, intrinsic in the model and/or induced by the nonperturbative parameters used. On the other hand, the relative size of these maximized contributions to the asymmetry, coming from different terms and models, is certainly under better control. One has to keep in mind that the ultimate goal of this comparison is to estimate the impact of ISIs and FSIs in the computation of such SSAs.

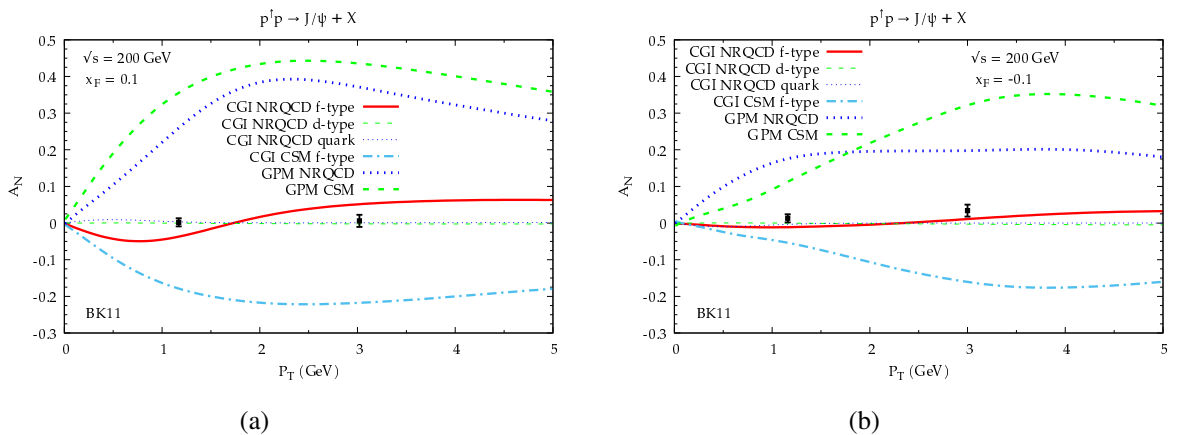


Figure 22: Maximized contributions to A_N estimates as a function of p_T for the process $p^\dagger p \rightarrow J/\psi + X$ at $\sqrt{s} = 200 \text{ GeV}$ and $x_F = 0.1$ (a) and $x_F = -0.1$ (b) adopting the CGI-GPM and GPM approaches, within the CS model and NRQCD. Data are taken from [26]. Reprinted figures from Ref. [21], ©(2020) by the American Physical Society under the Creative Commons Attribution 4.0 International License.

In Fig. 23(b) we show the analogous estimates for pp collisions at NICA energy, $\sqrt{s} = 27 \text{ GeV}$, this time at fixed p_T as a function of x_F . A word of caution is mandatory: at these energies the quark-initiated contribution to the unpolarized cross-section, when adopting the NRQCD framework, is not negligible and, starting around $p_T \simeq 2 \text{ GeV}$, becomes comparable with the gluon-initiated ones. On the other hand, when employing the parametrizations of the quark Sivvers functions (as extracted from SIDIS data) their contribution to the SSA turns out to be completely

negligible. Once again, in Fig. 23(b), we see that the largest maximized estimates are obtained within the GPM, both in the CSM and in NRQCD. In the CGI-GPM, the only sizeable contribution comes from the f -type GSF in the CS model. In this respect, a measurement of A_N at NICA could represent an important tool to disentangle among the different approaches and to constrain the GSF. Moreover, a detailed comparison with the analogous results obtained at RHIC kinematics could help in better understanding the role of quark and gluon initiated subprocesses both in the unpolarized cross-sections and in SSAs.

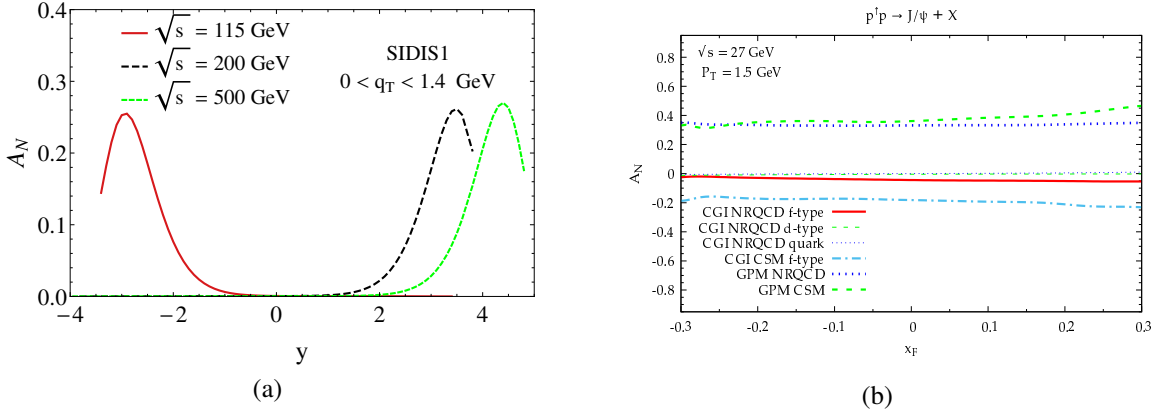


Figure 23: (a) Predictions for $A_N^{J/\psi}$ for $\sqrt{s} = 115$ GeV (AFTER), 200 GeV and 500 GeV (RHIC) as a function of rapidity y . Reprinted figure with permission from [301] © (2017) by the American Physical Society. (b) Maximized contributions to A_N estimates as a function of x_F for the process $p^+ p^- \rightarrow J/\psi + X$ at $\sqrt{s} = 27$ GeV and $p_T = 1.5$ GeV adopting the CGI-GPM and GPM approaches, within the CS model and NRQCD.

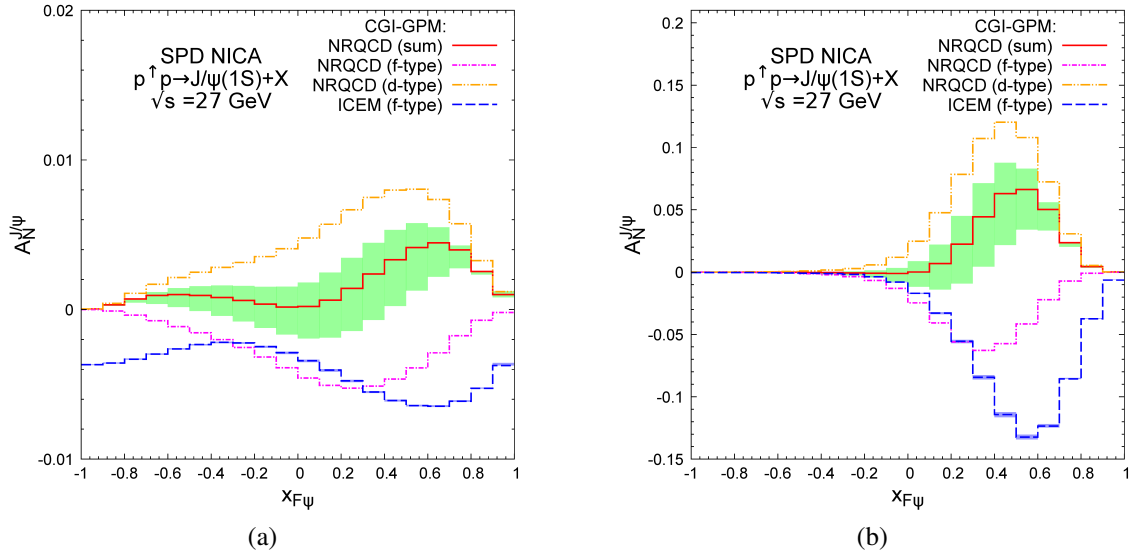


Figure 24: Comparisons of NRQCD and ICEM predictions for $A_N^{J/\psi}$ as function of x_F in p - p collisions at the energy $\sqrt{s} = 27$ GeV obtained in CGI-GPM with D'Alesio et al. (a) and SIDIS1 (b) parameterizations of Siverson function.

Predictions for $A_N^{J/\psi}$ in proton-proton collisions at NICA energy $\sqrt{s} = 27$ GeV, obtained in GPM + NRQCD approach, as function of x_F and p_T are shown in the Figure (24). For comparison, results are presented for SIDIS1 [309] and D'Alesio et al. [22, 197] parameterizations of proton Siverson function.

A measurement with open-heavy hadrons (both D - and B -mesons) was performed at RHIC (PHENIX, $\sqrt{s} = 200$ GeV) [27] using high- p_T muons from their semileptonic decays. Obtained results are affected by relatively large statistical uncertainties and do not exhibit any significant non-zero asymmetry. Nevertheless, the results do not contradict the predictions of the twist-3 approach from Ref. [303]. The Siverson effect contribution to the A_N^D asymmetry calculated within the Generalized Parton Model for $\sqrt{s} = 27$ GeV is presented in Fig. 25.

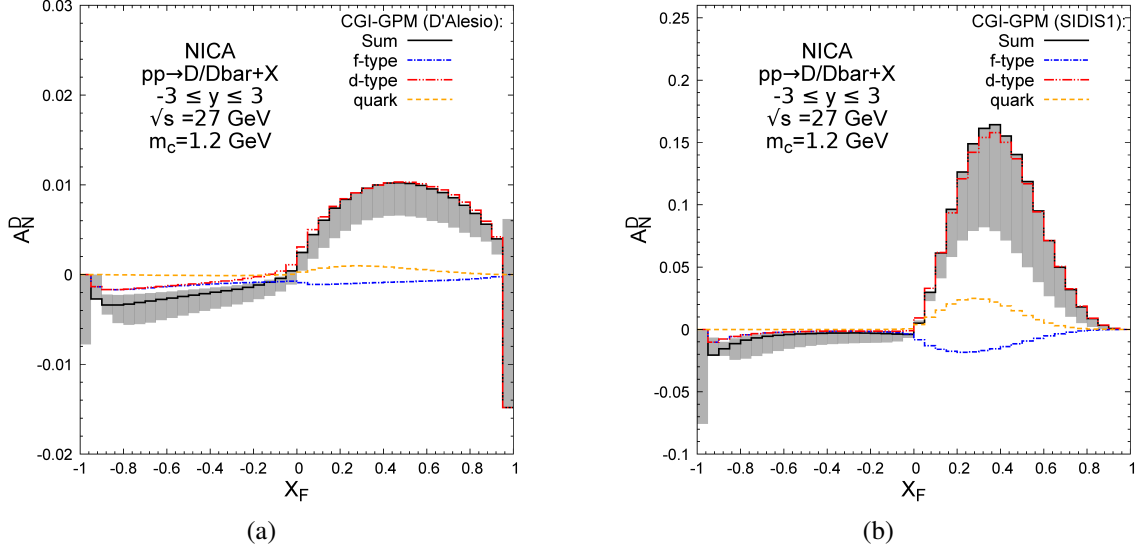


Figure 25: CGI-GPM predictions for single-spin asymmetry in inclusive D -meson production with gluon Sivvers function extracted in the D'Alesio *et.al.* [22, 197] fit (a) and SIDIS1 [309] fit (b)

Measurement of the A_N^γ for prompt photons provides a unique opportunity to study the Sivvers PDF and twist-3 correlation functions, since the corresponding hard process does not involve fragmentation in the final state and thus is exempt from the Collins effect. The first attempt to measure A_N^γ at $\sqrt{s} = 19.4$ GeV was performed at the fixed target experiment E704 at Fermilab in the kinematic range $-0.15 < x_F < 0.15$ and $2.5 \text{ GeV}/c < p_T < 3.1 \text{ GeV}/c$. The results were consistent with zero within large statistical and systematic uncertainties [321]. Figure 26(a) shows the results of our calculations of A_N^γ asymmetry as a function of x_F for $\sqrt{s} = 27$ GeV based on the SIDIS1 parameterization of the GSF. Quark and gluon contributions from the gluon Compton scattering, dominating at positive and negative values of x_F , respectively, are shown separately. The $q\bar{q}$ annihilation contribution is also presented. Dotted lines illustrate the twist-3 predictions for $\sqrt{s} = 30$ GeV and $p_T = 4$ GeV for negative [306] and positive [295] values of x_F . The p_T dependence of the A_N^γ asymmetry at $x_F = -0.5$ is shown for different values of \sqrt{s} in Fig. 26(b).

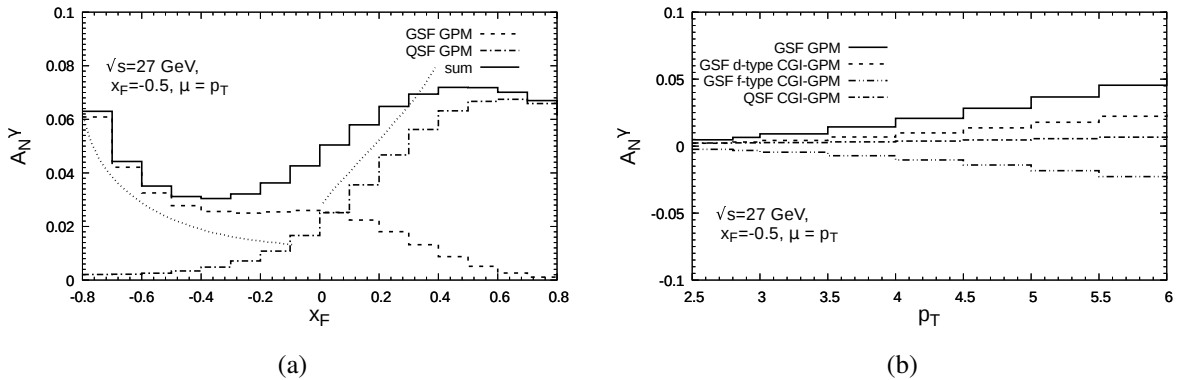


Figure 26: (a) x_F dependence of the asymmetry A_N^γ calculated adopting the SIDIS1 Sivvers function for $\sqrt{s} = 27$ GeV and $4 < p_T < 6$ GeV. Gluon and quark contributions are shown separately, see the legend in the plots. Dotted lines illustrate the twist-3 predictions for $\sqrt{s} = 30$ GeV and $p_T = 4$ GeV for negative [306] and positive [295] values of x_F . (b) p_T dependence of the A_N^γ asymmetry for different values of \sqrt{s} at $x_F = -0.5$.

5.3. Gluon transversity in deuteron

The transversely polarized parton densities (called transversity distributions) within transversely polarized proton and deuteron are extensively investigated both theoretically and experimentally. A remarkable difference of the

parton transverse distributions from the longitudinal ones is that the gluon transversity distribution does not exist in the spin-1/2 nucleons. For this reason, the Q^2 - evolution of the quark transversity in a nucleon is independent of the gluon contributions [322–324], whereas the quark and gluon helicities evolve with Q^2 in a close relation to each other according to the DGLAP equations [325].

The quark transversity PDFs are less constrained experimentally compared to the helicity functions [12], while the gluon transversity is presently unknown [326]. The latter one can be potentially studied in experiments with linearly polarized deuterons.¹³ Traditionally, the deuteron is considered as a weakly coupled spin-1 bound state of a proton and neutron. Since proton and neutron themselves do not contain the gluon transversity, one could expect vanishing gluon transversity in the deuteron. However, if sizable values for the gluon transversity are measured, this might indicate the presence of new (different from $|pn\rangle$ state) degrees of freedom in the deuteron.

The longitudinally and transversely polarized quark distributions in a nucleon are defined as matrix elements on the light-cone [326]¹⁴:

$$\begin{aligned} g_1^q(x) &= \int \frac{d\xi^-}{4\pi} e^{ixp^+\xi^-} \langle p_{S_L} | \bar{\psi}(0) \gamma^+ \gamma_5 \psi(\xi) | p_{S_L} \rangle_{\xi^+ = \xi_\perp = 0}, \\ h_1^q(x) &= \int \frac{d\xi^-}{4\pi} e^{ixp^+\xi^-} \langle p_{S_T j} | \bar{\psi}(0) i \gamma_5 \sigma^{j+} \psi(\xi) | p_{S_T j} \rangle_{\xi^+ = \xi_\perp = 0}, \end{aligned} \quad (38)$$

where gauge links which ensure gauge invariance are omitted; s_L and s_T indicate the longitudinal and transverse polarizations of the nucleon, respectively. In Eqs.(38), the antisymmetric tensor $\sigma^{\mu\nu}$ is defined by $\sigma^{\mu\nu} = \frac{i}{2}(\gamma^\mu \gamma^\nu - \gamma^\nu \gamma^\mu)$ while $a^\pm = (a^0 \pm a^3)/\sqrt{2}$.

According to the optical theorem, hadron structure functions are determined by the imaginary part of corresponding forward scattering amplitudes. Such an amplitude, $A_{\Lambda_i \lambda_i, \Lambda_f \lambda_f}$, is illustrated in Fig. 27, where the initial and final hadron (parton) helicities are denoted as Λ_i and Λ_f (λ_i and λ_f). The helicity conservation yields $\Lambda_i - \lambda_i = \Lambda_f - \lambda_f$. The quark densities (38) are expressed in terms of helicity amplitudes as follows:

$$\begin{aligned} g_1^q(x) &= q_+(x) - q_-(x) \sim \text{Im}(A_{+,+,+} - A_{+,-,-}), \\ h_1^q(x) &= q_\uparrow(x) - q_\downarrow(x) \sim \text{Im} A_{+,+,-}. \end{aligned} \quad (39)$$

The density $g_1^q(x)$ is determined by the distributions $q_+(x)$ and $q_-(x)$ which describe the quarks with spin oriented parallel and anti-parallel to the longitudinal nucleon spin, as shown in Fig. 28(a). The quark transversity distribution is given by $h_1^q(x) = q_\uparrow(x) - q_\downarrow(x)$, where subscripts “ \uparrow ” and “ \downarrow ” indicate the quark polarizations which are parallel and anti-parallel to the transverse nucleon spin, as illustrated in Fig. 28(b). The relation $h_1^q(x) \sim \text{Im} A_{+,+,-}$ indicates that the quark transversity distribution in a nucleon is described by the helicity-flip ($\lambda_i = +, \lambda_f = -$) amplitude. Note that the density $g_1^q(x)$ is a chiral-even function while the distribution $h_1^q(x)$ is a chiral-odd one.

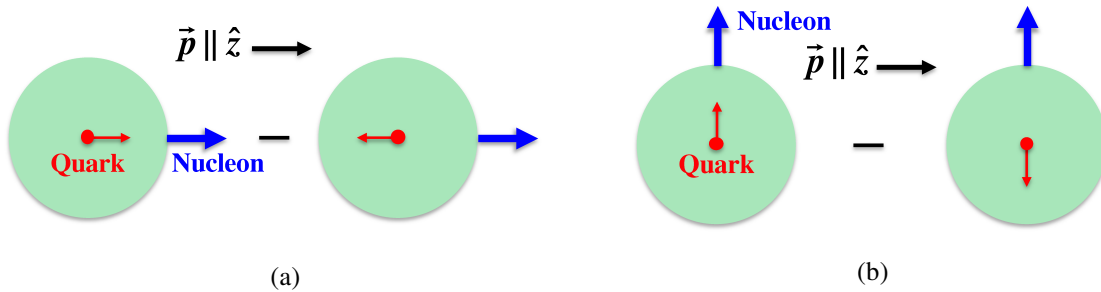


Figure 28: Schematic illustration for quark helicity (a) and transversity (b) distribution functions.

¹³In the case of the transversely polarized deuteron, one also needs to account for the contributions of the transverse and tensor spin components, see Table 6 and discussion below.

¹⁴Functions g_1^q and h_1^q are also referred to as $\mathcal{A}q(x)$ and $\mathcal{A}_T q(x)$ correspondingly.

.5 We see that the helicity and transversity functions, $g_1^q(x)$ and $h_1^q(x)$, have completely different nature and properties. For this reason, their contributions to the spin asymmetries differ essentially from each other. Possible way to access the transversity are measurements of single transverse spin asymmetries in lepton-proton and proton-proton collisions with interference dihadron fragmentation function used as a chiral-odd probe [329].

The transversity PDF may also be studied through the measurement of the double transverse spin asymmetry, A_{TT} , defined analogously to the double longitudinal spin asymmetry, A_{LL} . This is a unique opportunity for SPD NICA, where transverse polarization of both colliding beams will be available. Due to the absence of transversity gluon contributions, the transverse asymmetries in pp collisions are expected to be much smaller than the longitudinal ones, $A_{TT} \ll A_{LL}$. As an example, the asymmetry A_{TT}^γ in the prompt-photon production at 200 and 500 GeV coming from the $q\bar{q}$ annihilation process calculated in LO [327] and NLO [328] is shown in Fig. 29. Predicted values for the quantity A_{TT}^γ are of the order of one per cent. On the other hand, in case of pd or dd collisions a measurable value of A_{TT} could be expected in case of presence of sizable contributions of non-nucleon degrees of freedom in deuteron.

Note that the quark transversity distributions play important role in correct interpretation of data on the neutron electric dipole moment (EDM), which is used in search for physics beyond the standard model (BSM). The current experimental lower bound of the neutron EDM is close to the typical BSM predictions, 10^{-28} – 10^{-26} e·cm. For more accurate comparison with data, one needs to convert the quark-level BSM results for EDMs to the neutron one by using the quark transversity distributions [326]: $d_n = \sum_q d_q h_1^q$, where $h_1^q \equiv \int_0^1 dx [h_1^q(x) - \bar{h}_1^q(x)]$ and d_q is the quark EDM.

Let us discuss the polarized gluon distributions in the deuteron. The spin-1 states are described by the polarization vectors \mathbf{E} defined as

$$\mathbf{E}_\pm = \frac{1}{\sqrt{2}}(\mp 1, -i, 0), \quad \mathbf{E}_0 = (0, 0, 1), \quad \mathbf{E}_x = (1, 0, 0), \quad \mathbf{E}_y = (0, 1, 0). \quad (40)$$

The vectors \mathbf{E}_+ , \mathbf{E}_0 , and \mathbf{E}_- correspond to the spin states with z component equal to $s_z = +1, 0$, and -1 ; \mathbf{E}_x and \mathbf{E}_y describe the linear polarization. The vector, \mathbf{S} , and tensor, T^{ij} , polarizations of a spin-1 particle can be expressed in terms of vectors \mathbf{E} as

$$\mathbf{S} = \text{Im}(\mathbf{E}^* \times \mathbf{E}), \quad T^{ij} = \frac{1}{3} \delta^{ij} - \text{Re}(\mathbf{E}^{i*} \mathbf{E}^j). \quad (41)$$

We parameterize these polarizations in the form

$$\mathbf{S} = (S_T^x, S_T^y, S_L), \quad T^{ij} = \frac{1}{2} \begin{pmatrix} -\frac{2}{3}S_{LL} + S_{TT}^{xx} & S_{TT}^{xy} & S_{LT}^x \\ S_{TT}^{xy} & -\frac{2}{3}S_{LL} - S_{TT}^{xx} & S_{LT}^y \\ S_{LT}^x & S_{LT}^y & \frac{4}{3}S_{LL} \end{pmatrix}, \quad (42)$$

where $\{S_T^x, S_T^y, S_L, S_{LL}, S_{TT}^{xx}, S_{TT}^{xy}, S_{LT}^x, S_{LT}^y\}$ is the full set of parameters describing the vector and tensor polarizations.

For example, in the case of the polarization vector \mathbf{E}_+ , Eqs. (41) lead to the following set of parameters:

$$S_L = 1, \quad S_{LL} = 1/2, \quad S_T^x = S_T^y = S_{TT}^{xx} = S_{TT}^{xy} = S_{LT}^x = S_{LT}^y = 0. \quad (43)$$

The parameters of longitudinal, transverse, and linear polarizations of a spin-1 particle are listed in Table 6. The polarization \mathbf{E}_+ means that the spin is directed along z axis, $S_L = 1$. Note however that this polarization can also be described by the tensor parameter $S_{LL} = 1/2$.

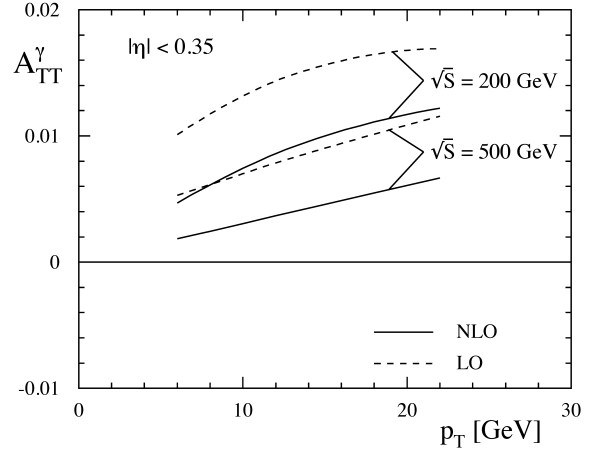


Figure 29: A_{TT}^γ asymmetry for the prompt-photon production at 200 and 500 GeV coming from the $q\bar{q}$ annihilation process calculated in LO [327] and NLO [328]. Adapted figure from [328] ©(2003) by the American Physical Society.

Polarizations	E	S_T^x	S_T^y	S_L	S_{LL}	S_{TT}^{xx}
Longitudinal $+z$	$\frac{1}{\sqrt{2}}(-1, -i, 0)$	0	0	+1	$+\frac{1}{2}$	0
Longitudinal $-z$	$\frac{1}{\sqrt{2}}(+1, -i, 0)$	0	0	-1	$+\frac{1}{2}$	0
Transverse $+x$	$\frac{1}{\sqrt{2}}(0, -1, -i)$	+1	0	0	$-\frac{1}{4}$	$+\frac{1}{2}$
Transverse $-x$	$\frac{1}{\sqrt{2}}(0, +1, -i)$	-1	0	0	$-\frac{1}{4}$	$+\frac{1}{2}$
Transverse $+y$	$\frac{1}{\sqrt{2}}(-i, 0, -1)$	0	+1	0	$-\frac{1}{4}$	$-\frac{1}{2}$
Transverse $-y$	$\frac{1}{\sqrt{2}}(-i, 0, +1)$	0	-1	0	$-\frac{1}{4}$	$-\frac{1}{2}$
Linear x	(1, 0, 0)	0	0	0	$+\frac{1}{2}$	-1
Linear y	(0, 1, 0)	0	0	0	$+\frac{1}{2}$	+1

Table 6: Longitudinal, transverse, and linear polarizations of the deuteron: vectors E and parameters of the vector, S , and tensor, T^{ij} , polarizations. All other parameters vanish for the considered cases, $S_{TT}^{xy} = S_{LT}^x = S_{LT}^y = 0$.

As mentioned above, the gluon transversity distribution is forbidden in the spin-1/2 nucleons; it however may contribute to a spin-1 hadron [330]. Similarly to the quark distribution (39), the gluon transversity¹⁵ is given by the helicity-flip amplitude:

$$h_1^g(x) \sim \text{Im} A_{+, -, -} . \quad (44)$$

We see that the function $h_1^g(x)$ is associated with the spin flip $\Delta s = 2$ amplitude as shown in Fig. 30. Therefore, in search for the gluon transversity, one should use hadrons with spin ≥ 1 . The most appropriate candidate is the deuteron: it is stable and can be polarized.

The gluon transversity distribution in the deuteron is defined in the matrix-element form as

$$h_1^g(x) = \varepsilon_{TT}^{\alpha\beta} \int \frac{d\xi^-}{2\pi} x p^+ e^{i x p^+ \xi^-} \langle p E_x | A_\alpha(0) A_\beta(\xi) | p E_x \rangle_{\xi^+ = \xi_1 = 0}, \quad (45)$$

where E_x describes the linear polarization of the deuteron along the positive x -axis. The tensor $\varepsilon_{TT}^{\alpha\beta}$ in Eq. (45) is defined by $\varepsilon_{TT}^{\alpha\beta} \equiv \varepsilon_x^\alpha \varepsilon_x^{\beta*} - \varepsilon_y^\alpha \varepsilon_y^{\beta*}$, where $\varepsilon_{x,y}^\alpha = (0, \varepsilon_{x,y})$ describe the linearly polarized gluons in the deuteron. So, one needs the linearly polarized deuteron target (or beam) for measuring the gluon transversity $h_1^g(x)$. As shown in Refs. [326, 331], measurements of the difference of cross-sections with the deuteron linearly polarized in "x" and "y" directions, $d\sigma(E_x) - d\sigma(E_y)$, will allow to determine the function $h_1^g(x)$.

Presently, experimental data on the gluon transversity are not available. There is only the JLab Letter of Intent [332] which proposes to measure $h_1^g(x)$ in the electron scattering off polarized deuteron [333]. The gluon-induced Drell-Yan process $qg \rightarrow q\gamma^* \rightarrow q\mu^+\mu^-$ was also proposed in Refs. [326, 331] as a way to access $h_1^g(x)$ in polarized pd collisions in the SpinQuest experiment at Fermilab [334].

In Fig. 31, we present predictions for the asymmetry $A_{E_y} = [d\sigma(E_x) - d\sigma(E_y)]/[d\sigma(E_x) + d\sigma(E_y)]$ in the pd Drell-Yan process with unpolarized proton as a function of $M_{\mu\mu}^2$. The results are given for the di-muon transverse momenta $q_T = 0.2, 0.5, \text{ and } 1.0$ GeV at the azimuthal angle $\phi = 0$ and rapidity $y = 0$. Note that, in these predictions, the gluon transversity is assumed to be equal to the longitudinally polarized gluon distribution. For this reason, the asymmetry $|A_{E_y}|$ presented in Fig. 31 may be overestimated. At NICA, the J/ψ production in pd and dd collisions with a linearly polarized deuteron can be used to access the gluon transversity. The asymmetry A_{E_y} in these processes is expected to be of the same order of magnitude, i.e. of the order of one per cent.

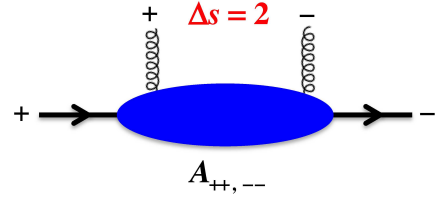


Figure 30: Gluon-hadron forward scattering amplitude with the spin flip of 2.

¹⁵Denoted as h_1^g or $A_T g$.

In the above examples, the single spin asymmetry in the reactions with linearly polarized deuterons was discussed. In principle, non-vanishing contributions of the gluon transversity $h_1^g(x)$ to the double transverse spin asymmetry, A_{TT} , are also possible. However, in the case of A_{TT} , one should take into account two more types of contributions: quark and anti-quark transversities and tensor-polarized PDFs. For this reason, the single spin asymmetry in the processes with linearly polarized deuterons, $A_{E_{xy}}$, seems to be most direct way to probe the function $h_1^g(x)$ [326, 331].

5.4. Tensor-polarized gluon distribution in deuteron

The polarized ep DIS is described in terms of four structure functions ($F_{1,2}$, $g_{1,2}$), whereas the ed DIS contains eight functions. The additional four structure functions, b_{1-4} , can be measured using an unpolarized lepton beam [335, 336]. Among them, b_1 and b_2 are twist-2 structure functions which are related to each other by the Callan-Gross type relation $b_2 = 2xb_1$, while b_3 and b_4 are higher-twist ones. In the LO in α_s , the b_1 (and b_2) structure function can be expressed in terms of tensor-polarized quark and anti-quark distribution functions $\delta_\tau q$ and $\delta_\tau \bar{q}$ as

$$b_1(x, Q^2)_{\text{LO}} = \frac{1}{2} \sum_i e_i^2 [\delta_\tau q_i(x, Q^2) + \delta_\tau \bar{q}_i(x, Q^2)]. \quad (46)$$

The tensor-polarized PDFs are defined by

$$\delta_\tau f(x, Q^2) \equiv f^0(x, Q^2) - \frac{f^{+1}(x, Q^2) + f^{-1}(x, Q^2)}{2}, \quad (f = q, \bar{q}, \text{ or } g), \quad (47)$$

where f^λ indicates an unpolarized parton distribution in the hadron spin state " λ ". In practice, the deuteron is best suited for measuring b_1 because it is stable and simplest spin-one hadron. In the framework of the parton model, the following sum rule was derived [337, 338]:

$$\int dx b_1(x)_{\text{LO}} = -\frac{5}{24} \lim_{t \rightarrow 0} t F_Q(t) + \sum_i e_i^2 \int dx \delta_\tau \bar{q}_i(x), \quad (48)$$

where $F_Q(t)$ is the electric quadrupole form factor of the considered hadron. Since the first term vanishes, non-zero values of b_1 could indicate nonvanishing tensor-polarized anti-quark distributions. Eq. (48) is an analogue of the Gottfried sum rule which was derived for the unpolarized ep DIS [339, 340]:

$$\int \frac{dx}{x} [F_2^p(x) - F_2^n(x)]_{\text{LO}} = \frac{1}{3} + \frac{2}{3} \int dx [\bar{u}(x) - \bar{d}(x)]. \quad (49)$$

This sum rule indicates that the light anti-quark distributions \bar{u} and \bar{d} are not identical if Eq. (49) deviates from 1/3. The first terms in r.h.s. of Eqs.(48) and (49) (0 and 1/3, respectively) differ essentially from each other because the number of valence quarks depends on the flavor but is independent of the tensor polarization. The deviation of the sum rule (49) from 1/3 was experimentally confirmed by the New Muon Collaboration (NMC) [341, 342] and later pp and pd Drell-Yan measurements [343–345]. Since large deviation from 1/3 cannot be explained within the perturbative QCD, the NMC result created a new field of hadron physics related to the flavor-asymmetric anti-quark distributions [340, 346, 347]. Similarly, a new field of tensor-polarized anti-quark distributions could be created if the b_1 sum (48) will be non-zero. Such an indication was obtained in the HERMES experiment, $\int dx b_1(x) = 0.35 \pm 0.10(\text{stat}) \pm 0.18(\text{sys})$ [250]. Furthermore, the conventional convolution calculations of b_1 based on the standard deuteron model are very different from the HERMES measurements [250] in magnitude and x dependence [348].

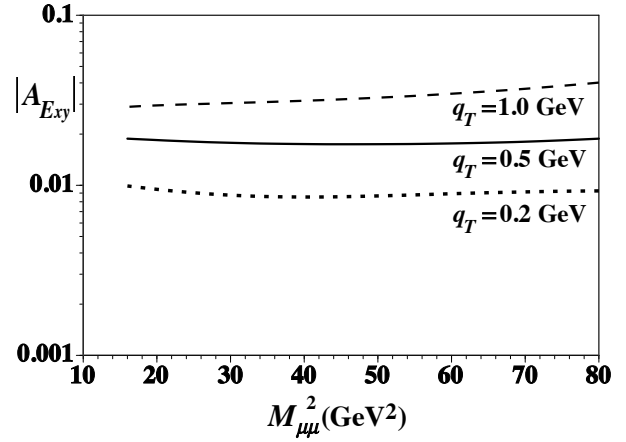


Figure 31: Spin asymmetry $|A_{E_{xy}}|$ for the proton-deuteron Drell-Yan process.

The tensor-polarized quark and anti-quark distributions were fitted to the HERMES data in Ref. [349]. The obtained results for the quark and anti-quark densities at $Q^2 = 2.5 \text{ GeV}^2$ (the averaged value of the HERMES measurements) are shown in Fig. 32 by dashed curves. Since experimental information on the gluon tensor polarization is presently unavailable, $\delta_T g = 0$ for $Q^2 = 2.5 \text{ GeV}^2$ has been assumed. However the tensor-polarized PDFs satisfy the same standard DGLAP evolution equations as the unpolarized ones [336, 350]. Due to this evolution, a non-zero tensor-polarized gluon distribution will appear at large values of Q^2 even if it does not exist at small Q^2 . The DGLAP predictions for $\delta_T f$ ($f = q, \bar{q}, g$) at $Q^2 = 30 \text{ GeV}^2$ are given in Fig. 32 by solid curves.

Further experimental studies of b_1 will be performed at JLab [351]. The tensor-polarized deuteron target for this experiment is under development [333]. Tensor-polarized quark and anti-quark distributions could be probed at Fermilab [334] using the proton-deuteron Drell-Yan process [350, 352, 353]. The tensor-polarized gluon distribution could be studied at NICA using the tensor-polarized deuteron in prompt-photon and J/ψ production processes.

5.5. Deuteron tensor polarization and shear forces

The availability of tensor polarized deuteron beam opens a possibility to study shear forces generated by quarks and gluons [354]. The natural way to get the traceless part of the energy-momentum tensor related to a shear is provided just by the tensor polarization, as the relevant tensor $S^{\mu\nu}$ is a traceless one by construction. The contribution of the "tensor-polarized" parton distribution C^T [336, 337] (introduced as an "aligned" one [355]) is constrained by the zero sum rule [355] for its second moment (complementing the Close-Kumano sum rule [337]) which may be decomposed into quark and gluon components [356]:

$$\sum_{i=q,\bar{q}} \int_0^1 \delta_{Ti}(x, Q^2) x dx = \delta_T(Q^2), \quad (50)$$

$$\int_0^1 \delta_{TG}(x, Q^2) x dx = -\delta_T(Q^2). \quad (51)$$

As a result, the matrix elements of the energy momentum tensors of quarks and gluons look as

$$\sum_i \langle P, S | T_i^{\mu\nu} | P, S \rangle_{Q^2} = 2P^\mu P^\nu (1 - \delta(Q^2)) + 2m_N^2 S^{\mu\nu} \delta_T(Q^2) \quad (52)$$

$$\langle P, S | T_g^{\mu\nu} | P, S \rangle_{\mu^2} = 2P^\mu P^\nu \delta(Q^2) - 2m_N^2 S^{\mu\nu} \delta_T(Q^2), \quad (53)$$

where the second terms describe the average (integrated over transverse distance) shear force. Here m_N is the nucleon mass.

The zero sum rules (50) were later interpreted [357] as yet another manifestation of Equivalence Principle (EP), as it was done earlier [358] for the Ji sum rules. In turn, the smallness of δ_T , compatible with the existing HERMES data, was suggested [357] to be the new manifestation of the Extended Equivalence Principle (ExEP) [359–361] valid separately for quarks and gluons in non-perturbative QCD due to the confinement and chiral symmetry violation. It was originally suggested for anomalous gravitomagnetic moments [359, 361]. In particular, it provides the rotation of spin in a terrestrial experiment with the angular velocity of Earth's rotation. Let us stress, that it may seem trivial if spin is considered just as a vector. However, it became highly non-trivial if one takes into account that the device which measures the spin is rotating together with Earth. This is a particular example of the practical importance of the quantum theory of measurement. Another example may be represented by the Unruh radiation in heavy-ion collisions [362], which implies that the particles production may be also considered as a quantum-mechanical measurement in a non-inertial hadronic medium.

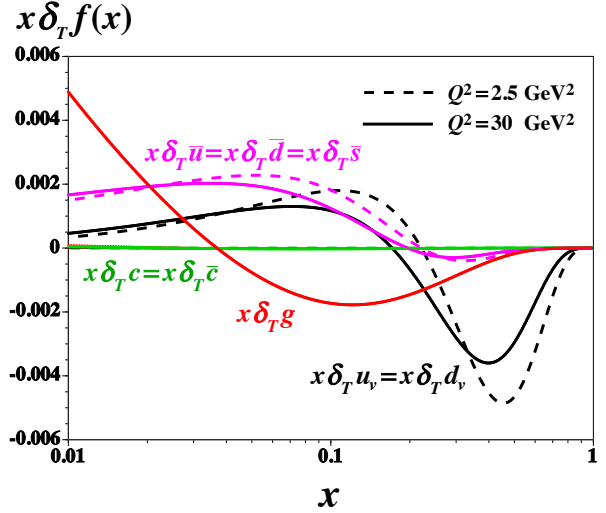


Figure 32: Q^2 evolution of the tensor-polarized PDFs.

Recently, ExEP was also discovered for the pressure [363].

To check ExEP for the shear force, one may use future studies of DIS at JLab and of Drell-Yan processes with tensor polarized deuterons [364]¹⁶.

Note that tensor polarized parton distribution may be also measured in *any* hard process with the relevant combination of deuteron polarizations, in particular, for large p_T pion production, providing much better statistics. The correspondent quantity can be the P-even single spin asymmetry

$$A_T = \frac{d\sigma(+)+d\sigma(-)-2d\sigma(0)}{d\sigma(+)+d\sigma(-)+d\sigma(0)} \sim \frac{\sum_{i=q,\bar{q},g} \int d\hat{\sigma}_i \delta_{Ti}(x)}{\sum_{i=q,\bar{q},g} \int d\hat{\sigma}_i f_i(x)}, \quad (54)$$

where the differential cross-section with a definite deuteron polarization appears.

Note that since the polarization tensor is traceless, the sum rule is valid for the three mutually orthogonal orientations of coordinate frame [355]:

$$\sum_i \rho_{00}^i = 1; \quad \sum_i S_{ii} = 0. \quad (55)$$

As a result, the leading twist kinematically dominant "longitudinal" tensor polarization can be obtained by accelerating *transversely* polarized deuterons which will be accessible at NICA.

6. Summary

In this Review we have discussed theoretical aspects of past and possible future measurements related to the study of the (un)polarized gluon content of the proton and deuteron, particularly focusing on the opportunities opening for the future Spin Physics Detector project at the NICA collider in Dubna. Proposed measurements at SPD are foreseen to be carried out performing a high-luminosity p - p , p - d and d - d collisions at the center-of-mass energy up to 27 GeV using longitudinally or transversely polarized proton and vector- or tensor-polarized deuteron beams. The SPD will have a unique possibility to probe gluon content employing simultaneously three gluon-induced processes: the inclusive production of charmonia (J/ψ and higher states), open charm production, and production of the prompt photons. The kinematic region to be covered by the SPD is unique and has never been accessed purposefully in polarized hadronic collisions. The data are expected to provide inputs for gluon physics, mostly in the region around $x \sim 0.1$ and above. The expected event rates for all three aforementioned production channels are sizable in the discussed kinematic range and the experimental setup is being designed to increase the registration efficiency for the final states of interest.

Despite certain phenomenological difficulties currently present in the heavy quarkonium production theory, charmonium production is an invaluable tool to study the gluon content of (un)polarized protons. Future measurements at the NICA SPD will provide complementary inputs for the study of heavy-quarkonium production mechanisms and explicit hadron structure aspects. In particular, SPD data should help to validate and constrain different theoretical models available on the market.

Precise data on the total cross-section of the open charm production at energies not so far from the production threshold should significantly reduce the present uncertainties in the c -quark mass and α_s at a GeV scale. This will essentially improve description of the processes with charmed particles in the framework of perturbative QCD. Measuring the $c\bar{c}$ pair production with large enough invariant mass, we will probe the gluon density at high values of x . Detailed information on the gluon distribution at large x is very important for various phenomenological applications: from infrared renormalon ambiguities in cross-sections to intrinsic charm content of the proton.

One of the important measurements would be the extraction of the classic double longitudinal spin asymmetry A_{LL} , which provides access to the gluon helicity function $\Delta g(x)$. Due to the quadratic dependence of the asymmetry on $\Delta g(x)$ in the charm production process and linear dependence in case of the prompt-photon production, the corresponding measurements at SPD will be highly complementary and will help to determine both the sign and the size of the gluon polarization.

A special attention should be drawn to the TMD observables. In particular, both the unpolarized gluon distribution and the gluon Boer-Mulders functions can be probed in (un)polarized collisions at SPD. The gluon Sivers function $\Delta_N^g(x, k_T)$ and higher-twist effects are planned to be studied via measurements of the single transverse spin asymmetry A_N . Due to the relatively small \sqrt{s} , the SPD results will provide inputs for the investigation of possible

¹⁶Complementary probes are provided by vector mesons [360].

application of the TMD factorization approach in the region of relatively large x . This, in turn, is related to gluonic contribution in the valence region to spin structure of particular hadrons and nuclei (protons and deuterons).

Unpolarized gluon content of the deuteron can be studied from the explicit comparison of the differential cross-sections for the p - p and d - d collisions for each of the probes. The effects related to possible non-nucleonic degrees of freedom and the Fermi motion can be investigated at high x . Exploration of the deuteron, the simplest nuclear system, is a bridge to another physics program at NICA – the study of hot and dense hadronic matter in heavy-ion collisions [365]. The single spin asymmetry in pd collisions with linearly polarized deuterons, and the double transverse spin asymmetry A_{TT} in dd reactions provide unique opportunities to access for the first time the gluon transversity function $h_1^g(x)$. The J/ψ and prompt-photon production measurements with tensor-polarized deuterons at the SPD would help to determine the tensor-polarized gluon distribution.

Main proposed measurements to be carried out at the SPD are summarized in Table 7.

Table 7: Study of the gluon content in proton and deuteron at SPD.

Physics goal	Observable	Experimental conditions
Gluon helicity $\Delta g(x)$	A_{LL} asymmetries	p_L - p_L , $\sqrt{s} = 27$ GeV
Gluon Sivers PDF $f_{1T}^{\perp g}(x, k_T^2)$, Gluon Boer-Mulders PDF $h_1^{\perp g}(x, k_T^2)$ TMD-factorization test	A_N asymmetries, Azimuthal asymmetries Diff. cross-sections, A_N asymmetries	p_T - p , $\sqrt{s} = 27$ GeV p - p , $\sqrt{s} = 27$ GeV p_T - p , energy scan
Unpolarized gluon density $g(x)$ in deuteron Unpolarized gluon density $g(x)$ in proton	Differential cross-sections	d - d , p - p , p - d $\sqrt{s_{NN}} = 13.5$ GeV p - p , $\sqrt{s} \leq 27$ GeV
Gluon transversity $h_1^g(x)$ "Tensor polarized" PDF $C_G^T(x)$	Double vector/tensor asymmetries Single vector/tensor asymmetries	d_{tensor} - d_{tensor} , $\sqrt{s_{NN}} = 13.5$ GeV d_{tensor} - d , p - d_{tensor}

The study of the gluon content in the proton and deuteron at NICA SPD will serve as an important contribution to our general understanding of the spin structure of hadrons and QCD fundamentals. The expected inputs from the SPD will be highly complementary to the ongoing and planned measurements at RHIC, and future facilities such as EIC at BNL and fixed-target LHC projects at CERN.

The physics program of the SPD facility is open for exciting and challenging ideas from theorists and experimentalists worldwide.

Acknowledgements

We thank D. Boer and all participants of the workshop "Gluon content of proton and deuteron with the Spin Physics Detector at the NICA collider" for useful and inspiring discussions. M.G.E. is supported by the Spanish MICINN grant PID2019-106080GB-C21. M.N. and V.S. are supported by the Ministry of education and science of Russia via the State assignment to educational and research institutions under project FSSS-2020-0014.

References

- [1] A. Kotzinian, Nucl. Phys. B **441**, 234 (1995), [hep-ph/9412283](#).
- [2] P. Mulders and R. Tangerman, Nucl. Phys. B **461**, 197 (1996), [Erratum: Nucl.Phys.B 484, 538–540 (1997)], [hep-ph/9510301](#).
- [3] D. Boer and P. Mulders, Phys. Rev. D **57**, 5780 (1998), [hep-ph/9711485](#).
- [4] K. Goeke, A. Metz, and M. Schlegel, Phys. Lett. B **618**, 90 (2005), [hep-ph/0504130](#).
- [5] A. Bacchetta, M. Diehl, K. Goeke, A. Metz, P. J. Mulders, and M. Schlegel, JHEP **02**, 093 (2007), [hep-ph/0611265](#).
- [6] R. Angeles-Martinez et al., Acta Phys. Polon. B **46**, 2501 (2015), [1507.05267](#).
- [7] M. Anselmino, M. Boglione, U. D'Alesio, S. Melis, F. Murgia, E. R. Nocera, and A. Prokudin, Phys. Rev. D **83**, 114019 (2011), [1101.1011](#).
- [8] S. Bastami et al., JHEP **06**, 007 (2019), [1807.10606](#).

- [9] S. Arnold, A. Metz, and M. Schlegel, Phys. Rev. D **79**, 034005 (2009), [0809.2262](#).
- [10] S. Bastami, L. Gamberg, B. Parsamyan, B. Pasquini, A. Prokudin, and P. Schweitzer (2020), [2005.14322](#).
- [11] A. Metz and A. Vossen, Prog. Part. Nucl. Phys. **91**, 136 (2016), [1607.02521](#).
- [12] M. Anselmino, A. Mukherjee, and A. Vossen (2020), [2001.05415](#).
- [13] H. Avakian, B. Parsamyan, and A. Prokudin, Riv. Nuovo Cim. **42**, 1 (2019), [1909.13664](#).
- [14] M. Grosse Perdekamp and F. Yuan, Ann. Rev. Nucl. Part. Sci. **65**, 429 (2015), [1510.06783](#).
- [15] M. Boglione and A. Prokudin, Eur. Phys. J. A **52**, 154 (2016), [1511.06924](#).
- [16] C. A. Aidala, S. D. Bass, D. Hasch, and G. K. Mallot, Rev. Mod. Phys. **85**, 655 (2013), [1209.2803](#).
- [17] J.-P. Lansberg, C. Pisano, and M. Schlegel, Nucl. Phys. **B920**, 192 (2017), [1702.00305](#).
- [18] F. Scarpa, D. Boer, M. G. Echevarria, J.-P. Lansberg, C. Pisano, and M. Schlegel, Eur. Phys. J. C **80**, 87 (2020), [1909.05769](#).
- [19] N. Abdulov, A. Lipatov, G. Lykasov, and M. Malyshev, EPJ Web Conf. **204**, 05010 (2019).
- [20] U. D’Alesio, F. Murgia, C. Pisano, and P. Taels, Phys. Rev. **D100**, 094016 (2019), [1908.00446](#).
- [21] U. D’Alesio, L. Maxia, F. Murgia, C. Pisano, and S. Rajesh, Phys. Rev. D **102**, 094011 (2020), [2007.03353](#).
- [22] U. D’Alesio, F. Murgia, C. Pisano, and P. Taels, Phys. Rev. **D96**, 036011 (2017), [1705.04169](#).
- [23] A. Bacchetta, F. G. Celiberto, M. Radici, and P. Taels, Eur. Phys. J. C **80**, 733 (2020), [2005.02288](#).
- [24] A. Adare et al. (PHENIX), Phys. Rev. D **90**, 012006 (2014), [1312.1995](#).
- [25] A. Adare et al. (PHENIX), Phys. Rev. D **82**, 112008 (2010), [Erratum: Phys.Rev.D 86, 099904 (2012)], [1009.4864](#).
- [26] C. Aidala et al. (PHENIX), Phys. Rev. D **98**, 012006 (2018), [1805.01491](#).
- [27] C. Aidala et al. (PHENIX), Phys. Rev. D **95**, 112001 (2017), [1703.09333](#).
- [28] C. Adolph et al. (COMPASS), Phys. Lett. B **772**, 854 (2017), [1701.02453](#).
- [29] A. Szabelski (COMPASS), PoS **DIS2016**, 219 (2016).
- [30] M. Garcon and J. W. Van Orden, Adv. Nucl. Phys. **26**, 293 (2001), [nucl-th/0102049](#).
- [31] J. J. Aubert et al. (European Muon), Phys. Lett. B **123**, 275 (1983).
- [32] V. Barone, A. Drago, and P. G. Ratcliffe, Phys. Rept. **359**, 1 (2002), [hep-ph/0104283](#).
- [33] S. J. Brodsky, F. Fleuret, C. Hadjidakis, and J. P. Lansberg, Phys. Rept. **522**, 239 (2013), [1202.6585](#).
- [34] C. Hadjidakis et al. (2018), [1807.00603](#).
- [35] C. A. Aidala et al., PoS **DIS2019**, 233 (2019), [1901.08002](#).
- [36] A. Accardi et al., Eur. Phys. J. **A52**, 268 (2016), [1212.1701](#).
- [37] I. Savin et al., EPJ Web Conf. **85**, 02039 (2015), [1408.3959](#).
- [38] R. Tsenov (SPD project team), PoS **SPIN2018**, 163 (2019).
- [39] A. Guskov (SPD Working Group), JPS Conf. Proc. **26**, 021018 (2019), [1904.04779](#).
- [40] The SPD project at JINR (2020).
- [41] I. N. Meshkov, Phys. Part. Nucl. **50**, 663 (2019).
- [42] V. M. Abazov et al. (2021), [2102.00442](#).
- [43] E. R. Nocera, R. D. Ball, S. Forte, G. Ridolfi, and J. Rojo (NNPDF), Nucl. Phys. **B887**, 276 (2014), [1406.5539](#).
- [44] C. Brenner Mariotto, M. B. Gay Ducati, and G. Ingelman, Eur. Phys. J. **C23**, 527 (2002), [hep-ph/0111379](#).
- [45] Run overview of the relativistic heavy ion collider (2020).
- [46] I. Abt et al. (HERA-B), Phys. Rev. D **79**, 012001 (2009), [0807.2167](#).
- [47] A. Adare et al. (PHENIX), Phys. Rev. D **85**, 092004 (2012), [1105.1966](#).
- [48] J.-P. Lansberg, Phys. Rept. **889**, 1 (2020), [1903.09185](#).
- [49] A. Andronic et al., Eur. Phys. J. **C76**, 107 (2016), [1506.03981](#).
- [50] N. Brambilla et al., Eur. Phys. J. C **71**, 1534 (2011), [1010.5827](#).
- [51] J. P. Lansberg, Int. J. Mod. Phys. **A21**, 3857 (2006), [hep-ph/0602091](#).
- [52] J. P. Leveille and T. J. Weiler, Nucl. Phys. B **147**, 147 (1979).
- [53] P. Aurenche, M. Fontannaz, J.-P. Guillet, E. Pilon, and M. Werlen, Phys. Rev. **D73**, 094007 (2006), [hep-ph/0602133](#).
- [54] A. V. Karpishkov, M. A. Nefedov, and V. A. Saleev, Phys. Rev. D **96**, 096019 (2017), [1707.04068](#).
- [55] C.-Y. Wong and H. Wang, Phys. Rev. C **58**, 376 (1998), [hep-ph/9802378](#).
- [56] T. Binoth, J. Guillet, E. Pilon, and M. Werlen, Eur. Phys. J. C **16**, 311 (2000), [hep-ph/9911340](#).
- [57] L. Apanasevich et al. (Fermilab E706), Phys. Rev. Lett. **81**, 2642 (1998), [hep-ex/9711017](#).
- [58] E. Anassontzis et al., Z. Phys. C **13**, 277 (1982).
- [59] W. Vogelsang and M. R. Whalley, J. Phys. **G23**, A1 (1997).
- [60] J. Badier et al. (NA3), Phys. Lett. B **164**, 184 (1985).
- [61] P. J. Mulders and J. Rodrigues, Phys. Rev. **D63**, 094021 (2001), [hep-ph/0009343](#).
- [62] S. Meissner, A. Metz, and K. Goetze, Phys. Rev. **D76**, 034002 (2007), [hep-ph/0703176](#).
- [63] C. Lorce’ and B. Pasquini, JHEP **09**, 138 (2013), [1307.4497](#).
- [64] D. Boer, S. Cotogno, T. van Daal, P. J. Mulders, A. Signori, and Y.-J. Zhou, JHEP **10**, 013 (2016), [1607.01654](#).
- [65] J. J. Ethier and E. R. Nocera, Ann. Rev. Nucl. Part. Sci. pp. 1–34 (2020), [2001.07722](#).
- [66] G. Bozzi, S. Catani, D. de Florian, and M. Grazzini, Phys. Lett. B **564**, 65 (2003), [hep-ph/0302104](#).
- [67] S. Catani and M. Grazzini, Nucl. Phys. B **845**, 297 (2011), [1011.3918](#).
- [68] M. G. Echevarria, T. Kasemets, P. J. Mulders, and C. Pisano, JHEP **07**, 158 (2015), [Erratum: JHEP05,073(2017)], [1502.05354](#).
- [69] D. Boer, S. J. Brodsky, P. J. Mulders, and C. Pisano, Phys. Rev. Lett. **106**, 132001 (2011), [1011.4225](#).
- [70] P. Sun, B.-W. Xiao, and F. Yuan, Phys. Rev. **D84**, 094005 (2011), [1109.1354](#).
- [71] D. Boer, W. J. den Dunnen, C. Pisano, M. Schlegel, and W. Vogelsang, Phys. Rev. Lett. **108**, 032002 (2012), [1109.1444](#).
- [72] C. Pisano, D. Boer, S. J. Brodsky, M. G. Buffing, and P. J. Mulders, JHEP **10**, 024 (2013), [1307.3417](#).
- [73] W. J. den Dunnen, J. P. Lansberg, C. Pisano, and M. Schlegel, Phys. Rev. Lett. **112**, 212001 (2014), [1401.7611](#).
- [74] D. Kharzeev, Y. V. Kovchegov, and K. Tuchin, Phys. Rev. D **68**, 094013 (2003), [hep-ph/0307037](#).
- [75] F. Dominguez, B.-W. Xiao, and F. Yuan, Phys. Rev. Lett. **106**, 022301 (2011), [1009.2141](#).
- [76] F. Dominguez, C. Marquet, B.-W. Xiao, and F. Yuan, Phys. Rev. D **83**, 105005 (2011), [1101.0715](#).
- [77] T. C. Rogers, Phys. Rev. D **88**, 014002 (2013), [1304.4251](#).
- [78] C. Bomhof, P. Mulders, and F. Pijlman, Eur. Phys. J. C **47**, 147 (2006), [hep-ph/0601171](#).

- [79] J.-P. Lansberg, C. Pisano, F. Scarpa, and M. Schlegel, Phys. Lett. B **784**, 217 (2018), [Erratum: Phys.Lett.B 791, 420–421 (2019)], [1710.01684](#).
- [80] D. Gutierrez-Reyes, S. Leal-Gomez, I. Scimemi, and A. Vladimirov, JHEP **11**, 121 (2019), [1907.03780](#).
- [81] U. D'Alesio, C. Flore, F. Murgia, C. Pisano, and P. Tael, Phys. Rev. D **99**, 036013 (2019), [1811.02970](#).
- [82] V. S. Fadin, E. Kuraev, and L. Lipatov, Phys. Lett. B **60**, 50 (1975).
- [83] E. A. Kuraev, L. N. Lipatov, and V. S. Fadin, Sov. Phys. JETP **44**, 443 (1976).
- [84] E. Kuraev, L. Lipatov, and V. S. Fadin, Sov. Phys. JETP **45**, 199 (1977).
- [85] I. Balitsky and L. Lipatov, Sov. J. Nucl. Phys. **28**, 822 (1978).
- [86] M. Hentschinski, A. Sabio Vera, and C. Salas, Phys. Rev. Lett. **110**, 041601 (2013), [1209.1353](#).
- [87] A. Besse, L. Szymanowski, and S. Wallon, JHEP **11**, 062 (2013), [1302.1766](#).
- [88] A. D. Bolognino, F. G. Celiberto, D. Yu. Ivanov, and A. Papa, Eur. Phys. J. **C78**, 1023 (2018), [1808.02395](#).
- [89] A. D. Bolognino, F. G. Celiberto, D. Yu. Ivanov, and A. Papa, Frascati Phys. Ser. **67**, 76 (2018), [1808.02958](#).
- [90] A. D. Bolognino, F. G. Celiberto, D. Yu. Ivanov, and A. Papa, Acta Phys. Polon. Supp. **12**, 891 (2019), [1902.04520](#).
- [91] A. D. Bolognino, A. Szczurek, and W. Schaefer, Phys. Rev. D **101**, 054041 (2020), [1912.06507](#).
- [92] F. G. Celiberto, Nuovo Cim. **C42**, 220 (2019), [1912.11313](#).
- [93] D. Brzeminski, L. Motyka, M. Sadzikowski, and T. Stebel, JHEP **01**, 005 (2017), [1611.04449](#).
- [94] I. Bautista, A. Fernandez Tellez, and M. Hentschinski, Phys. Rev. D **94**, 054002 (2016), [1607.05203](#).
- [95] A. Arroyo Garcia, M. Hentschinski, and K. Kutak, Phys. Lett. B **795**, 569 (2019), [1904.04394](#).
- [96] F. G. Celiberto, D. Gordo Gomez, and A. Sabio Vera, Phys. Lett. **B786**, 201 (2018), [1808.09511](#).
- [97] Z. Lu and B.-Q. Ma, Phys. Rev. **D94**, 094022 (2016), [1611.00125](#).
- [98] J. M. Pereira-Resina-Rodrigues, Ph.D. thesis, Vrije Univ. Amsterdam (2001).
- [99] A. Bacchetta, F. Conti, and M. Radici, Phys. Rev. **D78**, 074010 (2008), [0807.0323](#).
- [100] A. Bacchetta, M. Radici, F. Conti, and M. Guagnelli, Eur. Phys. J. **A45**, 373 (2010), [1003.1328](#).
- [101] L. P. Gamberg and G. R. Goldstein, Phys. Lett. B **650**, 362 (2007), [hep-ph/0506127](#).
- [102] L. P. Gamberg, G. R. Goldstein, and M. Schlegel, Phys. Rev. D **77**, 094016 (2008), [0708.0324](#).
- [103] R. Jakob, P. J. Mulders, and J. Rodrigues, Nucl. Phys. **A626**, 937 (1997), [hep-ph/9704335](#).
- [104] G. T. Bodwin, E. Braaten, and G. Lepage, Phys. Rev. D **51**, 1125 (1995), [Erratum: Phys.Rev.D 55, 5853 (1997)], [hep-ph/9407339](#).
- [105] H. Fritzsch, Phys. Lett. **67B**, 217 (1977).
- [106] F. Halzen, Phys. Lett. **69B**, 105 (1977).
- [107] V. D. Barger, W.-Y. Keung, and R. Phillips, Phys. Lett. B **91**, 253 (1980).
- [108] V. D. Barger, W.-Y. Keung, and R. Phillips, Z. Phys. C **6**, 169 (1980).
- [109] R. Gavaï, D. Kharzeev, H. Satz, G. Schuler, K. Sridhar, and R. Vogt, Int. J. Mod. Phys. A **10**, 3043 (1995), [hep-ph/9502270](#).
- [110] Y.-Q. Ma and R. Vogt, Phys. Rev. D **94**, 114029 (2016), [1609.06042](#).
- [111] V. Cheung and R. Vogt, Phys. Rev. D **96**, 054014 (2017), [1706.07686](#).
- [112] V. Cheung and R. Vogt, Phys. Rev. D **98**, 114029 (2018), [1808.02909](#).
- [113] R. Maciula, A. Szczurek, and A. Cisek, Phys. Rev. D **99**, 054014 (2019), [1810.08063](#).
- [114] J.-P. Lansberg, H.-S. Shao, N. Yamanaka, Y.-J. Zhang, and C. Notis, Phys. Lett. **B807**, 135559 (2020), [2004.14345](#).
- [115] J.-P. Lansberg and H.-S. Shao, JHEP **10**, 153 (2016), [1608.03198](#).
- [116] G. C. Nayak, J.-W. Qiu, and G. F. Sterman, Phys. Rev. D **72**, 114012 (2005), [hep-ph/0509021](#).
- [117] G. C. Nayak, J.-W. Qiu, and G. F. Sterman, Phys. Rev. D **74**, 074007 (2006), [hep-ph/0608066](#).
- [118] Z.-G. He, B. A. Kniehl, and X.-P. Wang, Phys. Rev. Lett. **121**, 172001 (2018), [1809.07993](#).
- [119] G. Lepage, L. Magnea, C. Nakhleh, U. Magnea, and K. Hornbostel, Phys. Rev. D **46**, 4052 (1992), [hep-lat/9205007](#).
- [120] R. Gastmans, W. Troost, and T. T. Wu, Phys. Lett. B **184**, 257 (1987).
- [121] M. Butenschoen and B. A. Kniehl, Phys. Rev. Lett. **106**, 022003 (2011), [1009.5662](#).
- [122] M. Butenschoen and B. A. Kniehl, Phys. Rev. D **84**, 051501 (2011), [1105.0820](#).
- [123] M. Butenschoen and B. A. Kniehl, Phys. Rev. Lett. **108**, 172002 (2012), [1201.1872](#).
- [124] M. Butenschoen and B. A. Kniehl, Mod. Phys. Lett. A **28**, 1350027 (2013), [1212.2037](#).
- [125] K.-T. Chao, Y.-Q. Ma, H.-S. Shao, K. Wang, and Y.-J. Zhang, Phys. Rev. Lett. **108**, 242004 (2012), [1201.2675](#).
- [126] B. Gong, L.-P. Wan, J.-X. Wang, and H.-F. Zhang, Phys. Rev. Lett. **110**, 042002 (2013), [1205.6682](#).
- [127] G. T. Bodwin, H. S. Chung, U.-R. Kim, and J. Lee, Phys. Rev. Lett. **113**, 022001 (2014), [1403.3612](#).
- [128] B. Gong, J.-X. Wang, and H.-F. Zhang, Phys. Rev. D **83**, 114021 (2011), [1009.3839](#).
- [129] K. Wang, Y.-Q. Ma, and K.-T. Chao, Phys. Rev. D **85**, 114003 (2012), [1202.6012](#).
- [130] B. Gong, L.-P. Wan, J.-X. Wang, and H.-F. Zhang, Phys. Rev. Lett. **112**, 032001 (2014), [1305.0748](#).
- [131] M. Nefedov, V. Saleev, and A. Shipilova, Phys. Rev. D **88**, 014003 (2013), [1305.7310](#).
- [132] G. T. Bodwin, E. Braaten, and J. Lee, Phys. Rev. D **72**, 014004 (2005), [hep-ph/0504014](#).
- [133] S. Chatrchyan et al. (CMS), Phys. Lett. B **727**, 381 (2013), [1307.6070](#).
- [134] S. Chatrchyan et al. (CMS), Phys. Rev. Lett. **110**, 081802 (2013), [1209.2922](#).
- [135] M. Butenschoen, Z.-G. He, and B. A. Kniehl, Phys. Rev. Lett. **114**, 092004 (2015), [1411.5287](#).
- [136] R. Aaij et al. (LHCb), Eur. Phys. J. C **75**, 311 (2015), [1409.3612](#).
- [137] R. Aaij et al. (LHCb), Eur. Phys. J. **C80**, 191 (2020), [1911.03326](#).
- [138] H.-F. Zhang, Z. Sun, W.-L. Sang, and R. Li, Phys. Rev. Lett. **114**, 092006 (2015), [1412.0508](#).
- [139] H. Han, Y.-Q. Ma, C. Meng, H.-S. Shao, and K.-T. Chao, Phys. Rev. Lett. **114**, 092005 (2015), [1411.7350](#).
- [140] H. Shao, H. Han, Y. Ma, C. Meng, Y. Zhang, and K. Chao, JHEP **05**, 103 (2015), [1411.3300](#).
- [141] J.-P. Lansberg, H.-S. Shao, N. Yamanaka, and Y.-J. Zhang, Eur. Phys. J. **C79**, 1006 (2019), [1906.10049](#).
- [142] Z.-G. He, B. A. Kniehl, M. A. Nefedov, and V. A. Saleev, Phys. Rev. Lett. **123**, 162002 (2019), [1906.08979](#).
- [143] Z.-G. He and B. A. Kniehl, Phys. Rev. Lett. **115**, 022002 (2015), [1609.02786](#).
- [144] J.-P. Lansberg and H.-S. Shao, Phys. Lett. **B751**, 479 (2015), [1410.8822](#).
- [145] J.-P. Lansberg and H.-S. Shao, Phys. Rev. Lett. **111**, 122001 (2013), [1308.0474](#).
- [146] Z.-B. Kang, J.-W. Qiu, and G. Sterman, Phys. Rev. Lett. **108**, 102002 (2012), [1109.1520](#).
- [147] Y.-Q. Ma and K.-T. Chao, Phys. Rev. D **100**, 094007 (2019), [1703.08402](#).

- [148] R. Li, Y. Feng, and Y.-Q. Ma, JHEP **05**, 009 (2020), [1911.05886](#).
- [149] A.-P. Chen and Y.-Q. Ma (2020), [2005.08786](#).
- [150] V. Saleev, M. Nefedov, and A. Shipilova, Phys. Rev. D **85**, 074013 (2012), [1201.3464](#).
- [151] A. Karpishkov, M. Nefedov, and V. Saleev, J. Phys. Conf. Ser. **1435**, 012015 (2020).
- [152] Y. Feng, J.-P. Lansberg, and J.-X. Wang, Eur. Phys. J. C **75**, 313 (2015), [1504.00317](#).
- [153] J. P. Lansberg and M. A. Ozelik (2020), (To appear).
- [154] M. G. Echevarria, JHEP **10**, 144 (2019), [1907.06494](#).
- [155] S. Fleming, Y. Makris, and T. Mehen (2019), [1910.03586](#).
- [156] J. Collins, Camb. Monogr. Part. Phys. Nucl. Phys. Cosmol. **32**, 1 (2011).
- [157] M. G. Echevarria, A. Idilbi, and I. Scimemi, JHEP **07**, 002 (2012), [1111.4996](#).
- [158] M. G. Echevarria, A. Idilbi, A. Schäfer, and I. Scimemi, Eur. Phys. J. C **73**, 2636 (2013), [1208.1281](#).
- [159] M. G. Echevarria, A. Idilbi, and I. Scimemi, Phys. Lett. B **726**, 795 (2013), [1211.1947](#).
- [160] M. G. Echevarria, A. Idilbi, and I. Scimemi, Phys. Rev. D **90**, 014003 (2014), [1402.0869](#).
- [161] I. Scimemi and A. Vladimirov, JHEP **08**, 003 (2018), [1803.11089](#).
- [162] U. D'Alesio, M. G. Echevarria, S. Melis, and I. Scimemi, JHEP **11**, 098 (2014), [1407.3311](#).
- [163] M. G. Echevarria, A. Idilbi, Z.-B. Kang, and I. Vitev, Phys. Rev. D **89**, 074013 (2014), [1401.5078](#).
- [164] A. Bacchetta, M. G. Echevarria, P. J. Mulders, M. Radici, and A. Signori, JHEP **11**, 076 (2015), [1508.00402](#).
- [165] A. Bacchetta, F. Delcarro, C. Pisano, M. Radici, and A. Signori, JHEP **06**, 081 (2017), [Erratum: JHEP 06, 051 (2019)], [1703.10157](#).
- [166] M. Anselmino, M. Boglione, U. D'Alesio, F. Murgia, and A. Prokudin, JHEP **04**, 046 (2017), [1612.06413](#).
- [167] I. Scimemi and A. Vladimirov, Eur. Phys. J. C **78**, 89 (2018), [1706.01473](#).
- [168] V. Bertone, I. Scimemi, and A. Vladimirov, JHEP **06**, 028 (2019), [1902.08474](#).
- [169] D. Gutierrez-Reyes, I. Scimemi, and A. Vladimirov, JHEP **07**, 172 (2018), [1805.07243](#).
- [170] A. Vladimirov, JHEP **04**, 045 (2018), [1707.07606](#).
- [171] M. G. Echevarria, I. Scimemi, and A. Vladimirov, JHEP **09**, 004 (2016), [1604.07869](#).
- [172] M. G. Echevarria, I. Scimemi, and A. Vladimirov, Phys. Rev. D **93**, 054004 (2016), [1511.05590](#).
- [173] M. G. Echevarria, I. Scimemi, and A. Vladimirov, Phys. Rev. D **93**, 011502 (2016), [Erratum: Phys.Rev.D 94, 099904 (2016)], [1509.06392](#).
- [174] A. Bacchetta and M. G. Echevarria, Phys. Lett. B **788**, 280 (2019), [1810.02297](#).
- [175] D. Boer, P. J. Mulders, C. Pisano, and J. Zhou, JHEP **08**, 001 (2016), [1605.07934](#).
- [176] D. Boer et al. (2011), [1108.1713](#).
- [177] T. Burton, in [20th International Workshop on Deep-Inelastic Scattering and Related Subjects](#) (2012), [1212.3590](#).
- [178] R. F. del Castillo, M. G. Echevarria, Y. Makris, and I. Scimemi (2020), [2008.07531](#).
- [179] L. Zheng, E. C. Aschenauer, J. H. Lee, B.-W. Xiao, and Z.-B. Yin, Phys. Rev. D **98**, 034011 (2018), [1805.05290](#).
- [180] J. Collins and J.-W. Qiu, Phys. Rev. D **75**, 114014 (2007), [0705.2141](#).
- [181] J. Collins (2007), [0708.4410](#).
- [182] T. C. Rogers and P. J. Mulders, Phys. Rev. D **81**, 094006 (2010), [1001.2977](#).
- [183] J. R. Gaunt, JHEP **07**, 110 (2014), [1405.2080](#).
- [184] M. D. Schwartz, K. Yan, and H. X. Zhu, Phys. Rev. D **97**, 096017 (2018), [1801.01138](#).
- [185] Y. Gao, C. S. Li, and J. J. Liu, Phys. Rev. D **72**, 114020 (2005), [hep-ph/0501229](#).
- [186] J.-Y. Chiu, A. Jain, D. Neill, and I. Z. Rothstein, JHEP **05**, 084 (2012), [1202.0814](#).
- [187] D. Neill, I. Z. Rothstein, and V. Vaidya, JHEP **12**, 097 (2015), [1503.00005](#).
- [188] D. Boer and C. Pisano, Phys. Rev. D **86**, 094007 (2012), [1208.3642](#).
- [189] J. Ma, J. Wang, and S. Zhao, Phys. Rev. D **88**, 014027 (2013), [1211.7144](#).
- [190] G.-P. Zhang, Phys. Rev. D **90**, 094011 (2014), [1406.5476](#).
- [191] J. Ma and C. Wang, Phys. Rev. D **93**, 014025 (2016), [1509.04421](#).
- [192] D. Boer, PoS [QCDEV2015](#), 023 (2015), [1510.05915](#).
- [193] R. Bain, Y. Makris, and T. Mehen, JHEP **11**, 144 (2016), [1610.06508](#).
- [194] A. Mukherjee and S. Rajesh, Phys. Rev. D **93**, 054018 (2016), [1511.04319](#).
- [195] A. Mukherjee and S. Rajesh, Phys. Rev. D **95**, 034039 (2017), [1611.05974](#).
- [196] A. Bacchetta, D. Boer, C. Pisano, and P. Taels, Eur. Phys. J. C **80**, 72 (2020), [1809.02056](#).
- [197] U. D'Alesio, F. Murgia, C. Pisano, and S. Rajesh, Eur. Phys. J. C **79**, 1029 (2019), [1910.09640](#).
- [198] M. Grewal, Z.-B. Kang, J.-W. Qiu, and A. Signori, Phys. Rev. D **101**, 114023 (2020), [2003.07453](#).
- [199] D. Boer, U. D'Alesio, F. Murgia, C. Pisano, and P. Taels (2020), [2004.06740](#).
- [200] M. G. Echevarria, Y. Makris, and I. Scimemi, JHEP **10**, 164 (2020), [2007.05547](#).
- [201] M. Beneke, I. Rothstein, and M. B. Wise, Phys. Lett. B **408**, 373 (1997), [hep-ph/9705286](#).
- [202] S. Fleming, A. K. Leibovich, and T. Mehen, Phys. Rev. D **68**, 094011 (2003), [hep-ph/0306139](#).
- [203] S. Fleming, A. K. Leibovich, and T. Mehen, Phys. Rev. D **74**, 114004 (2006), [hep-ph/0607121](#).
- [204] J. Ma, J. Wang, and S. Zhao, Phys. Lett. B **737**, 103 (2014), [1405.3373](#).
- [205] H.-L. Lai, M. Guzzi, J. Huston, Z. Li, P. M. Nadolsky, J. Pumplin, and C.-P. Yuan, Phys. Rev. D **82**, 074024 (2010), [1007.2241](#).
- [206] S. J. Brodsky, K. Y.-J. Chiu, J.-P. Lansberg, and N. Yamanaka, Phys. Lett. B **783**, 287 (2018), [1805.03173](#).
- [207] R. L. Jaffe and A. Manohar, Nucl. Phys. **B337**, 509 (1990).
- [208] X.-D. Ji, Phys. Rev. Lett. **78**, 610 (1997), [hep-ph/9603249](#).
- [209] X. Ji, J.-H. Zhang, and Y. Zhao, Phys. Rev. Lett. **111**, 112002 (2013), [1304.6708](#).
- [210] Y. Zhao, K.-F. Liu, and Y. Yang, Phys. Rev. D **93**, 054006 (2016), [1506.08832](#).
- [211] X. Ji, Sci. China Phys. Mech. Astron. **57**, 1407 (2014), [1404.6680](#).
- [212] X. Ji, J.-H. Zhang, and Y. Zhao, Phys. Lett. **B743**, 180 (2015), [1409.6329](#).
- [213] K. Y. Bliokh, J. Dressel, and F. Nori, New J. Phys. **16**, 093037 (2014), [1404.5486](#).
- [214] X.-S. Chen, X.-F. Lu, W.-M. Sun, F. Wang, and T. Goldman, Phys. Rev. Lett. **100**, 232002 (2008), [0806.3166](#).
- [215] Y.-B. Yang, R. S. Sufian, A. Alexandru, T. Draper, M. J. Glatzmaier, K.-F. Liu, and Y. Zhao, Phys. Rev. Lett. **118**, 102001 (2017), [1609.05937](#).

- [216] M. Deka et al., Phys. Rev. D **91**, 014505 (2015), [1312.4816](#).
- [217] C. Alexandrou, M. Constantinou, K. Hadjiyiannakou, K. Jansen, C. Kallidonis, G. Koutsou, A. Vaquero Avilés-Casco, and C. Wiese, Phys. Rev. Lett. **119**, 142002 (2017), [1706.02973](#).
- [218] Y.-B. Yang (Xqcd), PoS **LATTICE2018**, 017 (2019), [1904.04138](#).
- [219] Z.-Y. Fan, Y.-B. Yang, A. Anthony, H.-W. Lin, and K.-F. Liu, Phys. Rev. Lett. **121**, 242001 (2018), [1808.02077](#).
- [220] W. Detmold and P. Shanahan, Phys. Rev. D **94**, 014507 (2016), [Erratum: Phys.Rev.D 95, 079902 (2017)], [1606.04505](#).
- [221] I. Abt et al. (ZEUS) (2020), [2003.08742](#).
- [222] A. M. Sirunyan et al. (CMS), Eur. Phys. J. C **77**, 459 (2017), [1703.01630](#).
- [223] H. Abdolmaleki and A. Khorramian, Phys. Rev. D **99**, 116019 (2019), [1903.02583](#).
- [224] C. Lourenco and H. Wohri, Phys. Rept. **433**, 127 (2006), [hep-ph/0609101](#).
- [225] A. Accardi et al., Eur. Phys. J. C **76**, 471 (2016), [1603.08906](#).
- [226] P. Bärnreuther, M. Czakon, and A. Mitov, Phys. Rev. Lett. **109**, 132001 (2012), [1204.5201 \[hep-ph\]](#).
- [227] M. Czakon and A. Mitov, JHEP **1**, 080 (2013), [1210.6832 \[hep-ph\]](#).
- [228] M. Czakon, P. Fiedler, and A. Mitov, Phys. Rev. Lett. **110**, 252004 (2013), [1303.6254 \[hep-ph\]](#).
- [229] P. Nason, S. Dawson, and R. Ellis, Nucl. Phys. B **303**, 607 (1988).
- [230] P. A. Zyla et al. (Particle Data Group), PTEP **2020**, 083C01 (2020).
- [231] G. F. Sterman, Nucl. Phys. B **281**, 310 (1987).
- [232] S. Catani and L. Trentadue, Nucl. Phys. B **327**, 323 (1989).
- [233] H. Contopanagos, E. Laenen, and G. F. Sterman, Nucl. Phys. B **484**, 303 (1997), [hep-ph/9604313](#).
- [234] N. Kidonakis, G. Oderda, and G. F. Sterman, Nucl. Phys. B **531**, 365 (1998), [hep-ph/9803241](#).
- [235] N. Ivanov, Nucl. Phys. B **615**, 266 (2001), [hep-ph/0104301](#).
- [236] S. Catani, M. L. Mangano, P. Nason, and L. Trentadue, Nucl. Phys. B **478**, 273 (1996), [hep-ph/9604351](#).
- [237] E. L. Berger and H. Contopanagos, Phys. Rev. D **54**, 3085 (1996), [hep-ph/9603326](#).
- [238] N. Kidonakis, Phys. Rev. D **64**, 014009 (2001), [hep-ph/0010002](#).
- [239] S. Forte, G. Ridolfi, J. Rojo, and M. Ubiali, Phys. Lett. B **635**, 313 (2006), [hep-ph/0601048](#).
- [240] S. Brodsky, P. Hoyer, C. Peterson, and N. Sakai, Phys. Lett. B **93**, 451 (1980).
- [241] S. J. Brodsky, C. Peterson, and N. Sakai, Phys. Rev. D **23**, 2745 (1981).
- [242] L. Ananikyan and N. Ivanov, Nucl. Phys. B **762**, 256 (2007), [hep-ph/0701076](#).
- [243] A. Efremov, N. Ivanov, and O. Teryaev, Phys. Lett. B **772**, 283 (2017), [1706.03125](#).
- [244] A. Efremov, N. Y. Ivanov, and O. Teryaev, Phys. Lett. B **777**, 435 (2018), [1711.05221](#).
- [245] A. Efremov, N. Y. Ivanov, and O. Teryaev, Phys. Lett. B **780**, 303 (2018), [1801.03398](#).
- [246] N. Y. Ivanov, Nucl. Phys. B **666**, 88 (2003), [hep-ph/0304191](#).
- [247] N. Y. Ivanov and B. Kniehl, Eur. Phys. J. C **59**, 647 (2009), [0806.4705](#).
- [248] J. Collins and T. Rogers, Phys. Rev. D **91**, 074020 (2015), [1412.3820](#).
- [249] J.-W. Qiu, M. Schlegel, and W. Vogelsang, Phys. Rev. Lett. **107**, 062001 (2011), [1103.3861](#).
- [250] A. Airapetian et al. (HERMES), Phys. Rev. Lett. **95**, 242001 (2005), [hep-ex/0506018](#).
- [251] M. Harvey, Nucl. Phys. A **352**, 301 (1981), [Erratum: Nucl.Phys.A 481, 834 (1988)].
- [252] G. A. Müller, Phys. Rev. C **89**, 045203 (2014), [1311.4561](#).
- [253] P. Hoyer and D. Roy, Phys. Lett. B **410**, 63 (1997), [hep-ph/9705273](#).
- [254] H. Mäntysaari and B. Schenke, Phys. Rev. C **101**, 015203 (2020), [1910.03297](#).
- [255] F. Winter, W. Detmold, A. S. Gambhir, K. Orginos, M. J. Savage, P. E. Shanahan, and M. L. Wagman, Phys. Rev. D **96**, 094512 (2017), [1709.00395](#).
- [256] J. Ashman et al. (European Muon), Nucl. Phys. B **328**, 1 (1989).
- [257] D. L. Adams et al. (FNAL E581/704), Phys. Lett. **B336**, 269 (1994).
- [258] A. Airapetian et al. (HERMES), JHEP **08**, 130 (2010), [1002.3921](#).
- [259] B. Adeva et al. (Spin Muon (SMC)), Phys. Rev. **D70**, 012002 (2004), [hep-ex/0402010](#).
- [260] E. S. Ageev et al. (COMPASS), Phys. Lett. **B633**, 25 (2006), [hep-ex/0511028](#).
- [261] M. Alekseev et al. (COMPASS), Phys. Lett. **B676**, 31 (2009), [0904.3209](#).
- [262] C. Adolph et al. (COMPASS), Phys. Lett. **B718**, 922 (2013), [1202.4064](#).
- [263] C. Adolph et al. (COMPASS), Phys. Rev. **D87**, 052018 (2013), [1211.6849](#).
- [264] C. Adolph et al. (COMPASS), Eur. Phys. J. **C77**, 209 (2017), [1512.05053](#).
- [265] A. Deur, S. J. Brodsky, and G. F. De Téraumont, Rept. Prog. Phys. **82** (2019), [1807.05250](#).
- [266] J. Adam et al. (STAR), Phys. Rev. D **98**, 032013 (2018), [1805.09745](#).
- [267] A. Adare et al. (PHENIX), Phys. Rev. **D90**, 012007 (2014), [1402.6296](#).
- [268] A. Adare et al. (PHENIX), Phys. Rev. Lett. **103**, 012003 (2009), [0810.0694](#).
- [269] A. Adare et al. (PHENIX), Phys. Rev. **D79**, 012003 (2009), [0810.0701](#).
- [270] U. A. Acharya et al. (PHENIX), Phys. Rev. D **102**, 032001 (2020), [2004.02681](#).
- [271] P. Djawotho (STAR), Nuovo Cim. **C036**, 35 (2013), [1303.0543](#).
- [272] L. Adamczyk et al. (STAR), Phys. Rev. D **95**, 071103 (2017), [1610.06616](#).
- [273] J. Adam et al. (STAR), Phys. Rev. D **98**, 032011 (2018), [1805.09742](#).
- [274] A. Adare et al. (PHENIX), Phys. Rev. **D87**, 012011 (2013), [1209.3278](#).
- [275] A. Adare et al. (PHENIX), Phys. Rev. **D94**, 112008 (2016), [1606.01815](#).
- [276] E. Leader, A. V. Sidorov, and D. B. Stamenov, Phys. Rev. **D91**, 054017 (2015), [1410.1657](#).
- [277] D. de Florian, R. Sassot, M. Stratmann, and W. Vogelsang, Phys. Rev. Lett. **113**, 012001 (2014), [1404.4293](#).
- [278] D. de Florian, G. A. Lucero, R. Sassot, M. Stratmann, and W. Vogelsang, Phys. Rev. **D100**, 114027 (2019), [1902.10548](#).
- [279] J. J. Ethier, N. Sato, and W. Melnitchouk, Phys. Rev. Lett. **119**, 132001 (2017), [1705.05889](#).
- [280] D. de Florian, R. Sassot, M. Stratmann, and W. Vogelsang, Phys. Rev. Lett. **101**, 072001 (2008), [0804.0422](#).
- [281] C. Aidala, G. Bunce, and A. Et, Technical Report, BNL-73798-2005 (2005).
- [282] T. Gehrmann and W. J. Stirling, Z. Phys. C **65**, 461 (1995), [hep-ph/9406212](#).
- [283] M. Anselmino, E. Andreeva, V. Korotkov, F. Murgia, W. D. Nowak, S. Nurushev, O. Teryaev, and A. Tk-

- ablazde, in *Future physics at HERA. Proceedings, Workshop, Hamburg, Germany, September 25, 1995-May 31, 1996*. Vol. 1, 2 (1996), [hep-ph/9608393](#).
- [284] L. E. Gordon and W. Vogelsang, *Phys. Lett.* **B387**, 629 (1996), [hep-ph/9607442](#).
- [285] E. Leader, Cambridge University Press (2011) (2011).
- [286] Y. Feng and H.-F. Zhang, *JHEP* **11**, 136 (2018), [1809.04894](#).
- [287] W. Vogelsang, in *Deep inelastic scattering. Proceedings, 8th International Workshop, DIS 2000, Liverpool, UK, April 25-30, 2000* (2000), pp. 253–254, [hep-ph/0006199](#).
- [288] L. E. Gordon, *Phys. Lett.* **B406**, 184 (1997), [hep-ph/9609403](#).
- [289] Q.-h. Xu and Z.-t. Liang, *Phys. Rev.* **D70**, 034015 (2004), [hep-ph/0406119](#).
- [290] Z.-T. LIANG and C. BOROS, *International Journal of Modern Physics A* **15**, 927–982 (2000), ISSN 1793-656X, URL [http://dx.doi.org/10.1142/S0217751X0000046X](#).
- [291] E. C. Aschenauer, U. D’Alesio, and F. Murgia, *The European Physical Journal A* **52** (2016), ISSN 1434-601X, URL [http://dx.doi.org/10.1140/epja/i2016-1140-4](#).
- [292] C. Aidala, Y. Akiba, M. Alfred, V. Andrieux, N. Apadula, H. Asano, B. Azmoun, V. Babintsev, A. Bagoly, N. Bandara, et al., *Physical Review D* **98** (2018), ISSN 2470-0029, URL [http://dx.doi.org/10.1103/PhysRevD.98.012006](#).
- [293] A. Efremov and O. Teryaev, *Sov. J. Nucl. Phys.* **36**, 140 (1982).
- [294] A. Efremov and O. Teryaev, *Phys. Lett. B* **150**, 383 (1985).
- [295] J.-w. Qiu and G. F. Sterman, *Phys. Rev. Lett.* **67**, 2264 (1991).
- [296] A. Efremov, V. Korotkiian, and O. Teryaev, *Phys. Lett. B* **348**, 577 (1995).
- [297] D. Pitonyak, *Int. J. Mod. Phys. A* **31**, 1630049 (2016), [1608.05353](#).
- [298] D. W. Sivers, *Phys. Rev. D* **41**, 83 (1990).
- [299] U. D’Alesio and F. Murgia, *Prog. Part. Nucl. Phys.* **61**, 394 (2008), [0712.4328](#).
- [300] D. Boer, C. Lorcé, C. Pisano, and J. Zhou, *Adv. High Energy Phys.* **2015**, 371396 (2015), [1504.04332](#).
- [301] R. M. Godbole, A. Kaushik, A. Misra, V. Rawoot, and B. Sonawane, *Phys. Rev.* **D96**, 096025 (2017), [1703.01991](#).
- [302] M. Anselmino, M. Boglione, U. D’Alesio, E. Leader, and F. Murgia, *Phys. Rev. D* **70**, 074025 (2004), [hep-ph/0407100](#).
- [303] Y. Koike and S. Yoshida, *Phys. Rev. D* **84**, 014026 (2011), [1104.3943](#).
- [304] Z.-B. Kang, J.-W. Qiu, W. Vogelsang, and F. Yuan, *Phys. Rev.* **D78**, 114013 (2008), [0810.3333](#).
- [305] R. M. Godbole, A. Kaushik, and A. Misra, *Phys. Rev.* **D94**, 114022 (2016), [1606.01818](#).
- [306] N. Hammon, B. Ehrnsperger, and A. Schaefer, *J. Phys.* **G24**, 991 (1998).
- [307] K. Kanazawa and Y. Koike, *Phys. Lett.* **B720**, 161 (2013), [1212.3071](#).
- [308] U. D’Alesio, F. Murgia, and C. Pisano, *JHEP* **09**, 119 (2015), [1506.03078](#).
- [309] M. Anselmino, M. Boglione, U. D’Alesio, A. Kotzinian, F. Murgia, and A. Prokudin, *Phys. Rev. D* **72**, 094007 (2005), [Erratum: *Phys.Rev.D* 72, 099903 (2005)], [hep-ph/0507181](#).
- [310] M. Anselmino, M. Boglione, U. D’Alesio, A. Kotzinian, S. Melis, F. Murgia, A. Prokudin, and C. Turk, *Eur. Phys. J. A* **39**, 89 (2009), [0805.2677](#).
- [311] S. Kretzer, *Phys. Rev. D* **62**, 054001 (2000), [hep-ph/0003177](#).
- [312] D. de Florian, R. Sassot, and M. Stratmann, *Phys. Rev. D* **75**, 114010 (2007), [hep-ph/0703242](#).
- [313] L. Gamberg and Z.-B. Kang, *Phys. Lett. B* **696**, 109 (2011), [1009.1936](#).
- [314] U. D’Alesio, L. Gamberg, Z.-B. Kang, F. Murgia, and C. Pisano, *Phys. Lett. B* **704**, 637 (2011), [1108.0827](#).
- [315] J. C. Collins, *Phys. Lett. B* **536**, 43 (2002), [hep-ph/0204004](#).
- [316] S. J. Brodsky, D. S. Hwang, and I. Schmidt, *Nucl. Phys. B* **642**, 344 (2002), [hep-ph/0206259](#).
- [317] C. Bomhof and P. Mulders, *JHEP* **02**, 029 (2007), [hep-ph/0609206](#).
- [318] M. Anselmino, M. Boglione, U. D’Alesio, A. Kotzinian, F. Murgia, and A. Prokudin, *Phys. Rev. D* **71**, 074006 (2005), [hep-ph/0501196](#).
- [319] J. Pumplin, D. Stump, J. Huston, H. Lai, P. M. Nadolsky, and W. Tung, *JHEP* **07**, 012 (2002), [hep-ph/0201195](#).
- [320] D. Boer and W. Vogelsang, *Phys. Rev.* **D69**, 094025 (2004), [hep-ph/0312320](#).
- [321] D. L. Adams et al. (E704), *Phys. Lett.* **B345**, 569 (1995).
- [322] S. Kumano and M. Miyama, *Phys. Rev. D* **56**, 2504 (1997), [hep-ph/9706420](#).
- [323] S. Kumano and M. Miyama, in *10th Summer School and Symposium on Nuclear Physics: QCD, Light cone Physics and Hadron Phenomenology (NuSS 97)* (1997), pp. 266–270, [hep-ph/9709298](#).
- [324] M. Hirai, S. Kumano, and M. Miyama, *Comput. Phys. Commun.* **111**, 150 (1998), [hep-ph/9712410](#).
- [325] M. Hirai, S. Kumano, and M. Miyama, *Comput. Phys. Commun.* **108**, 38 (1998), [hep-ph/9707220](#).
- [326] S. Kumano and Q.-T. Song, *Phys. Rev. D* **101**, 054011 (2020), [1910.12523](#).
- [327] J. Soffer, M. Stratmann, and W. Vogelsang, *Phys. Rev. D* **65**, 114024 (2002), [hep-ph/0204058](#).
- [328] A. Mukherjee, M. Stratmann, and W. Vogelsang, *Phys. Rev. D* **67**, 114006 (2003), [hep-ph/0303226](#).
- [329] M. Radici and A. Bacchetta, *Phys. Rev. Lett.* **120**, 192001 (2018), [1802.05212](#).
- [330] R. Jaffe and A. Manohar, *Phys. Lett. B* **223**, 218 (1989).
- [331] S. Kumano and Q.-T. Song, *Phys. Rev. D* **101**, 094013 (2020), [2003.06623](#).
- [332] M. Jones et al., A Letter of Intent to Jefferson Lab PAC 44, LOI12-16-006 (2016).
- [333] D. Keller, D. Crabb, and D. Day, *Nucl. Instrum. Meth. A* **981**, 164504 (2020), [2008.09515](#).
- [334] A. Klein et al., Letter of Intent Report No. P1039 (2013) (2013).
- [335] L. Frankfurt and M. Strikman, *Nucl. Phys. A* **405**, 557 (1983).
- [336] P. Hoodbhoy, R. Jaffe, and A. Manohar, *Nucl. Phys. B* **312**, 571 (1989).
- [337] F. Close and S. Kumano, *Phys. Rev. D* **42**, 2377 (1990).
- [338] S. Kumano, *J. Phys. Conf. Ser.* **543**, 012001 (2014), [1407.3852](#).
- [339] K. Gottfried, *Phys. Rev. Lett.* **18**, 1174 (1967).
- [340] S. Kumano, *Phys. Rept.* **303**, 183 (1998), [hep-ph/9702367](#).
- [341] P. Amaudruz et al. (New Muon), *Phys. Rev. Lett.* **66**, 2712 (1991).
- [342] M. Arneodo et al. (New Muon), *Phys. Rev. D* **50**, 1 (1994).
- [343] A. Baldit et al. (NA51), *Phys. Lett. B* **332**, 244 (1994).
- [344] E. Hawker et al. (NuSea), *Phys. Rev. Lett.* **80**, 3715 (1998), [hep-ex/9803011](#).

- [345] R. Towell et al. (NuSea), Phys. Rev. D **64**, 052002 (2001), [hep-ex/0103030](#).
- [346] G. T. Garvey and J.-C. Peng, Prog. Part. Nucl. Phys. **47**, 203 (2001), [nucl-ex/0109010](#).
- [347] J.-C. Peng and J.-W. Qiu, Prog. Part. Nucl. Phys. **76**, 43 (2014), [1401.0934](#).
- [348] W. Cosyn, Y.-B. Dong, S. Kumano, and M. Sargsian, Phys. Rev. D **95**, 074036 (2017), [1702.05337](#).
- [349] S. Kumano, Phys. Rev. D **82**, 017501 (2010), [1005.4524](#).
- [350] S. Kumano and Q.-T. Song, Phys. Rev. D **94**, 054022 (2016), [1606.03149](#).
- [351] J.-P. Chen et al., Proposal to Jefferson Lab PAC-38, PR12-11-110 (2011).
- [352] S. Hino and S. Kumano, Phys. Rev. D **59**, 094026 (1999), [hep-ph/9810425](#).
- [353] S. Hino and S. Kumano, Phys. Rev. D **60**, 054018 (1999), [hep-ph/9902258](#).
- [354] O. Teryaev, PoS **DIS2019**, 240 (2019).
- [355] A. Efremov and O. Teryaev, Sov. J. Nucl. Phys. **36**, 557 (1982).
- [356] A. Efremov and O. Teryaev, in International Symposium: Dubna Deuteron 93 (1994), [hep-ph/9910555](#).
- [357] O. Teryaev, Mod. Phys. Lett. A **24**, 2831 (2009).
- [358] O. V. Teryaev (1999), [hep-ph/9904376](#).
- [359] O. Teryaev, Czech. J. Phys. **53**, 47 (2003), [hep-ph/0306301](#).
- [360] O. Teryaev, AIP Conf. Proc. **915**, 260 (2007), [hep-ph/0612205](#).
- [361] O. Teryaev, Front. Phys. (Beijing) **11**, 111207 (2016).
- [362] G. Y. Prokhorov, O. V. Teryaev, and V. I. Zakharov, Phys. Rev. D **99**, 071901 (2019), [1903.09697](#).
- [363] M. V. Polyakov and H.-D. Son, JHEP **09**, 156 (2018), [1808.00155](#).
- [364] S. Kumano and Q.-T. Song, in 22nd International Symposium on Spin Physics (2017), [1702.01477](#).
- [365] V. Golovatyuk, V. Kekelidze, V. Kolesnikov, O. Rogachevsky, and A. Sorin, Nucl. Phys. A **982**, 963 (2019).